Technische Universiteit Delft

Standardized Thermal Control

SOLUTIONS FOR POCKETQUBES

R. Ávila de Luis

TU Delft

Standardized Thermal Control

SOLUTIONS FOR POCKETQUBES

by

R. Ávila de Luis

to obtain the degree of Master of Science
at the Delft University of Technology,
to be defended publicly.

Student number:	4621840		
Thesis defense:	February 19, 2019 10:00		
Project duration:	March 26, 2018 – January 21, 2019		
Thesis committee:	Ir. B.T.C. Zandbergen,	TU Delft	Space Systems Engineering
	J. Bouwmeester,	TU Delft	Space Systems Engineering
	Dr. M.J. Heiligers,	TU Delft	Astrodynamics & Space Missions

An electronic version of this thesis is available at `http://repository.tudelft.nl/`

TU Delft

Summary

An innovative approach for thermal analysis and design of small satellites consisting in the study of its thermal behavior and properties from a global perspective is investigated in this research project.

Spacecraft analysis and design is usually carried out in a tailored manner, based on the particular characteristics of each mission. The increasing interest in PocketQubes as space platforms, which share multiple design features, opens the possibility to develop general thermal control procedures applicable to multiple satellites independently of their payloads, configurations and orbits, within certain ranges.

An exploration of the design and environmental parameters that influence the thermal behavior of picosatellites is carried out along with a sensitivity analysis in order to better understand their influence on temperatures. The Delfi-PQ satellite has been chosen as a case study for which a finite element model has been developed using ESATAN. As well, a Matlab tool has been developed for processing the data generated.

Based on the results produced from these analyses, generalized conclusions on how thermal control could be achieved for satellites such as the Delfi-PQ and similar PocketQubes are derived.

This study aims to set the basis for approaching thermal control of highly standardized spacecraft from a global perspective, opening new possibilities of lowering the costs and increase its reliability and performance. The outcomes and lessons learned could be later applied to other categories of similar satellites such as CubeSats.

Acknowledgments

First of all I would like to thank my supervisor, Jasper Bouwmeester, for all his support. Jasper gave me the opportunity to get involved in the development of an actual satellite, the Delfi-PQ, while performing research in spacecraft thermal control, a discipline which I decided to specialize in. Thank you for your commitment, all the feedback and advice, and for being understanding with my sometimes chaotic ways of scheduling my thesis.

As well I'm very thankful for all the support received from Alexander Maas, which sparked my interest in spacecraft thermal control when attending his lectures, and provided excellent technical support for the project as an experienced thermal engineer working for Airbus Defence & Space.

Furthermore I can't forget to mention my colleague, Timo Ruhl for his support through the entire project. Also, I would like to thank Lorenzo Pasqualetto for providing me with useful input based on his experience working with CubeSats at the thermal engineering department of ESA ESTEC and Sevket Uludag for his advice as part of the team developing the Delfi-PQ satellite.

Moreover I feel grateful for the opportunity given by the European Space Agency to present the results of this research project at the European Space Thermal Engineering Workshop which was organized by the European Space Agency in Noordwijk in October 2018.

Thanks to the TU Delft as an educational institution for giving me so many opportunities to grow as a professional in the space sector and push me forward to step into the future. In particular to Barry Zandbergen for trusting in me to help him with his lectures as a teacher assistant and to the VSV Leonardo da Vinci for organizing an amazing Study Tour around Europe and the Middle East. Studying at the TU Delft has been a true adventure and a life-changing experience.

Finally, I would like to dedicate a special mention to my friends, family and all the people around the TU campus who contributed to make my time in Delft and unforgettable experience. Sergio, Mario, Alvaro, Alicia, Michelle, Akash, João, Loo, Francesca, Jean Pascal, Chase, Andres, Kristhi, Mathijs, Matys, and so many more. Thank you all!

Preface

The space sector is currently going through a process of democratization, allowing larger numbers of research groups, companies and institutions to make use of it. Rather than a extraordinary case, space technology seems to be following the natural evolutionary path that other technologies previously followed. Take for example, the Internet, automobiles, computers or smart phones. When they were first conceived, little users had access to them, their cost were prohibitive and only a select collective of people was allowed to make use of those. Advancements such as standardization, mass production, serial manufacturing and miniaturization of technology all contributed to lower the costs and make this platforms available to the a wider public. The generalization in the use of these technologies opened up a world of new services and possibilities that keep pushing our societies forward.

The case of space technology is somehow different due to the inherent difficulties of safely deploying and operating platforms in space. Traditionally this sector has been dominated by governmental agencies financed by the most wealthy nations (NASA, ESA, ISRO, JAXA, CNSA, ROSCOSMOS) which could afford the costs and assume the risks. However, new players are entering the game. Commercial companies such as Space Exploration Technologies Corp., founded just a decade ago, have successfully developed launching capabilities, injecting heavy payloads into orbit and have plans to offer space platforms as a means of transportation for the general public in the coming years.

The year 2013 could be set as a the turning point in the process of democratization of space, when the explosive growth in the launch of CubeSats –small space platforms owned and developed by universities, research groups and private companies– started. A total count of 88 CubeSats were deployed during this year. Since then, the interest in the use of these platforms have been growing exponentially. In the coming six years SpaceWorks predicts more than 1500 CubeSats will be launched to space according to their latest Nano/Microsatellite Market Forecast.

While CubeSats continue gaining popularity, a new category of satellites, PocketQubes, even more reduced than the previous ones seem to be taking off. Research institutions such as the TU Delft and private companies like Alba Orbital and GAUSS SRL are investing on them. It is the aim of this research project to contribute to the process of democratizing space and facilitate access to it by lowering the costs and reducing the risks of these recently conceived platforms.

Contents

List of Tables

List of Figures

List of Abbreviations

ADCS	Attitude Dynamics and Control
ADS-B	Automatic dependent surveillance - broadcast
AIS	Automatic identification system
COTS	Commercial-of-the-shelve
DPQ	Delfi-PQ
ECSS	European cooperation for space standardization
EO	Earth observation
EPS	Electrical power subsystem
ESA	European Space Agency
FEM	Finite element method
GNSS-R	Global navigation satellite systems reflectometry
GSD	Ground sampling distance
ID	Identification
IOD	In orbit demonstration
IoT	Internet of things
IOV	In orbit validation
IR	Infrared
ISS	International Space Station
ITEMS	Integrated Thermal Energy Management System
LEO	Low Earth orbit
LTAN	Local time of the ascending node
NASA	National Aeronautics and Space Administration
MRFOD	Morehead-Rome Femtosatellites Orbital Deployer
MPPT	Maximum Power Point Tracker
NGTS	Non-geometrical thermal node
PDR	Preliminary design review
OBC	On board computer
OBDH	On board data handling
OLR	Outgoing longwave radiation
PCB	Printed circuit board
PQ	PocketQube
RAAN	Right ascension of the ascending node
SSO	Sun-synchronous orbit
TRL	Technology readiness level
TT&C	Telemetry and telecommand
TVAC	Thermal vacuum

List of Symbols

Greek symbols

α	Optical absorptivity
β	Beta angle
β^*	Critical beta angle
δ	Declination
ε	Optical emissivity
σ	Stephan-Boltzmann constant
τ	Thermal time constant
Ω	Right ascension

Astronomycal symbols

$\odot$	Sun
$\earth$	Earth

Latin symbols

A	Surface area
a	Semi-major axis
Ap	Apogee
C_p	Heat capacity
C_{Sp}	Specific heat
d	Distance
E	Eccentric anomaly
e	Eccentricity
f_E	Eclipse fraction
G	Universal gravity constant
GL	Linear thermal coupling
GR	Radiative thermal coupling
h	Orbital altitude
i	Orbital inclination
k	Thermal conductivity
k_c	Coefficient of thermal contact conductance
l	Longitude
M	Mass
Pe	Perigee
Q	Thermal flux
Q_0	Average in-orbit thermal flux
R	Radius
T	Temperature
T_0	Average in-orbit temperature
t	Time
t_0	Initial time
Z	Thickness

Simulation parameter symbols

o_1	α/ϵ external side shear panels
o_2	ϵ internal side shear panels
o_3	ϵ PCB boards
o_4	ϵ battery
t_1	Orbital altitude
t_2	Orbital inclination
t_3	Right ascension of the ascending node
t_4	Earth Albedo
t_5	Earth Infrared
t_6	Solar radiation
c_1	Shear panel heat capacity, single material
c_2	Shear panel heat capacity, multiple materials
c_3	Internal boards heat capacity
c_4	Battery heat capacity
c_5	Electronics components heat capacity
c_6	Structural elements heat capacity
k_1	Conductivity of PCBs
k_2	Conductance board to board via spacers
k_3	Conductance internal to external structure via standoffs
k_4	Conductance battery to board
k_5	Conductance soldered or attached components to board
k_6	Conductance solar cells to shear panels
g_1	Single stack, cylindrical battery, current configuration
g_2	Single stack, cylindrical battery, reversed order of the stack
g_3	3-stack solution, pouch battery

1 Introduction

The introduction of the CubeSat standard [1] in the year 1999 was a game changer for the space sector. Restricting a number of design parameters such as the dimensions and mass of this platform while allowing at the same time enough flexibility for them to cover multiple purposes and missions was a key element that contributed to their success. The geometrical restrictions facilitated the development of standardized deployers that could be easily incorporated as secondary payloads in regular launchers or installed on board the International Space Station. Precisely the cover of this report shows the moment in which two CubeSats were released from the NanoRacks deployer on board the ISS. These developments helped to reduce the launching costs and ease the development process.

Because of their reduced mass, the costs of sending them to orbit were significantly reduced compared to average-sized platforms. The use of mass-produced, commercial-of-the-shelve (COTS) components rather than tailored-designed ones contributed as well to the reduction of the costs. The performance and reliability of these missions was not expected to be as good as the ones that bigger satellites could provide. Nevertheless, thanks to the advancements in technology miniaturization, high performances could be achieved. The design philosophy for CubeSats could be associated with the principle of factor sparsity. This implies that around 80% of the scientific or technical potential that a regular satellite is expected to deliver could be achieved with a CubeSat platform for 20% of the cost.

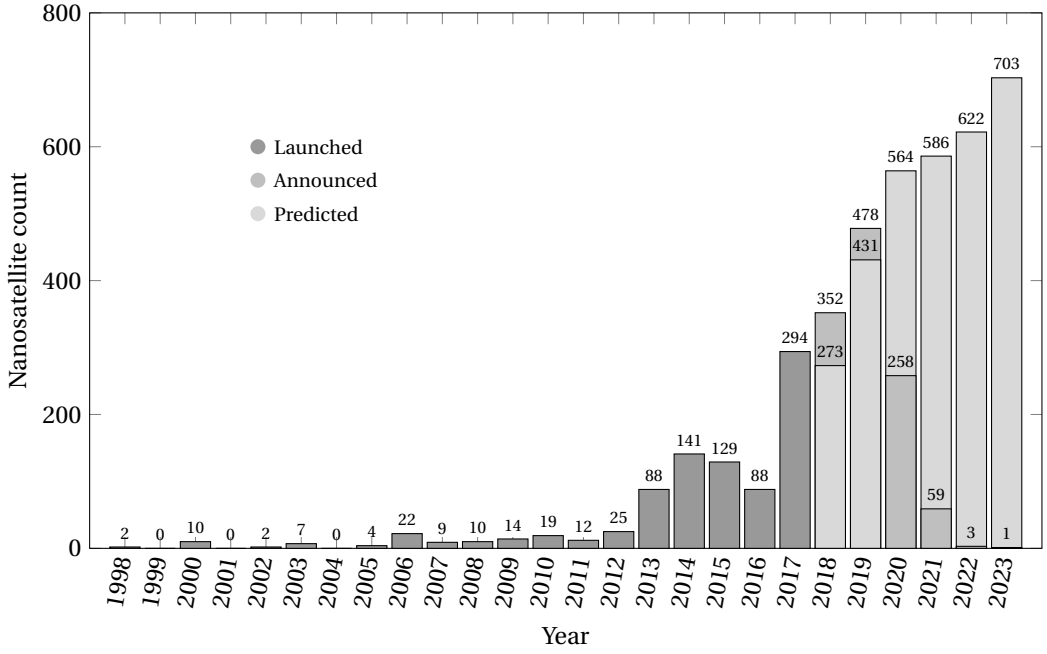

Figure 1.1: Nanosatellite launches, data retrieved from [2] in 2018.

CubeSats share a lot of features, reason why numerous companies flourished providing standardized parts for them such as structures, solar cells, components and even entire subsystems. Some of them, space graded. This contributed to lower even more the costs and make more accessible, reliable and easy to develop space missions.

CubeSats have demonstrated to be a success, opening up their own place in the space market and enabling new services and applications. The interest in this platforms is clearly depicted in Figure 1.1, showing the launches per year. The Delft University of Technology, conscious of their potential launched a couple of them: Delfi-C^3 and the Delfi-n3Xt; and investigated future missions such as DelFFi or OLFAR. However the quest for miniaturizing and lowering the costs do not stop at CubeSats. A new category of satellites, PocketQubes, promise to be the new step in miniaturization.

1.1. The potential of PocketQubes

PocketQubes offer the possibility of miniaturizing space systems even more, economize them and enable access to more research groups and academia. If the building unit of CubeSats is a 10×10×10 cm cube, PocketQubes cut these dimensions down by a factor of 2 as illustrated by figure 1.2, yielding a volume 8 times smaller and therefore a mass reduced in the same order of magnitude, assuming CubeSat and PocketQubes have similar densities. While CubeSats fall in the category of nanosatellites, PocketQubes are considered picosatellites.

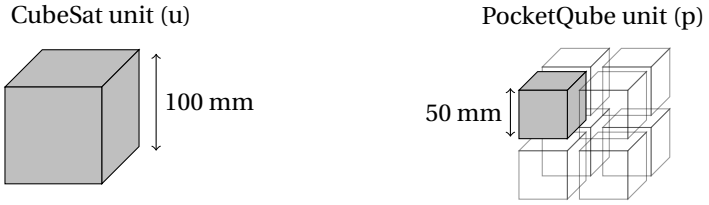

Figure 1.2: CubeSat vs PocketQube dimensions.

The potential applications of PocketQubes are numerous. Optical payloads are one of the candidates for this type of spacecraft. Although volume constraints are generally a concern for optical instruments due to physical limitations in resolution, Alba Orbital has recently passed the PDR in partnership with ESA of a 3p platform (triple PocketQube), the Unicorn-2, which could carry optical instruments achieving sub 10 meter resolution on ground sampling distance (GSD). The use of non diffraction-limited instruments such as uncooled micro-bolometers could be considered as well as a great option for EO missions with PockeQubes as suggested by Bouwmeester et al. in [3].

Given its super reduced-mass, deployment of big constellations becomes more affordable providing smaller revisiting times and even continuous coverage of certain areas of interest. As well, using PocketQubes as distributed space systems offer the potential of multi point sensing at a low cost.

Plane tracking could be another application for PocketQubes, as ADS-B (Automatic dependent surveillance - broadcast) payloads for these satellites are commercially available at the moment provided by companies such as SkyFox Labs. Ship tracking could be possible as well via AIS (Automatic Identification System).

Applications related to communications are being studied as well. A swarm of PocketQubes could connect devices across the world with reduced latency for time-critical applications. This could help to cope with the increasing number of devices that will be connected to the Internet in the years to come (IoT). Encrypted communications could be a potential application to be implemented with PocketQubes as well.

In orbit demonstration (IOD) and in-orbit validation (IOV) are other areas of application where PocketQubes could potentially provide services. Science missions, spectrum monitoring, weather forecasting via Global Navigation Satellite Systems Reflectometry (GNSS-R) is being considered too. Training and education opportunities for academia applications are always an option.

The same way CubeSats will never substitute specific missions and tasks that can only be achieved with bigger and more specialized spacecraft, PocketQubes will most probably not substitute CubeSats. In any case, they might be bound to the same success story of CubeSats in their own fields of application.

1.2. Spacecraft Thermal Control

Thermal Control is one of the concerns every team developing a space mission has to deal with. The space environment can be harsh. The lack of atmosphere has a double effect on the temperature of spacecraft: on one hand, the absence of a great mass of fluid surrounding the spacecraft does not help with keeping the temperatures constant (such as it happens on the surface of the Earth); on the other, the lack of fluids around prevent convection processes to happen naturally, restricting heat exchange with the environment. Heat exchange via conduction happens within the spacecraft as its different subsystems and components are in physical contact, usually through the structure. There is no heat conduction to the environment.

Therefore, there is only one heat transport mechanism possible: radiation. Indeed, spacecraft is subject to thermal inputs in form of radiation coming from the Sun, planets and other celestial objects. The Sun itself, at a distance of 150 million km from the Earth, exerts already 1.4 kW of power per square meter of surface facing it [4]. If not handled carefully, this power input could impact the performance and even damage a spacecraft. A planet like the Earth, because of the energy it reflects from the Sun and its own infrared radiation, could transfer power to a nearby spacecraft in the order of hundreds of Watts per square meter [4].

Spacecraft radiates energy on its own as well. According to the Stephan-Boltzmann law, physical objects are subject to radiate energy to the environment in function of their temperature. This means that a spacecraft constantly radiates energy to the environment. Therefore, if not receiving any thermal inputs from the Sun or the Earth, it will gradually decrease its temperature in time up to the point it reaches an equilibrium with the space (dictated by the cosmic microwave background) with a temperature around –270°C [4].

Because satellites are constantly moving in space, the thermal inputs form the environment vary with time. Take for example a satellite orbiting the Earth at low altitudes. At a given moment this spacecraft could be on the 'day' side of the Earth directly under the influence of the Sun and the reflected radiation from the planet. Half an hour later, it could have moved to the 'night' side of the Earth, subject to the cold space conditions. The cycle repeats every 90 minutes, which is the usual time it takes a satellite in Low Earth Orbit (LEO) to complete an orbit around the planet.

Thermal control of spacecraft is fundamental to ensure proper operation of the satellite in space, avoid failure of the embarked components and extend the lifetime of its subsystems. Most of the components that integrate the spacecraft can only be operated in a certain temperature range to ensure optimal performance and reliability, and prevent early degradation. Some components are more restrictive. For example, is better to keep batteries close to room temperatures (0 to 20 °C). If the temperature increases too much, they might suffer from thermal runaway and could even explode. If the temperature drops, the power delivered by the batteries diminishes. Some optical instruments and detectors require very low temperatures (close to zero absolute) to ensure noise levels are reduced as much as possible. Propellant tanks might have strict limitation in temperature to avoid freezing or overpressure. Some other hardware such as structural elements or solar cells tolerate very extreme temperatures both in the hot and the cold side.

It is the task of the thermal engineer to ensure the spacecraft will provide an optimal temperature environment for all its instruments and subsystems no matter what are the external inputs from the environment at a given moment. If thermal control is not performed properly the risk of failure of the mission increases.

1.2.1. Common approach to thermal control

Spacecraft thermal control is usually achieved by:

1. Determining and specifying the operational and non-operational temperature range of all subsystems.
2. Analyzing the thermal environment and behavior of the satellite.
3. Developing a tailored thermal design for the spacecraft.
4. Carrying out a number of tests to validate the analysis and ensure the spacecraft temperatures behave as expected.

This process is resource and time consuming. It requires trained personnel in the subject, in most cases the use of specific software such as ESATAN or THERMICA and costly test campaigns in TVAC (thermal vacuum) chambers. This impacts the time and budget of space missions.

Because thermal control depends on a great number of parameters involving the orbit in which the spacecraft will be set, its external geometry, internal configuration of subsystems, payloads on-board, the pointing

of the satellite in orbit, the power harvested, produced and stored as well as how it is managed, amongst others; the process of achieving thermal control is done in a case-by-case basis. This means that each mission is analyzed, designed and tested individually from a thermal point of view. The assumptions used in the model developed for one spacecraft do not generally apply to other ones. As well, the design proposed for one spacecraft is not, in general, compatible with other spacecraft.

When considering super-reduced budget missions such as CubeSats and PocketQubes, developers generally take two different approaches to the thermal problem. Option one considers skipping thermal control to cut down budget, time and personnel or do it in a very rough way. This option comes with the risk of failure, malfunction, reduced lifetimes, etc. Option two consists in performing proper thermal control to reduce the aforementioned risks, but incurs in analysis, design and test campaigns which raise costs and resources. Neither of them seem to be ideal for these missions.

1.2.2. An innovative approach to thermal control for standardized spacecraft

This research explores an innovative approach for PocketQube (and potentially CubeSat) thermal control. It aims to reduce thermal analysis and design efforts while ensuring a stable temperature environment for the mission. This could be achieved by following general design guidelines, which, no matter what the configuration, mission, or orbit (within certain boundaries) in which a PocketQube is set, thermal control is ensured.

This statement could seem counterintuitive after mentioning how thermal control depends on multiple parameters that are very particular to each mission. The fact that PocketQubes are standardized and that they share a great number of features, makes it easier to understand its thermal behavior from a global point of view rather than from a particular perspective. The same applies to CubeSats. Because of the standardization restrictions, numerous missions have been launched, each and every of them with different objectives and instruments, but still sharing a great number of commonalities such as orbits, geometry, structure, internal configuration, power budgets, etc.

Standardization of subsystems and components dedicated to CubeSats and PocketQubes already exists and are quite popular. Products are numerous and generally accessible from companies such as ISIS, GOMSpace, GAUSS SRL, Alba Orbital, etc. They provide flight proven platforms, subsystems and hardware. For example, a CubeSat developer in charge of providing a structure for its mission could opt for an in-house design, which requires to follow the already indicated steps of a) analyzing, b) designing and c) testing, or could just opt for buying an already-proven structure from one of the aforementioned providers. The costs and time are reduced when the second option is chosen. The same way, a PocketQube developer could opt to implement a set of predefined thermal measures according to the characteristics of its satellite without going though the entire process earlier described to achieve thermal control.

1.2.3. State of the art

Organizations such as the ECSS (European Cooperation for Space Standardization), among others, produced manuals containing standard recommendations for conducting thermal analysis and developing thermal designs for spacecraft. However, their aim is to provide thermal analysts and designers with practical guidelines to support high-quality thermal modeling, analysis and designs rather than a standard thermal design proposal itself.

By studying the software utilized for developing thermal models of a number of CubeSat missions it can be concluded that there is not a standard or preferred solution. ESATAN-TMS, Thermica, Thermal Desktop or ANSYS are reference software that several nanosatellite developers use but Matlab or Python tailored models seems to be gaining popularity among nanosatellite thermal analysts.

Willingness to develop thermal analysis software for small satellites is clear and initiatives are being proposed, although they are currently in early design phases. Regarding design, a paper on an algorithm for automatic optimization of a thermal design solution for nanosatellites based on coating patterns has been studied by Escobar [5]. Based on the conclussions of this report, a very simple but accurate thermal analysis software could be proposed.

In the field of standardized components for thermal subsystems, it is possible to find a variety of them in the market from numerous manufacturers which provide coatings, insulation materials, Kapton foil heaters and thermal straps among others. NASA provides a list of the most important suppliers of these components as well as their technology readiness level (TRL) [6].

Although these standard exists at component level, standardization at a subsystem level seems to be lack-

ing in the market. At the end of the day, although standard components are commonly used, the thermal design itself is made in a tailored way for each nanosatellite mission.

Thermal Control Subsystems
Literature regarding standardized thermal control subsystems is scarce, but a couple of concepts on this topic has been proposed. In this regard, the ITEMS (Integrated Thermal Energy Management System) was proposed by JPL in 2001 [7]. It consists of a series of thermal lines that connect the different thermally isolated subsystems, controlled by thermal switches, see figure 1.3. Excess heat produced by subsystems is transferred to other ones in need of thermal energy. In combination with variable emissivity radiators and heat storage devices that make uses of phase change materials (PCM) thermal control of any spacecraft in a wide range of environments is achieved.

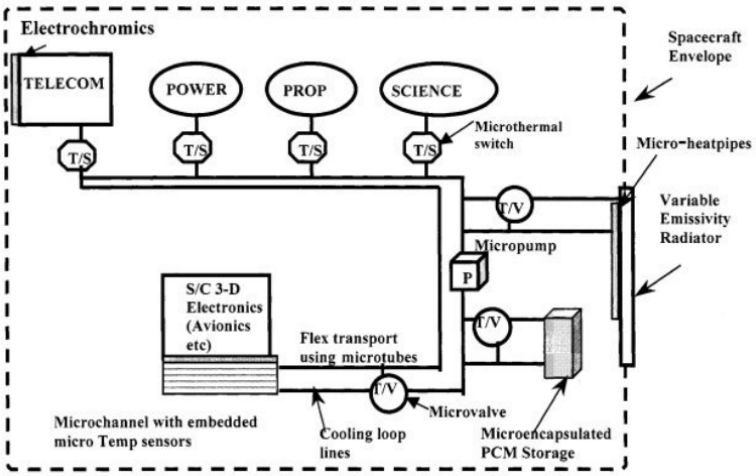

Figure 1.3: Schematic concept of the ITEMS standardized thermal control subsystem, extracted from [7].

However, such a subsystem seems to be highly complex, bulky, massive, power-consuming and, in conclusion, not suitable for pico- and nanosatellites. It assumes thermal isolation of the different components which is far from the reality of CubeSats and PocketQubes where subsystems are packed close together. The paper states the advantages of a system like this in terms of speeding up the design cycle and reducing costs.

Baturkin proposed in 2005 a thermal design approach for small spacecraft consisting of standardized buses where the payload has to be adapted to a predefined thermal environment [8]. Barton proposes a similar concept or modular thermal design for LEO spacecraft [9]. These proposal could actually be considered as a standardized thermal control subsystem although any record on their development or their implementation in nanosatellites has been found.

In conclusion, specific literature about standardized guidelines for thermal analysis for nanosatellites is scarce although some research work has been found. The level of application of these standard guidelines to nanosatellite missions seems to be limited as no recognized institution or publications proposing these guidelines have been found.

Standardized components for thermal control purposes are provided by numerous manufacturers and present high TRL. These components are extensively used in nanosatellite missions. At subsystem level, commercially available subsystems have not been found. Few concepts proposing standardized thermal control subsystems exists. Publications on the development or implementation of these concepts in actual nanosatellite missions have not been found.

1.3. Research framework

This research project is framed by the space systems engineering and spacecraft thermal control disciplines. The object under study is the relatively new category of satellites: PocketQubes. They are investigated under the point of view of thermal performance and control.

This research project is in line with the vision and projects under development at the Space Systems Engineering department of the Delft University of Technology. Being Delfi-PQ the first PocketQube mission in

development at the department and scheduled for launch in 2019, there was the need to perform a thermal analysis and design for it.

Rather than opting for a conventional tailored thermal design approach and given that the Delfi-PQ program aims to keep on developing and producing spacecraft on a yearly basis, it was decided to opt for a holistic approach in thermal engineering and start considering the possibility of a universal thermal analysis and design for the Delfi-PQ satellites.

This work was implemented into a master thesis project aiming to include not only the possible future Delfi-PQ satellites but extending the scope of the research to the whole PocketQube family looking for a more challenging and relevant research project.

1.4. Objectives

The ulterior goal of this research project is to contribute to make space platforms more accessible to the general public, decreasing its costs, development time and increasing their reliability. In order to achieve this, the following set of goals oriented the research.

- To provide the PocketQube community with validated results on the expectable temperatures these spacecraft will be subject to.
- To provide the PocketQube community with validated results on the expectable impact of design parameters on the thermal behavior of the spacecraft.
- To investigate the possibility of approaching thermal control from a general perspective and provide insight on whether or not and up to which extend this is an interesting approach to follow in future PocketQube developments.

1.4.1. Research questions

The main research question for this master thesis project, which once answered marks the completion of the research project is the following:

How standardized thermal analysis and design solutions could be applied to PocketQubes to ensure thermal control?

The proposed subquestions helping to find an answer to the main question and achieve the aforementioned goals are the following:

- Which are the expectable thermal behaviors and temperatures of PocketQubes in orbit?
- What are the main parameters that affect thermal control of small satellites and up to which extend could they be modified?
- How do these parameters impact the satellite temperatures?

1.5. Methodology

To extract valuable information on how design and environmental parameters impact the temperatures of PocketQubes, a sensitivity analysis is performed. This requires first to define a baseline or nominal case; where all the parameters to be studied are set to their nominal values. Then, the results extracted when varying the parameters can be compared to this baseline. The configuration of the Delfi-PQ satellite at the time when the study begun was chosen as a baseline for the research project.

Chapter 3 describes how the properties of the satellite have been determined and implemented into a finite element model based on ESATAN. Furthermore, temperature results for the nominal case are extracted which provide useful information on the expected temperature ranges and behavior of the satellite, which are used in later stages of the research.

Afterwards,some of the parameters that are expected to influence the most the temperatures of the satellite are analyzed, and boundary values are defined for them. By taking the Delfi-PQ as a baseline and varying

some of its design parameters within the determined ranges different variants (which could be considered even other similar PocketQubes) are defined.

Then, several cases are computed to extract temperature data from the Delfi-PQ thermal model, where each of these parameters under study is slightly modified. These variations on parameters are made one-at-a-time (only one parameter is altered for each case) in order to isolate the effect of the parameter on the temperature, allowing to establish correlations.

Considerable amounts of temperature data are produced from this cases and processed by using a Matlab tool in order to extract meaningful quantitative information. Chapter 4 reflects this process.

In a final step, all these processed data is compared and reviewed to give a general idea on which are the most important parameters to take into consideration for thermal control of PocketQubes. This information is contained in Chapter 5. Conclusions are drawn and further steps proposed in Chapter 6.

1.6. Outcome

The outcome of this study could be summarize in the following points:

- A survey study of the properties and design parameters of PocketQubes.
- Data on the expected thermal behavior and temperatures of common PocketQubes.
- A quantitative and qualitative study on how design and environmental parameters affect the thermal behavior of picosatellites.
- Recommendations on how to implement thermal control for PocketQubes from a general perspective.

The data and conclusions produced in this research study aim to increase the knowledge of thermal behavior of PocketQubes, hopefully facilitating future developments of these platforms and striving to improve reliability and reduce costs and development time.

The conclusions of this research project were presented by the author at the European Space Thermal Engineering Workshop organized by the European Space Agency in Noordwijk, The Netherlands, in October 2018.

2

Characterization of PocketQubes

The first step into approaching the research problem is to explore the properties which define the PocketQubes. The methodology is based in looking into literature and requesting information to the institutions and companies currently developing picosatellite platforms.

Let's start by reviewing the current missions set to be developed in the coming years. Table 2.1 enlists the missions planned according to [2]. For the moment this lists does not surpass 30 missions but might experience a similar growth to the one that CubeSats had in previous years.

Name	Type	Organisation	Mission	Status
WREN	1p	Stadoko UG	Tech. demonstrator	Inactive
QubeScout-S1	2.5p	Maryland Univ.	Unknown	Inactive
Eagle-1	2.5p	Morehead & Sonoma Univ.	Education	Inactive
Eagle-2	1.5p	Amateur Group	Unknown	Decayed
ArduOrbiter-1	1p	Reid Technologies	Unknown	Unknown
Arduiqube	1p	GAUSS	STEM	Unknown
OZQube-1	1p	Picosat Systems	Earth observation	In development
SMOG-1	1p	Budapest Univ. / GAUSS	Radiation measurement	In development
FossaSat-1	1p	FOSSA systems	Amateur	In development
TFTQube	1p	The Flame Trench	Amateur	In development
Discovery 1A	1p	Beyond Earth	Earth observation	In development
UOMBSat1	1p	Malta & Birmingham Univ.	Tech. demonstrator	In development
Exploration I	1p	British Columbia IT	Structural tests	In development
APRS PQ	1p	Chiao-Tung Univ.	Ground tracking	In development
TRSI (ADS-B Sat)	1p	Union Aerospace	Picking ADS-B packets	In development
Nepal-PQ1	1p	Orion Space	Education	In development
SMOG-P	1p	BME	Spectrum monitoring	In development
TBA	1p	Croatian Makers	STEM	In development
UBO	1p	Sat. Applications Catapult	Outreach	In development
Myansat-1	1p	Independant	LEO-GEO relay test	In development
Unicorn-1	2p	Alba Orbital / GAUSS	Structural test	In development
ATL-1	2p	Advanced Technology Laser	Isolation material test	In development
EASAT-2	2p	AMSAT EA	Amateur Mission	In development
SATLLA	2p	Ariel University	Laser comms. test	In development
Delfi-PQ	3p	Delft University of Tech.	Tech. demonstrator	In development
Unicorn-2A	3p	Alba Orbital	Tech. demonstrator	In development

Table 2.1: Announced PocketQube missions, retrieved from [2] in 2018.

For the moment only 4 PocketQubes have been deployed, all from the UniSat-5 satellite carrying the MRFOD (Morehead-Rome Femtosatellites Orbital Deployer). It was the case of the Eagle I and Eagle II devel-

oped by the Morehead State University in the USA; Wren developed by StaDoKo UG in Aachen, Germany and QubeScout-S1, developed by the University of Maryland. All of them are currently decayed or inactive.

The geometry of a satellite has an impact on its temperature behavior as it plays an important role when determining 1) the amount of power the satellite radiates to space via its external surface area 2) the amount of power the satellite receives from external sources such as the Sun or Earth and 3) radiative couplings among subsets of the satellite (for example the energy exchanged between deployable panels and the main body of the satellite).

PocketQubes follow the geometry guidelines set by Bob Twiggs in 2009 that establishes the basic unit for PocketQubes as a 5 cm cube [10]. These units are referred as 'p-units' and could be assembled together to form larger PocketQubes (2p, 3p, etc.). Of the total number of PocketQubes listed in Table 2.1, two thirds fall under the 1p category, being these the more popular ones for the moment. Some examples of 1p PocketQubes are illustrated in Figure 2.1. Very recently, a standard for PocketQubes has been developed, lead by Alba Orbital, the Delft University of Technology and Gauss SRL which further defines their geometrical constraints [11].

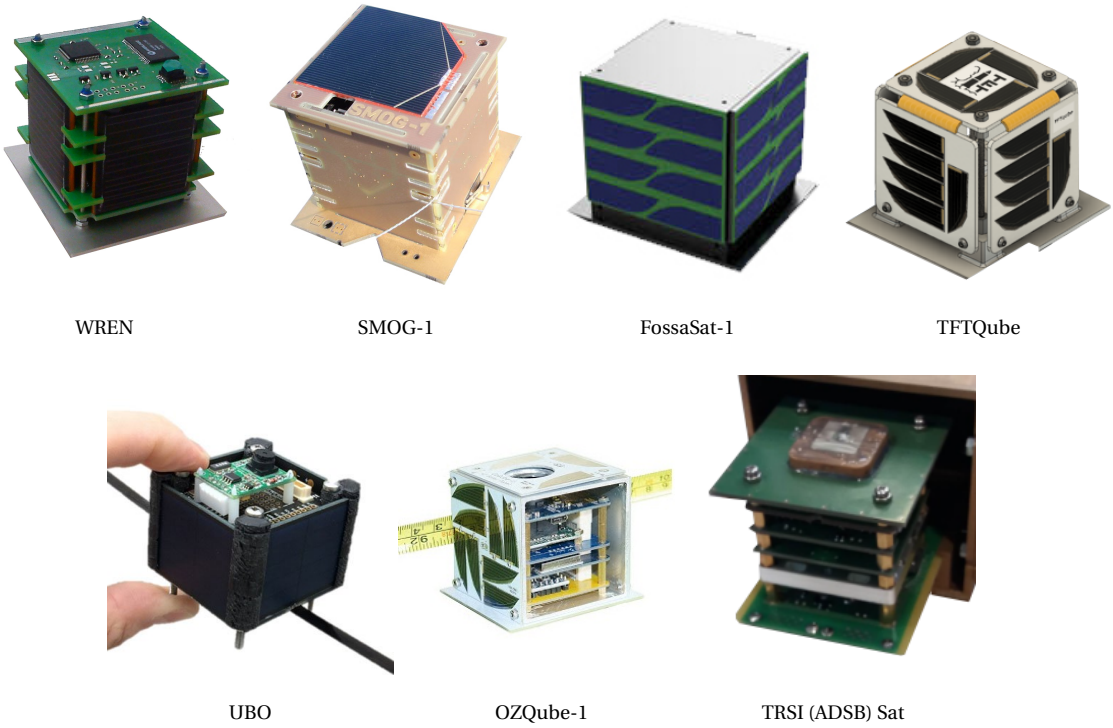

Figure 2.1: Examples of 1p PocketQubes: size and external configuration.

Gauss SRL developed the first (and up to the moment only) deployer carrying PocketQubes to orbit and Alba Orbital is developing a brand new one, the AlbaPOD which will accommodate 1p, 1.5p, 2p and 3p PocketQubes including optional deployables and/or antennas. Unicorn 2-A, Delfi-PQ, ATL-1, TRSI Sat, Discovery, SMOG-P and TBA are expected to fly in 2019 aboard the AlbaPOD. Therefore, it is expected that the aforementioned standard sets the geometrical constrains for all future PocketQubes. The most important guidelines included in the standard could be summarized as follows:

- The 1p unit picosatellites should be contained in a 50 mm cube.
- A stand-off distance of 7 mm surrounding the cube si available for attaching external components such as deployable antennas or solar panels.
- When the satellite is comprised of more than 1p, the stand-off distance between units could be incorporated into the internal volume of the satellite (see Figure 2.2).
- A baseplate exceeding in 4 to 7 mm the dimensions of the PocketQube body is used as sliding plate during the deployment of the spacecraft. This is clearly visible in Figures 2.1 and 2.5.

Figure 2.2 illustrates how in the process of integration of PocketQubes bigger than 1p, the reserved volume dedicated to deployables is absorbed, increasing the total length of the spacecraft by 2×7 mm in the case of the 2p and 4×7 mm in the case of the 3p.

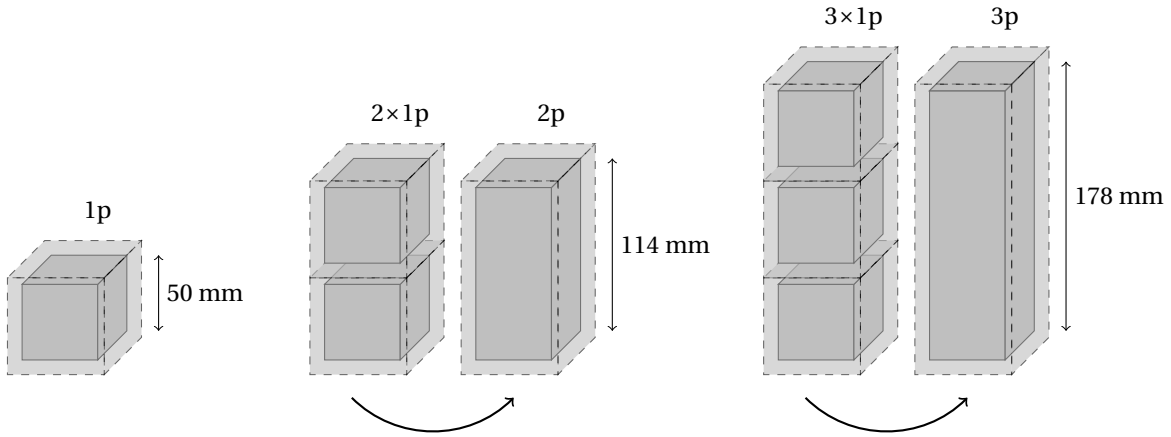

Figure 2.2: 1p, 2p and 3p PocketQube dimensions including reserved volume for deployables.

Deployable solar panels are expected to be incorporated in some spacecraft such as the Unicorn-1 and Unicorn-2 (see figure 2.5) .They are a couple of millimeters smaller both in length and width than the structure of the PocketQube. Figure 2.3 shows the dimensions and configuration of these possible deployables.

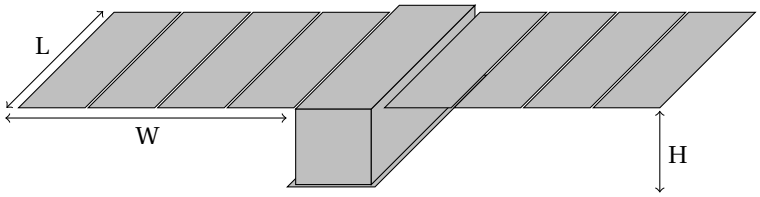

Figure 2.3: Quadruple deployable solar panel satellite based on the design of the Unicorn-2 PocketQube.

As well, the amount of external surface covered by solar cells or other devices (optical instruments, radiators, antennas) have an impact on the thermal behavior of the satellite. And not only the external geometry but the internal configuration of the PocketQubes might play an impact on how the temperatures of the satellite and different components within it. A common internal configuration for PocketQubes such as the Delfi-PQ is presented in figure 2.4.

Figure 2.4: External and internal configuration of a common PocketQube.

Besides geometry and internal configuration, design parameters such as the thermal conductive properties of the materials, thermal capacity, conductive couplings among subsets of the satellite, optical properties of its surfaces, internal dissipation, power management and pointing have an impact on the temperatures of the satellite as well. Not to forget the environmental inputs such as the solar power, Albedo and OLR, outgoing long wave radiation coming out from planet Earth in form of IR radiation.

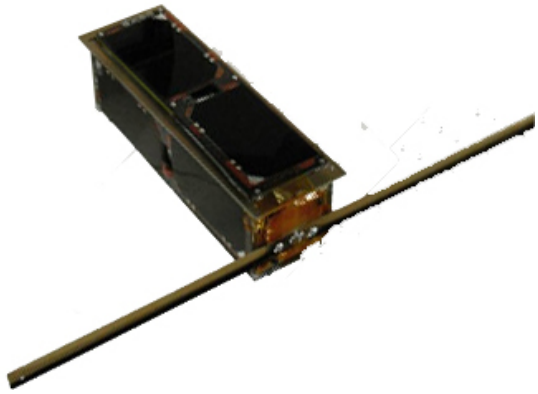

QubeScout-S1

Eagle-1

Eagle-2

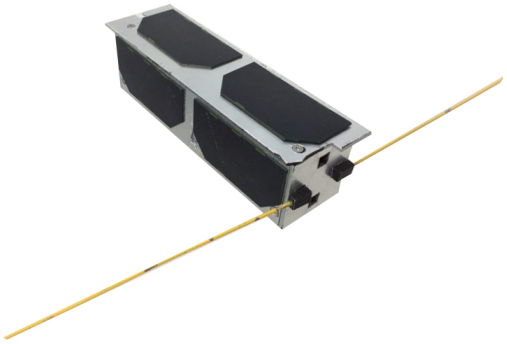

Delfi-PQ

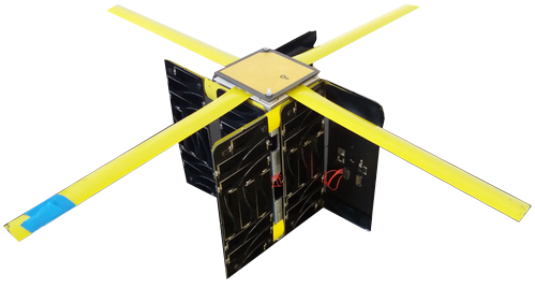

Unicorn-1

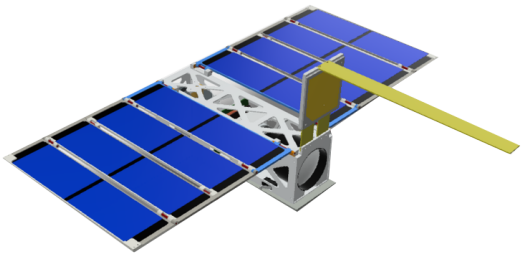

Unicorn-2

Figure 2.5: Examples of PocketQubes larger than 1p: size and external configuration.

3

Delfi-PQ Thermal Analysis

The Delfi-PQ PocketQube is chosen as case study for this research project. Its nominal configuration is used as a baseline to later investigate the sensitivity of temperature to a number of design and environmental parameters. Therefore, accurately characterizing the properties of the satellite and developing a thermal model serves as the foundation of this study. This model is modified and solved recurrently to obtain the results presented in Chapter 4.

In the following sections, the relevant elements for the model from a thermal point of view are described, from the geometry to the internal dissipation, specifying its values. Furthermore nominal, hot and cold cases for the satellite are defined and solved and the results presented and analyzed. This gives an overview on the expectable thermal behavior of the satellite under nominal and extreme conditions and provides useful input when compared to the temperature results extracted from the sensitivity analysis presented in chapter 4. A section on validation of the model is presented as well.

Model Definition

The model is implemented and solved with ESATAN TMS, being this an industry standard. The modeling process aims to simplify the complex reality of the satellite while retaining its more fundamental characteristics which influence its thermal behavior. It is essentially comprised of a number of parameters that could be classified in the categories itemized below. How well each one of the parameters is chosen will influence the accuracy of the results obtained. Therefore, the most realistic values possible have been chosen, based on literature survey and estimations. The exact procedure is detailed in the following sections.

1. Geometry
2. Materials
3. Thermal Capacity
4. Optical sets
5. Linear couplings
6. Thermal environment
7. Internal dissipation
8. Definition of cases
9. Solution routines

First of all, the physical dimensions of the satellite and its components are imputed in the model by using a combination of simple geometries such as surfaces and volumes. Secondly, the physical properties of the subsets of the satellites are inputed in the model. This is commonly done by defining 'materials' and 'optical sets'. A material contains information about conductivity, density and thermal capacity. It can be defined

as isotropic or orthotropic. An 'optical set' contains information about emissivity and absorptivity. This properties are assigned to the geometries of the satellite model.

The next step consists in dividing each one of the geometries into a number of smaller parts named 'elements'. These elements are then transformed into 'nodes', non-geometrical entities that retain the properties of the mother geometry and represents it. This process is a fundamental part of simplifying the problem: instead of solving the temperature in continuous surfaces or volumes, the problem is reduced to solving the temperature in a discrete number of points or 'nodes'. The number of nodes each surface is divided into has been chosen out of a trade-off between level of detail of the results and computation time. An idea of the size and number of nodes in the model can be inferred from Figures 3.1 and 3.2.

These nodes are then connected to each other via thermal couplings which could be manually inputed or automatically computed by the software. Thermal couplings determine how energy is exchanged between nodes. There are two types of thermal couplings in this problem: conductive and radiative. The first one is related to energy exchange via elements directly in contact (which is linear with the temperature difference between the two nodes). The second one is related to energy exchange via black-body radiation (proportional to temperature to the fourth power).

After that, boundary conditions are set. For example, the dissipation of the equipment on board the satellite is modeled by setting a thermal input at selected nodes where dissipating components are placed. To finish, the thermal cases are defined (this is, the orbital parameters, attitude of the satellite, environmental constants, which will define the power inputs from the Sun and Earth. The solution routines, or which methods the software uses to solve the problem and the type of solution required is specified at this point as well.

3.1. Geometry

The satellite model geometry represents its physical configuration by using simple elements such as 1) surfaces, 2) volumes and 3) non-geometrical thermal nodes (NGTM). The definition of the geometry is used to estimate the radiative couplings among all the nodes of the satellites and space as well as other properties such as the thermal capacity of each node. The geometries of this model have been divided into six categories named: 'battery', 'boards', 'components', 'panels', 'solar' and 'structure'.

- The 'battery' category is comprised of 2 cylindrical volumes representing the 2 electrical power cells and 5 rectangles conforming the battery plastic case.
- The 'boards' category is comprised of 9 squared shells representing the internal configuration of the satellite. These surfaces correspond to the EPS (x2), ADCS, OBDH, telemetry (x2) and spare boards (x3).
- The 'components' category is comprised, for the moment, of 4 cylindrical shells representing the 4 antennas and 3 nodes representing the components of the ADCS, EPS and antenna boards.
- The 'panels' category is comprised of 6 subgroups, representing each one of the external structural panels of the satellite. Each subgroup contains up to 50 geometries in the form of triangular, quadrilateral and rectangular shells.
- The 'structure' category is comprised of 28 NGTN representing the 3 standoffs (gray nodes), and the 4 structural rods with their spacers (blue nodes).
- The 'solar' category is comprised of 16 surfaces, representing the solar cells. There are 8 solar cells in total, two per side panel. Each one has been recreated by using two simple geometries: a rectangle and a trapezoid.

The dimensions of the aforementioned surfaces as well as their disposition with respect to the coordinate axis of the model have been defined to accurately represent the satellite, according to the most recent specifications available (see Figures 3.1 and 3.2). Each one of the geometries are assigned three properties: a material, an optical set, and a thickness. In the case of the NGTN only one property is assigned, its thermal capacity. The properties associated to the different geometries are listed in table A.1 and A.2. The thickness of the surfaces is presented in Table A.3 and the thermal capacity of the NGTN in Table A.4. All this data can be found in Appendix A.

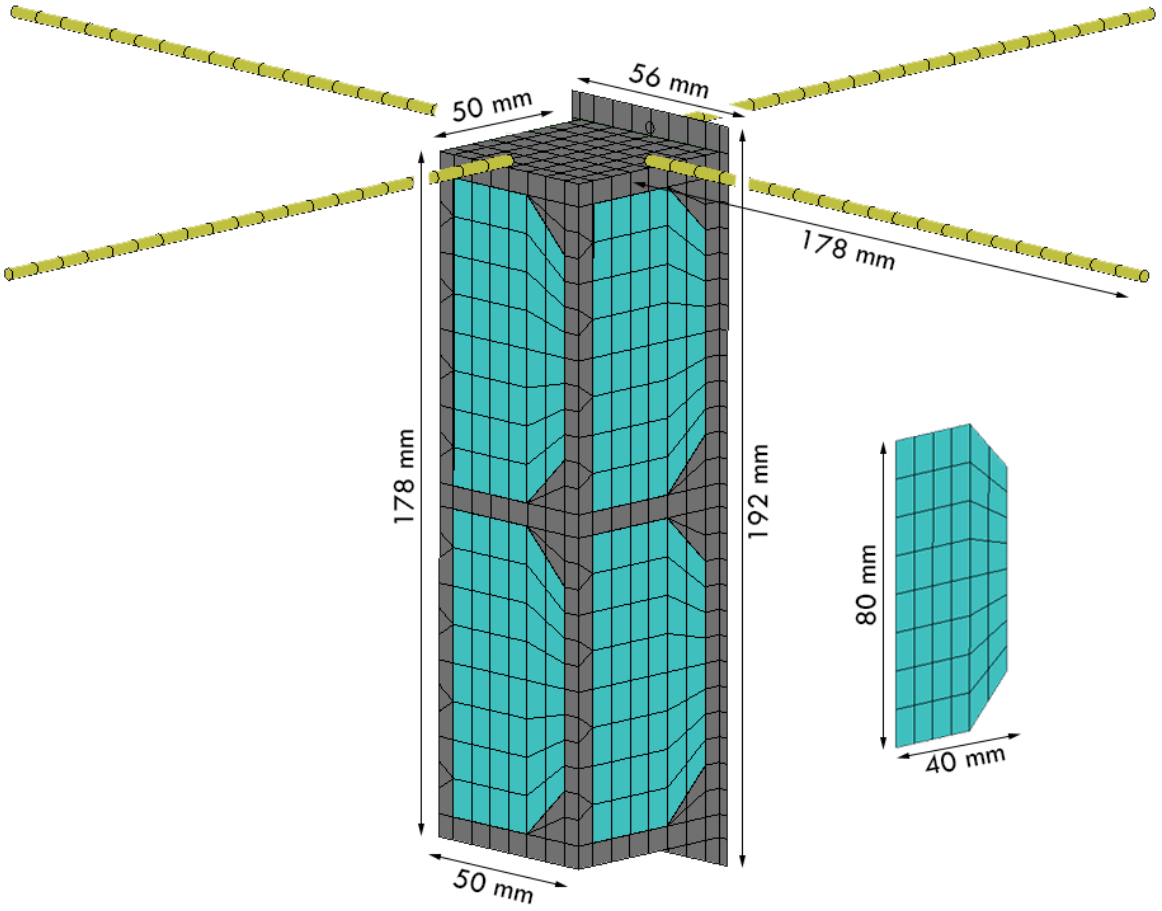

Figure 3.1: Finite element model representing the satellite external geometry.

Elements such as standoffs, spacers, rods, washers, nuts and bolts have not been assigned a geometry. Because of their limited surface area, they do not play a significant role in radiative heat exchange. Nonetheless, their contribution to the total heat capacity of the satellite has been taken into account by implementing them as NGTN. This is a common approach used before in thermal analysis of CubeSats. C. Macco, in a master thesis regarding thermal design of the Delfi-n3Xt, omits the geometry of similar elements in the thermal model providing grounded reasons for doing so (see [12], section 5.2.1, page 33). Further results obtained in this research project validate this assumption. These elements have an influence in thermal conductivity which has been taken into account by using node-to-node couplings. This process is explained in detail further ahead in section 3.4 and illustrated in Figure 3.7.

Components such as ADCS equipment, which its specific geometry and disposition was not specified at the moment, have been represented with NGTN to take into account their contribution to the total heat capacity of the satellite.

Some of the surfaces have been defined as 'double sided' meaning that for each node created on one side of the surface another one is created on the other side, coupled by the corresponding thermal resistance. This allows to compute temperature gradients through thin surfaces, which is important in orthotropic materials with low though-plane conductivity, like the printed circuit boards. The values provided in Table A.3 are in accordance with the specifications of the manufacturers and the last information available at the time regarding the design of the satellite. When creating a 'double sided' surface, the modeling software divides it in two subsurfaces, with independent properties. The thickness of each subsurface has to be inputed separately. Therefore, a value of half of the real thickness of the surface is used (see Table A.3, Appendix A).

The side panels have been modeled by using a large number of triangular, quadrilateral and rectangular shapes, rather than a simple rectangle, in order to properly accommodate the geometry of the solar cells, which are resting on top of them. This is meant to produce more accurate and realistic results and is a recommended guideline based on experience in thermal engineering projects. Figure 3.3 presents the computed

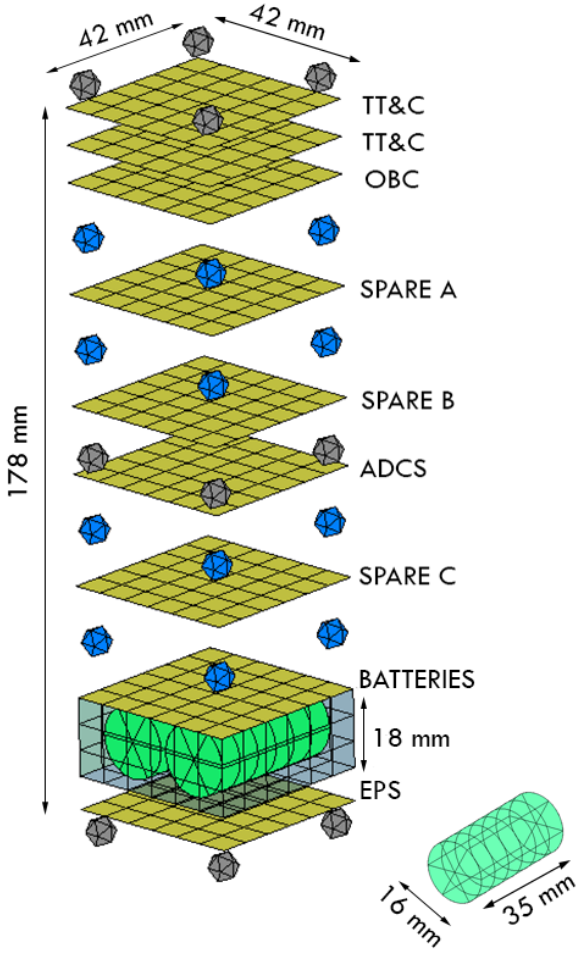

Figure 3.2: Finite element model representing the satellite internal geometry.

incoming power from the Sun at one of the external panels, showing how a refined mesh in accordance with the geometry of the solar cells provides more accurate results.

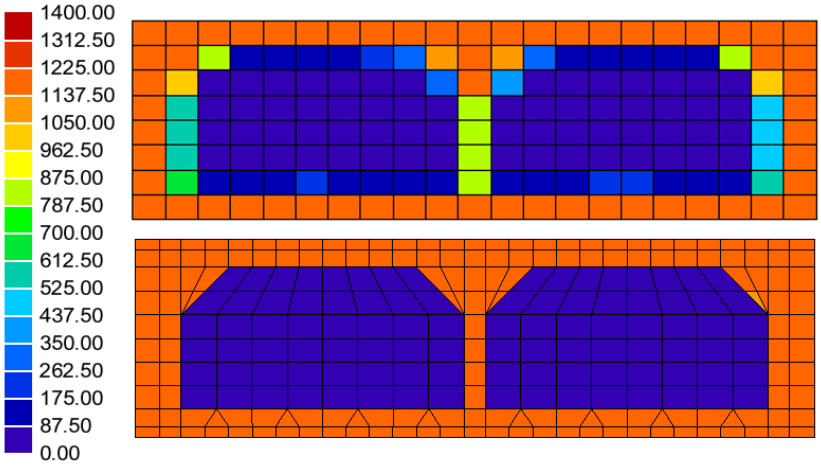

Figure 3.3: Computed solar input [W/m^2] for simple rectangular geometry (top) and refined mesh (bottom) of solar cells of the Delfi-PQ.

3.2. Materials

Five materials are defined: 'antenna', 'battery', 'cell', 'pcb' and 'plastic'; for which a total of three properties are specified, being those their density (see table A.5), specific heat (see table A.6) and thermal conductivity (see table A.7). These materials are assigned to the geometries according to table A.1 which can be found in Appendix A. In the following paragraphs an investigation on how the properties of these materials are defined is presented.

Antennae

The material of the antennae is known to be brass, which density is 8730 kg/m^3, a specific heat of 380 J/kg K and a thermal conductivity of 109 W/mK.

Battery

The battery to be mounted in the satellite is comprised of two identical 'AW 16340 ICR123 750mAh' cells which specifications can be extracted from [13]. According to it, each cell weights 18.3 grams, has a diameter of 16.6 mm and a length of 35 mm. Taken into account that they are manufactured in a cylindrical format, its volume and therefore its density can be estimated in 2416 kg/m^3. This will be used a the nominal value for the model. A study carried out by H. Maleki investigating thermal properties of lithium-ion batteries, indicates that their density lies somewhere in between 2680 and 2780 kg/m^3 (see [14], Table IV, page 952). This value is close to the computed one, giving confidence to the estimation. M. Muratori, on a paper about thermal modeling of cylindrical lithium-ion batteries uses a value for the cell density of 1824 kg/m^3 (see [15], Table I, page 3). This value is considered to differ greatly from the battery used in the DPQ. Nevertheless, in future versions of the satellite different batteries could be chosen with values closer to the one presented by Muratori. Therefore it has been considered as a possible lower boundary for battery density.

Regarding the specific heat, Maleki provides experimental data with values ranging from 960 to 1040 J/kg K (see [14], Table III, page 950). Muratori uses a value of 825 J/kg K (see [15], Table I, page 3). T. van Boxtel carries out an experiment to determine the thermal capacity of the lithium-ion batteries for the DelFFi satellite, presenting a value of 55 J/K (see [16], equation 5.7, page 71), although the researcher later uses a value of 39.06 J/K per cell in the thermal model (see [16], table 6.3, page 78). C. Macco, proposing a design for the Delfi-n3Xt nanosatellite, uses a value of 930 J/kg K (see [12] Section 5.5.3, page 56) which, taking into account that the batteries weight 46 grams, yields a thermal capacity of 42.8 J / K per battery, a very close value to the one used by Boxtel. Due to the similarity in the values presented by Macco, Boxtel and Maleki, they have been chosen as nominal.

Maleki estimates the cross-plane conductivity of these batteries to be within 3.39 and 3.40 W/mK and the in-plane conductivity between 20.06 and 28.05 W/mK (see [14], Table IV, page 952). Muratori uses a value for conductivity of 0.488 W/mK (see [15], Table I, page 3). The same researcher in an study of thermal characterization of lithium-ion batteries, pouch configuration, provides values of 0.70 W/ m K for cross-plane conductivity (see [17], Table 5.4, page 111) and values of 73.98 W / m K for in-plane conductivity, (see [17], Table 5.5, page 112). Because the battery modeled by Maleki seems to better represent the one actually used, the values he provides have been chosen as nominal.

Solar cells

The solar cells to be used are the 30% Triple Junction GaAs solar cells 3G30C advanced 80 µm from Azur Space, which specifications can be checked in the data sheet [18]. A density value of 50 mg/cm^2, a cell surface area of 30.18 cm^2 and a thickness of 80 micrometers is provided. This yields a mass of 1.509 grams per cell, a volume of 2.414×10^{-7} m^3 and therefore a density of 6520 kg/m^3, which will be used as a nominal value for the model. The solar cells are mainly comprised of Gallium Arsenide which have a density of 5318 kg/m^3. From previous satellite thermal studies carried at the Delft University of Technology, similar values are found: M. Graziosi uses a value of 5316 kg/m^3 for the density of the solar cells (see [19], Table 9.7, page 56).

Regarding the specific heat, gallium arsenide, the reference material, has a value of 350 J/ kg K. M. Graziosi uses a value of 325 J/kg K (see [19], Table 9.7, page 56), Macco a value of 493 J/ kg K (see [12], Table 5-3, page 50) and Boxtel refers to the value used by Macco. L. Jaques, in his master thesis proposing the thermal design of the Oufti-1 nanosatellite, uses a value of 700 J / kg K for thermal conductivity (see [20] section 4.3.2, page 47). The value presented by Macco has been considered the most accurate and applicable to this model and therefore it has been chosen as nominal.

Gallium Arsenide has a thermal conductivity value of 55 W/m K. Graziosi uses a value of 50 W/m K (see [19], Table 9.7, page 56), Macco a value of 56.7 W/m K (see [12], Table 5-3, page 50) and Boxtel refers to the

value used by Macco. Jaques uses a value of 100 W / m K for thermal conductivity (see [20] section 4.3.2, page 47). The value presented by Macco seems to be the more reasonable one and therefore it has been chosen as nominal.

Printed Circuit Boards
Printed circuit boards are associated with the 'pcb' material. They are mainly comprised of a substrate of FR4 which is a type of glass-epoxy with a several layers of embedded copper. For nanosatellite applications, the number of layers usually range from 2 to 6, according to the specification of the DPQ and a study carried out on CubeSat thermal modeling by L. Pasqualetto [21]. A typical PCB has a thickness of about 1.6 mm of which each layer of copper usually represents 35 micrometers. With this information, and given that FR4 has a density of 1850 kg/m^3 and copper of 8960 kg/m^3, the density of PCBs can be estimated to be between 2161 (two Cu layers) and 2783 kg/m^3 (six Cu layers). Graziosi uses a 50/50 FR-4/Cu proportion for the model of PCBs (see [19], section 9.2.1, page 53), which is far from reality, therefore the value he presented will be disregarded.

Because PCBs are not a material itself but rather a product comprised of layers of copper and FR-4, some insight on its thermal properties is required to model it properly. K. Azar in a experimental investigation of thermal conductivity of printed wiring boards (see [22]), comes to the following conclusions:

- There is negligible thermal resistance in the boundary epoxy-copper (perfectly thermally coupled).
- The heat is mainly carried by the copper within the PCB.
- There is no correlation between the conductivity and the configuration of copper layers (circuitry, distribution of the layers).
- There is a correlation between the relative thickness of copper in the PCB and the in-plane conductivity.
- There is little correlation between the relative thickness of copper and the through-plane conductivity, which is two orders in magnitude lower than the in-plane conductivity.

Based on the equations proposed by Azar (see [22], equations 8 and 10), which are presented in this document with equation numbers 3.1 and 3.2 respectively, and taking into account that 2 layers of copper yield a relative thickness (Z_{Cu}/Z) of 4.38% and six layers of 13.13%, the ranges for in-plane conductivity of copper should be between 17.7 and 51.4 W/m K and for through-plane conductivity between 0.32 and 0.36 W/m K. Graziosi uses a value of 200 W/ m K (see [19], Table 9.1, page 54), which is considered to be far from reality. Pasqualetto reports values of 37.2, 40.8, and 55 W/ m K been used for in-plane conductivity of Delfi-N3Xt, DelFFI and a generic ESA CubeSats (see [21] Table 3, page 20). This values are in accordance with the previously calculated one and correspond to 4-copper-layer boards. In the same report it is stated that a value of 0.3 W/ m K have been used for the through-conductivity of PCBs on satellite thermal models, which is as well in agreement with the previously calculated one (see [21] Table 5, page 22). The value of the through conductivity might be increased if thermal vias are added to the design of the PCB.

$$k_{\text{in-plane}}[\text{W/mK}] = 385\frac{Z_{Cu}}{Z} + 0.87 \tag{3.1}$$

$$k_{\text{through-plane}}[\text{W/mK}] = \left[3.23\left(1 - \frac{Z_{Cu}}{Z}\right) + 0.0026\frac{Z_{Cu}}{Z}\right]^{-1} \tag{3.2}$$

Considering that the copper has a thermal capacity of 385 J/kg K and FR-4 of 600 J/kg K, the averaged thermal capacity is 589 J/kg K for 2 layers of Cu and 567 J/kg K for 6 layers of Cu. If the electronic components soldered to the board are included in the computations, these values might change. Graziosi uses a value of 790 J/kg K (see [19], Table 9.1, page 54). Macco presents values for mass and thermal capacitance of the PCBS of the Delfi-n3Xt (see [12], table 5-6, page 57). From them the specific heat of the PCBs can be computed, which are in the range of 752 J/kg K to 1440 J/kg K, with an average of 1127 J/kg K. He includes in the estimation of the heat capacitance of the PCBs its electronic components. Boxtel, reviewing the data presented by Macco concludes that he is overestimating the specific heat of the boards. He carries out tests to determine the thermal capacitance of the boards and comes up with values of 47 J/K and 68 J/K, values which are in accordance with his more accurate computations (see [16], Table 5.6, page 60). The boards of the DelFFI seem to have a mass ranging 70 to 90 grams, and therefore its thermal capacity should be in the range of 587 J/kg K to 850 J/kg K. Giving this information, a nominal value of 567 J/kg K has been chosen as nominal.

Plastic elements
The physical properties for the 'plastic' are extracted straight forward by taking a look at the data sheet of a polycarbonate product.

Based on the most recent version of the mass budget for the Delfi-PQ, the ADCS components should have a mass of 22 grams approximately. Boxtel presents a mass for the ADCS of the DelFFi of 700 grams (see [16], section 2.2.8, page 11) and a heat capacity of 525 J/K (see [16], Table 4.3, page 34). This yields a specific heat for the subsystem of around 750 J/kg K. Assuming the components of the DPQ ADCS are similar and therefore have similar thermal properties, a heat capacity of 17 J/K will correspond to this subsystem. Flecht uses a value for the specific heat of magnetorquers of 100 J/kg K assuming they are mainly made of copper (see [23], Table 4.8, page 24), which seems erroneous as the copper has a thermal capacity of 385 J/kg K. If this value is used for the DPQ model, it yields a thermal capacity of 8 J/K.

The EPS components, without including the batteries, are expected to represent a mass of around 15 grams. Macco presents values for the components of the EPS of 70 J/K, with masses of 59 grams (see [12], Table 5-6, page 57), yielding a specific heat of 1186 J/kg K. When this value is used, a value of 18 J/K corresponds to the EPS components and will be used as nominal. Graziosi gives the power amplifiers a value between 700 and 880 J/kg K (see [19] Table 9.9, page 57) which, if used for the DPQ, translates into a thermal capacity between 10 and 13 J/K. The components of the bottom antenna board are expected to sum up to 15 grams. Its composition is considered to be similar to the EPS components and so the same values are used.

Fix elements
The rods and the spacers have been considered together. It has been decided to distribute their thermal capacity in 16 NGTN arranged in groups of 4, at 4 different heights along the Z axis of the satellite (see figure 3.7). The rods are manufactured in steel and have a diameter of 2.5 mm. The spacers are hollow cylinders with a inner diameter of 2.7 mm and external diameter of 4.5 mm. Assuming that there are four sets of rod/spacers with a length of approximately 178 mm, the total volume occupied by the rods is 8.738×10^{-7} (thread not considered) and by the spacers is 1.812×10^{-6}. Considering the spacers are manufactured in aluminum and the rods in stainless steel, which have a density of 2700 and 7700 kg/m^3 respectively, the total mass should reach 12 grams. The current best estimates give masses for just the spacers of 10 grams, which is considered to be an overestimation. The specific heat of aluminum is 897 J/kg K and the one of stainless steel is 502 J/kg K, which yields a total value of thermal capacity for the rods and spacers of 8 J/K. As there are 16 NGTN representing the rods and spacers a thermal capacity of 0.5 J/K will be assigned to each of them.

For the standoffs, it has been assumed that they are manufactured in aluminum 6060 which has a density of 2700 k/m^3 and a specific heat of 897 J/kg K. The standoffs have been modeled as 7 mm sided cubes. Therefore their volume is estimated in 3.430×10^{-7}, its mass in 1 gram and its thermal capacity in 0.8 J/K.

3.2.1. Thermal time constant

Once the thermal capacity of the elements of the satellite has been estimated, the thermal time constant could be computed. This is important as it affects the transient behavior of the satellite. Determining the value of the thermal time constant gives an idea on how quick temperatures change in the satellite when subjected to different environment inputs or internal loads. The total weight of the antennae of the satellites is estimated in 24 grams, so 6 grams are assigned to each antenna. Flecht provides a value for the specific heat of the antennae, assuming they are made out of aramid, of 1420 J/kg K. Based on this information, each DPQ antenna might have a thermal capacity of around 9 J/K.

The masses and thermal capacities of each component of the satellite represented in the model are estimated (see Tables A.8, A.9, A.10) and summed up. The total mass of the model seems to cover 93% of the total mass currently estimated in the mass budget. A specific heat of 290 J/K for the satellite is estimated. The total capacitance of 3U Cubesats such as the DelFFI is estimated to be 2934 J/K (see [16], section 4.1.3, page 34). This is 10 times less thermal capacity. This value seems to be realistic. Considering that a 3U PoquetQube has 8 times less volume than a 3U CubeSat, if considered that both are comprised of more or less the same components, the heat capacity should around 8 times less. The value computed in this example is lower for the reason that the satellite modeled carries no payloads in contrast with the DelFFi which was fully loaded. The satellite model estimates a mass for the DPQ of around 400 grams while the maximum (satellite fully loaded) should be around 750 grams. Scaling up the thermal capacitance assuming the same specific heat, from the current model to the fully loaded satellite yields a hypothetical thermal capacitance of 544 J/K. That's 5.3 times less the thermal capacity of the DelFFi. In the case of the Delfi n-3Xt, a heat capacity of 3457 J/K is estimated by Macco (see [12], section 6.1.1, page 66). This is 12 times more than the current DPQ and

6.3 times more than the hypothetical fully loaded DPQ.

Based on the Stephan-Boltzmann law and the specific heat equation, the temperatures variations in time for satellites are in general governed by a exponential equation of the kind $e^{-t/\tau}$ being t the time and τ the so called thermal time constant. The higher the thermal constant the slower the reaction of the temperature of the system to external fluxes. The thermal constant can be computed, according to [24], section 2.1, page 10, in the two different ways presented in equations 3.3 and 3.4. The total mass of the system is given by M, C_p represent the heat capacity of the satellite, T_0 the average temperature in orbit, Q_0 the average thermal flux, A the external surface area of the satellite, ε the emissivity of the external surfaces and σ the Stephan-Boltzmann constant.

The thermal time constant seems to be about 9 minutes, 8 times lower than the ones of the DelFFI and Delfi-n3Xt.

$$\tau = \frac{M \cdot C_p \cdot T_0}{4 \cdot Q_0} = \frac{0.4\ \text{kg} \cdot 290\ \text{J/K} \cdot 293\ \text{K}}{4 \cdot 15\ \text{W}} = 566\ \text{s} \approx 9\ \text{min}. \tag{3.3}$$

$$\tau = \frac{M \cdot C_p}{4 \cdot A \cdot \varepsilon \cdot \sigma \cdot T_0^3} = \frac{0.4\ \text{kg} \cdot 290\ \text{J/K}}{4 \cdot 0.04\ \text{m}^2 \cdot 0.9 \cdot 5.67 \times 10^{-8}\ \text{W/m}^2\text{K}^4 \cdot (293\ \text{K})^3} = 565\ \text{s} \approx 9\ \text{min}. \tag{3.4}$$

3.3. Optical sets

Optical sets are implemented in the model containing absorptivity and emissivity values. In this model 10 optical sets are defined: 'antenna', 'battery', 'board_top', 'board_bottom', 'solar_cell_int', 'solar_cell_ext', 'panels_ext', 'panels_int', 'plastic_int' and 'plastic_ext'. Optical sets are required for calculating radiative couplings among nodes. A description of how the optical properties are estimated for the model is described in the following paragraphs.

Antennae

The antennae are known to be gold-coated, with an absorptivity of 0.25 and an emissivity of 0.02.

Battery

The optical properties of the battery are not accurately known, but can be estimated taking into account that is wrapped in a black plastic cover. Optical properties of black plastics don't vary notably depending on its composition. As an example, polyethylene black plastic has values of 0.92 for emissivity. Jaques uses a value of 0.80 for emissivity of plastic wrapped batteries (see [20] Table 4.1, page 42). A paper on Optical Properties of Nanosatellite Hardware by NASA (see [25], section 5) estimates the emittance of a battery with plastic wrapping to be around 0.85. This value has been chosen as nominal. If required, the batteries could be covered with a low emittance wrap, to prevent them to loose heat, such as aluminized kapton, which has an emissivity value of 0.05 (see [26] Table 11.4). The absorptivity value of the battery does not play a role as they are not subject to solar radiation or albedo.

Shear panels and PCBs

Regarding the boards and the panels, two optical sets have been defined, one for the top/exterior and one for the bottom/interior parts. In principle, equal optical properties are assigned to both but it has been implemented in a way that makes it easier to change the optical properties of each of the sides independently if required. Boards and panels are both manufactured with a gold-coated, black paint finish for the dpq-2. Macco uses a value of emissivity of 0.89 and absorptivity of 0.90 for the PCBs (see [12] Table 5.1, page 36). Jaques uses a value of 0.91 for emissivity of PCB (see [20] Table 4.1, page 42) J. Nicolics, in a paper on thermal analysis of PCB (see [27], Table 2, page 49) present values for emissivity of FR-4 of 0.89. NASA (see [25], section 3) gives experimental values for emittance of PCB in the range of 0.80 to 0.91 (except for a very reduced number of cases), being the most popular value 0.89. Based on the presented information an emissivity value of 0.89 has been chosen as nominal. Because black coatings have absorptivity values of 0.95 according to Fortescue (see [26] Table 11.4) this has been chosen as nominal.

The boards could be thermally isolated from the rest of the satellite in radiative terms if covered with a low emittance material such as aluminized kapton, which has a value of 0.05 for emissivity (see [26] Table 11.4) or covered with an absorptive coating to raise the emissivity up to 0.98. (see [27], Table 2, page 49). The external

side of the lateral panels could be covered with a high alpha-to-epsilon coating such as aluminum tape with a value of 0.21 for absorptivity, 0.04 for emissivity and a ratio alpha to epsilon of 5.25 (hot case). On the other hand, it could be covered with a aluminized kapton, with a value of 0.40 for absorptivity, 0.63 for emissivity and a ratio alpha to epsilon of 0.63 (cold case).

Solar cells
The solar cells have an absorptivity of 0.91 or less according to the data sheet (see [18]) assuming a CMX 100 AR coverglass is applied. Qioptiq, manufacturer of this covers, which are made of oxides of titanium and aluminum, states a minimum emittance of 0.88 for it (see [28]). Therefore these values will be used as nominal for the solar cells. When the solar cells are producing electric power, the absorptivity value decays as much as the efficiency of the solar cell which is, according once again to the data sheet of the manufacturer 30%, so a minimum value of 0.71 for the absorptivity of the solar cells is applied. Jaques uses a value of 0.91 for absorptivity and 0.81 for emissivity of solar cells (see [20] Table 4.1, page 42). NASA (see [25], section 4) gives emissivity values for solar cells in the range 0.83 to 0.85 and absorptivity values in the range 0.74 to 0.93. According to Fortescue, solar GaAs solar cells have an absorptivity of 0.88 and an emissivity of 0.80. The interior of the solar cells, because they are glued to the solar panels, only exchange heat in form of radiation and so their radiative properties have been disabled (null absorptivity and emissivity).

Plastic elements
Two optical sets have been defined for 'plastic', for the same reasons as stated before. Emissivity of plastics is close to 1. For example, polypropylene has a emissivity of 0.97 and polyethylene of 0.92. This value will be chosen as nominal. Nevertheless, the emissivity of the plastic case could be reduced if covered with a low emittance material such as aluminized kapton, which has an emissivity value of 0.05 for (see [26] Table 11.4). The absorptivity value of the plastic case does not play a role as they are not subject to solar radiation or albedo.

3.4. Linear couplings

Linear couplings determine how the different geometries of the satellite exchange energy with each other via conduction. There are three types of linear couplings implemented in the model: 1) conductive interfaces, 2) contact zones and 3) user defined conductors.

Components modeled by using different geometries are connected together via 'fused' conductive interfaces, which means that the software will consider that the thermal resistance in the edge shared by the geometries is null. This is the case of the solar cells, which have been defined by a rectangle and a trapezoid or the battery plastic case which has been defined by using 5 rectangles (see Figure 3.4, fused couplings shown in yellow). It is the case of the external lateral panels of the satellite which, have been constructed as an integration of different geometries (see Figure 3.5, fused couplings shown in yellow).

Components that are glued, soldered or just in contact with each other via its edges are connected together via 'contact' conductive interfaces, which means that the software will consider that there is a thermal resistance in the edge shared by the geometries which must be specified by the user. This is the situation of the battery plastic case which is in contact with the battery board (see Figure 3.4, contact couplings shown in orange) and the case of the external panels which are not glued but in contact with each other via the edges (see Figure 3.5, contact couplings shown in orange). Depending on the roughness of the surfaces and the contact pressure among the edges this value can scale down to practically 0 or up to 2500W/m^{2}K.

Assuming that a typical epoxy glue has a thermal conductivity of 0.4 W/mK where the thickness of the glue layer is usually 0.1mm, the thermal coupling can be estimated just by dividing the two aforementioned values, resulting in a thermal conductivity of 4000 W/m^{2}K. The software automatically computes the surface area shared by the geometries. Note that the thermal resistance at the interface glue-material is considered null. Due to the viscosity and properties of the glue itself it bonds very well to the surfaces leaving virtually no gaps. If thermally conductive adhesive is used, then its conductivity can scale up to 15000 W/mK yielding a value of 15 W/m^{2}K. Worst case scenario, the glue layer is thicker than nominal, let's assume 0.2mm, yielding in that case a conductivity of 2000 W/m^{2}K.

For the external panels mechanically in contact, it is known that polished surfaces can present values of up to 25000 W/mK. Nevertheless this value is considered far too optimistic for the panels in contact as they are not bolted or glued against each other and the borders of the PCBs do not have an special surface

treatment. Numerous gaps between the surfaces are expected and with no air acting as interface material the conductivity is expected to drop. A moderate value of 500 W/m^{2}K will be set as nominal. In case the panels are glued together or filled with some material in order to enhance their thermal conductivity, this value could mount up to 4000 W/m^{2}K as in the previous case. Minimum values can scale down to 0 W/m^{2}K.

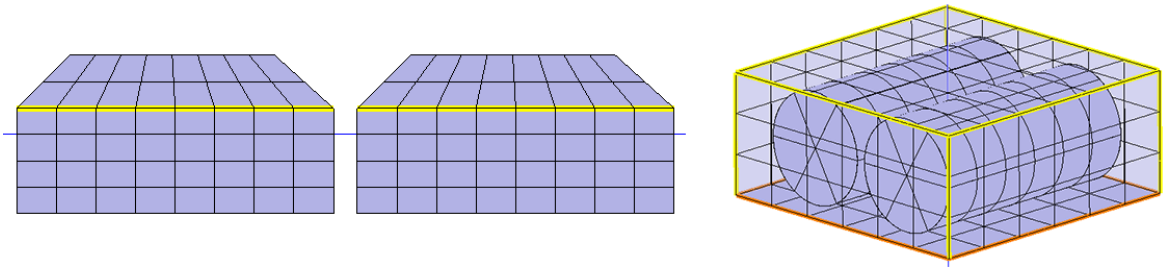

Figure 3.4: Fused (yellow) and contact (orange) conductive interfaces of the solar cells (left) and battery case (right).

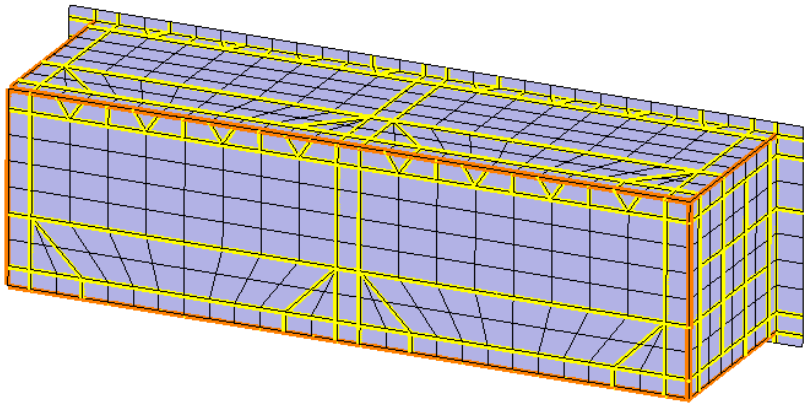

Figure 3.5: Fused (yellow) and contact (orange) conductive interfaces of the external (shear) panels of the DelfiPQ.

Contact zones are defined for components that are glued or attached together sharing a relatively large surface area. This is the case of the solar cells with are glued to the external panels. A value for the thermal resistance among the surfaces is estimated by assuming these cells are glued using a common epoxy based resin. The resin is covering the entire area with a thickness of 0.1 to 0.2 mm. If thermally conductive adhesive is used, then its conductivity can scale up to 1.5 W/mK. Because of the great capacity of the glue to adapt to the surfaces they are attached to, the thermal resistance among glue-component interfaces can be considered negligible. As in the previous cases, the estimations are similar, minimum values of 2000 W/m^{2}K, nominal of 4000 W/m^{2}K and maximum of 15000 W/m^{2}K. Values for glued surfaces in general, are in the range of 1000 to 2000 W/m^2 K are according to Pasqualetto, (see [21], section 5.2.3, page 33).

User defined conductors are used to couple nodes to other nodes individually. This are recommended to model the conductance through standoffs, pin connectors and spacers where two particular nodes (for example the corner node of one of the boards to corner node of the next board) are coupled together via a conductive link. In order to calculate the conductance, equation 3.5 will be used, where GL is the conductance, A the surface area in contact and l the length of the thermal path.

$$GL = k\frac{A}{l} \tag{3.5}$$

Board to board via spacers, 'spacers'
Pasqualetto (see [21], section 5.2.1.4, page 27) reports that usually contact conductance for the spacers, k_c, are estimated to be around 600 to 6000 W/m^2 K. Using OUFTI-1 as a reference, and considering 60601-T6 aluminum spacers, such as the one the DPQ mounts, the conductance is estimated to be 0.00321 W/K. The conductance through spacers for the DPQ can be computed as the inverse of the sum of three resistances in

series, according to figure 3.6 as stated in equation 3.6. The inner diameter of the spacers is 2.7 mm and the external 4.5 mm. Therefore, the contact area, which coincides with the cross sectional area, denoted by A is 1.0179×10^{-5}. The length of the thermal path, l, varies from 7 to 24 mm. The conductivity of aluminum 6061, k_{Al}, is 167 W/m K. The results show very low theoretical conductances. Including the effect of the four spacers, the total PCB to PCB conductance is 4 times larger, around 0.00384, which is comparable to the value presented earlier for the OUFTI-1. Graziosi [19] states in section 8.2.3, page 50, that the threaded rods (very similar as the ones used in the Delfi-PQ) have only a marginal effect on the conductive heat exchange on Delfi-C3. Nevertheless this calculations have to be reviewed and checked against the ones presented in Macco, as he states that the coupling among the different PCBs are in the order of 0.01 to 0.04 W/ K (see [12], Table 5-2, page 39).

$$GL = \frac{1}{\frac{1}{k_c \cdot A} + \frac{l}{k_{Al} \cdot A} + \frac{1}{k_c \cdot A}} = [0.000069, 0.00024]\, W/K \tag{3.6}$$

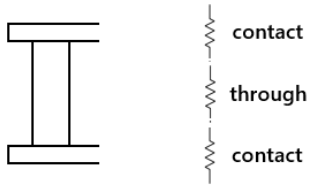

Figure 3.6: Schematics for computation of conductance via spacers.

Board to board via pin connectors, 'pins'
Boxtel provides data on this as well, measuring a experimental values ranging from 0.17 to 0.26 W/m K. The connectors on the DPQ are similar to the ones analized at Boxtel, but with just 9 pins. Pasqualetto presents value for conductances from different satellites (see [21], Table 6, page 24), where they range from 0.005 W/K for the Delfi-n3Xt, up to 1.092 W/K for a generic ESA CubeSat. Nevertheless, the conductance through pins has not been incorporated into the model for priority reasons as it is impact in the temperature results of the satellite is considered to be marginal.

Panels to spacers via standoffs, 'standoffs'
These connections are the only conductive coupling between the internal structure and the external panels, which are subject to the environmental inputs. The values of this conductive couplings are usually low, due to the high thermal resistance between the standoff and surfaces in contact with it. This link could be enhanced by placing some conductive fillers between the interfaces of surfaces. Pasqualetto presents the values of conductances PCBs to external panels trhough stand-offs of five different missions (see [21], Table 5, page 23) being those values similar to each other and between 0.009 and 0.031 W/K, with the exception of the satellite OUFTI-1 which uses a value of 0.12 W/ K, and has been disregarded as it differs greatly from the others. Jaques Table 4.7, page 49, uses values comprised between 0.12 and 1.42 W/K.

Pasqualetto dedicates a section to analize the pcb-to-structure conductance through stand-offs (see [21], section 5.2.1.2, pages 23 and 24), declaring that a theoretical value, considering perfect contact conductance, yields a value around 0.68 W/m K. Nonetheless, contact conductance has a notable impact on the thermal link, increasing the resistance. More reasonable values around 0.065 W/m K are expected to be found in this kind of link. This values are actually extracted from experimental data from Boxtel (see [16], Table 5.7, page 63). Values on literature can be found from 0.0087 used by a generic ESA Cubesat to 0.0315 for the DelFFI. The value proposed by Boxtel will be take as nominal.

Battery to board, 'battery'
The batteries are glued to the EPS board. Therefore, the nominal value to be used as explained before for the thermal conductivity through the glue interface is, in the worst case 2000 W/m^2 K, nominally 4000 W/m^2 K and in the best case 15000 W/m^2 K. The total surface area of one of the cylindrical power units is 1.76×10^{-3} m^2. Lets assume that, in the worst case, the batteries are only glued along a line, an arc of 5° (1/100 of total surface area) and that the lower conductivity value for the glue is used. Then the linear coupling is 0.05 W/K, to share with 6 nodes (0.01 W/K per node). Lets assume that the batteries are attached through a special

accommodation that keeps in contact at least an arc of 45° (1/8 of total surface area) and the nominal value for glue conductivity is used. Then the value of the linear coupling is 0.88 W/K, to be divided among 6 nodes yields 0.15W/K per node. In the best case, lets assume a brace for the batteries is designed that is perfectly attached to the PCB and keeps at least half of the surface of the batteries in contact with the PCB. Using as well especial thermally conductive glue, a value for the linear coupling of up to 13.2 W/K is obtained. Divided among 6 nodes, the result is 2.2W/K per node.

Components to board, 'components'

Components are usually glued to the PCBs in a similar way as described before. Of the total surface area of a PCB (42x42mm) lets assume around 30% is covered with components in the worst case and 70% in the best case. A nominal value of 50% of PCB surface occupation will be used. For the first case, and using the lowest value for conductivity of the glue, the conductance yields a value of 1 W/K, divided among 4 nodes is 0.25W/K per node. In the nominal case, this value amounts up to 3.5 W/K (0.9W/K per node). In the best case, and using conductive thermal glue the value obtained is 18.5 W/K which shared among four couplings means 4.6W/K per coupling.

All the user defined conductors are shown in figure 3.7 as segments connecting two nodes. Some of them has been used to couple the NGTN representing the components of the boards (magenta nodes) to the boards itself.

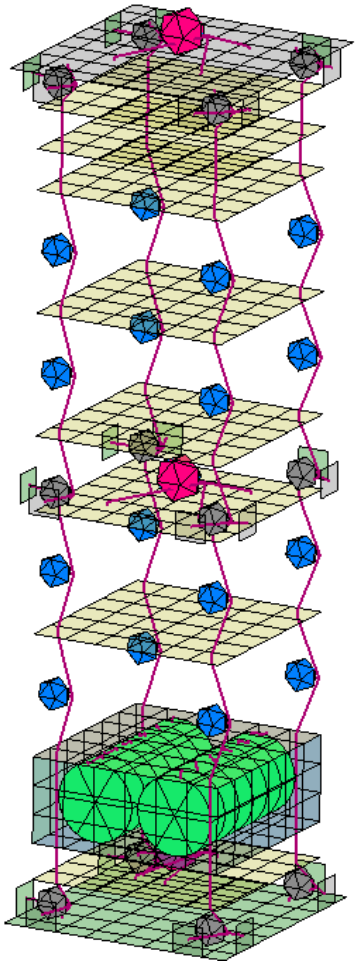

Figure 3.7: Disposition of the NGTN representing the structure of the satellite.

3.5. Thermal environment

The orbit in which the spacecraft is placed defines the energy inputs from the environment. The Delfi-PQ is to be injected in a LEO orbit, nominal altitude of 350 km, maximum of 650 km in order to comply with space debris regulation (so the spacecraft reentries within 25 years), and for tracking purposes and orbital occupation considerations. The orbit is expected to be sun-synchronous with an inclination of approximately 97 degrees. Minimum inclination of 52 degrees is required to ensure visibility from the TU Delft ground station. The orbit is assumed to be circular, or near circular due to injection inaccuracies and orbital perturbations.

The right ascension of the ascending node is an important parameter as it influences the Sun beta angle and therefore the duration of the eclipses. In any case, this parameter is not fixed due to the influence of the Earth gravity field perturbations, specially the term J2. This phenomena is known as nodal regression. Indeed for sun-synchronous orbits, the variation rate of the value is expected to be 1.1×10^{-5} deg/s. The orbital parameters used in the model are summarized in table 3.1

In the vicinity of Earth, there are three main thermal inputs to be considered: solar radiation, Bond albedo and infrared power coming from the planet. The influence of other power sources such as free molecular heating and charged-particle impingement are found to be negligible for the case under study. In the following sections these inputs are estimated providing expected average as well as upper and lower values. The thermal capacity of the satellite is estimated as well, which is useful for computing the thermal inputs coming from the Earth.

3.5.1. Solar radiation

Solar radiation is the main heat source for a satellite in the vicinity of the Earth. This energy comes from the Sun which radiates energy to space similarly as a black body with a temperature of 5777 K will do according to the Stephan-Boltzmann law (see equation 3.7) where $Q_\odot$ is the power radiated by the Sun, σ is the Stephan-Boltzmann constant, equal to 5.6704×10^{-8}W m^2 K^{-4}, $T_\odot$ is the Sun's surface temperature equal to 5777 K and $R_\odot$ is the radius of the Sun equivalent to 6.96×10^8 m. All the astronomical data used in this section is extracted from [4]. The left hand side factor in equation 3.7 corresponds to the Sun's surface area. The power emitted by the Sun is considered to be constant as all the parameters it depends on are too.

$$Q_\odot = 4\pi R_\odot^2 \cdot \sigma T_\odot^4 = 3.8354 \times 10^{26} \text{ W} \tag{3.7}$$

Power density decreases with the square of distance from the source point. Therefore the power arriving to the Earth could be calculated using equation 3.8 where $Q_{\odot\to♁}$ is the power arriving to the vicinity of the Earth, $Q_\odot$ is the power radiated by the Sun and $d^2_{\odot\to♁}$ the distance from the Sun to the Earth.

$$Q_{\odot\to♁} = \frac{Q_\odot}{4\pi d^2_{\odot\to♁}} \tag{3.8}$$

Because the Earth orbit around the Sun is slightly eccentric, the distance from the Sun to the Earth is not constant and have notable effects on the amount of power arriving to the Earth. Being the semimajor axis of the Earth $a_♁$ =1.496 $\times$ 10^{11} m and its eccentricity $e_♁$ =0.017 according to [4], the perihelion, $Pe_♁$, or point of minimum distance to the Sun and the aphelion, $Ap_♁$, or point of maximum distance to the Sun can be computed by using equations 3.9.

$$Pe_♁ = (1-e_♁)a_♁ = 1.471 \cdot 10^{11} \text{ m} \qquad Ap_♁ = (1+e_♁)a_♁ = 1.521 \times 10^{11} \text{ m} \tag{3.9}$$

The perihelion occurs few days after the beginning of a year (next one will occur on the 3^{rd} of January 2019, at 6:19 CET). At this moment the power coming from the Sun to the vicinity of the Earth will be maximum in intensity. The distance from the Sun to Earth at any other point in time can be calculated by solving Kepler's equation (see equation 3.10) where $Me_♁$ is the mean anomaly and $E_♁$ is the eccentric anomaly.

$$Me_♁ = E_♁ - sin(E_♁) \tag{3.10}$$

The mean anomaly can be computed as indicated in equation 3.11, where $T_♁$ is the orbital period of the Earth, G =6.674×10^{-11} m^{3}kg^{-1}s^{-2} the gravitational constant, t the current time in seconds counted from the 1^{st} of January of 2019 at 00:00 and $t_0 = 195,540$ s the origin of time set at the perihelion. According to the third law of Kepler, the orbital period of a planet can be expressed in terms of the semimajor axis of the orbit and the mass of the central body.

$$Me_{\oplus} = \frac{2\pi}{T_{\oplus}} \cdot (t - t_0) = \frac{2\pi}{2\pi\sqrt{\frac{a_{\oplus}^3}{GM_{\odot}}}} \cdot (t - t_0) = \sqrt{\frac{GM_{\odot}}{a_{\oplus}^3}} \cdot (t - t_0) \tag{3.11}$$

For a given time, the mean anomaly can be computed and therefore the eccentric anomaly and from it the distance from the focal point to the satellite can be computed according to equation 3.12.

$$d_{\oplus \to \odot} = a_{\oplus}(1 - e_{\oplus} cos(E_{\oplus})) \tag{3.12}$$

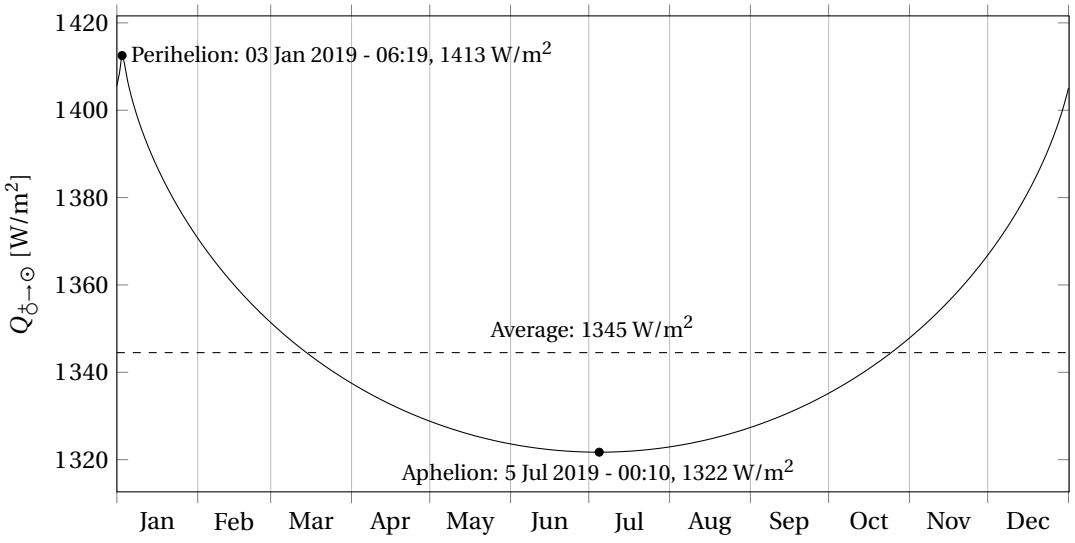

Figure 3.8: Computed Sun power arriving to the vicinity of the Earth.

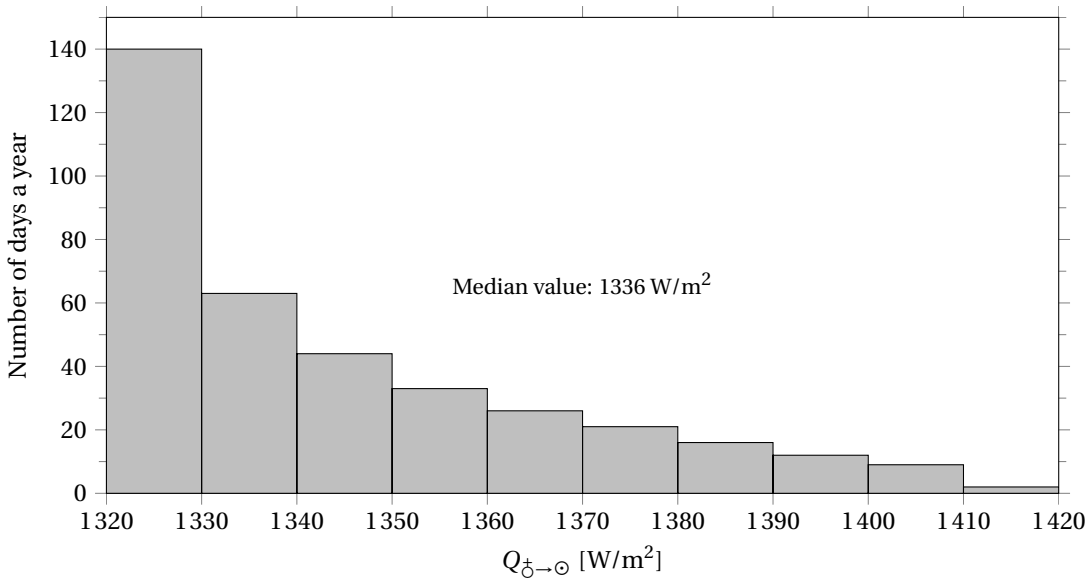

Figure 3.9: Histogram of Sun power arriving to the vicinity of the Earth.

According to Kepler's second law, the closer a planet is to the Sun, the faster it moves, reaching its maximum velocity at the perihelion and the minimum at the aphelion. This explains the shape of the histogram. Out of the 365 days an Earth orbit lasts, most of them are spent on the region the furthest from the Sun, where its power density is fainter. The pass through the nearest region to the Sun last only a few days.

The values calculated are in accordance with solid references in spacecraft thermal control. Gilmore states the sun radiation in the vicinity of the Earth varies from 1322 to 1414 W m^{-2} which are recommended values by the World Radiation Center in Davos, Switzerland, and believed to be accurate to within 0.4% (see [29], section 2, page 22).

Eclipses

A spacecraft orbiting the Earth is expected to receive a power input from the Sun in accordance to the values presented earlier at all times except when another celestial object is blocking it (eclipse). For a spacecraft injected in low Earth orbit, Earth eclipses are likely to happen. Moon eclipses might happen as well, although the chances of this event are fairly low and therefore they will not be considered.

In a circular orbit, the portion of it shadowed by the Earth is given by its altitude, h, and beta angle, β, which is defined as the angle from the solar vector (direction of the solar rays in the neighborhood of the Earth) to the orbital plane of the satellite, according to equation 3.13 where $\delta_\odot$ is the Sun declination, $\Omega_\odot$ is the Sun right ascension, i is the inclination of the orbit of the satellite and Ω its right ascension of the ascending node.

$$\beta = \arcsin\left(\cos\left(\delta_\odot\right)\cdot\sin\left(i\right)\cdot\sin\left(\Omega-\Omega_\odot\right)+\sin\left(\delta_\odot\right)\cdot\cos\left(i\right)\right) \tag{3.13}$$

The maximum eclipse occurs when the beta angle is 0 and decreases in time until the critical beta angle, β^*, is reached (equation 3.14). For $\beta > \beta^*$ until 90°there are no eclipses (see figure 3.10).

$$\beta^* = \arcsin\left(\frac{R_\oplus}{R_\oplus + h}\right) \tag{3.14}$$

The fraction of eclipse can then be calculated by using equation 3.15 (see [29], equation 2.7, page 41) which can be deduced from geometrical principles. The eclipse fractions vary from 40% for the 300 km orbit to 35% for the 760 km one. To compute eclipse times, the eclipse fraction should be multiplied by the orbital period, which can be computed based on Kepler's third law (refer to equation 3.16). Maximum eclipse times are 2194 s for a 300 km, orbit and 2110 s for the 760 km orbit, which amounts to approximately 35 minutes of eclipse in both cases.

$$f_E = \frac{1}{180}\arccos\left(\frac{\sqrt{h^2+2R_\oplus h}}{\left(R_\oplus+h\right)cos\beta}\right) \quad \text{if} \quad |\beta| < \beta^* \tag{3.15}$$

$$T = 2\pi\sqrt{\frac{\left(R_\oplus+h\right)^3}{\mu}} \tag{3.16}$$

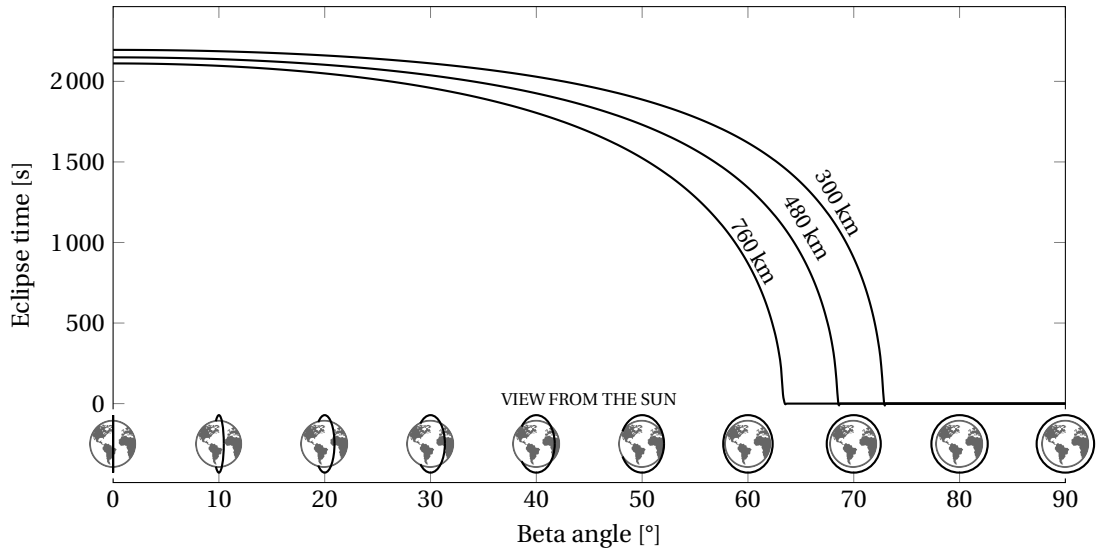

Figure 3.10: Eclipse duration as a function of the beta angle for 300, 480 and 760 km altitude orbits.

The maximum possible eclipse occurs with a beta angle of 0°, the minimum possible eclipse occurs with a beta angle higher than the critical one and for the nominal case, an average value of the eclipse time will be

chosen, which happens to be, according to the data presented in figure 3.10, 1488 s, corresponding to a beta angle of 62.7°.

At this point is interesting to determine a hot, nominal and cold case for Sun radiation. The hot case will be the one with maximum power input. Therefore, the satellite will be located near the perihelion (3 Jan 2019, 06:19). At this moment of the year the solar declination happens to be -22.9° and the Sun right ascension 283°. The beta angle will be higher than the critical one to ensure continuous sunlight. A RAAN of 15° produces a beta angle of 74°, which is greater than the critical one no matter what the altitude of the orbit (within the boundaries defined earlier).

For the cold, case the satellite will be situated close to the aphelion (5th July 2019, 00:10). At this moment of the year the solar declination happens to be 22.9° and the Sun right ascension 103°. A RAAN of 107° produces a beta angle of 0°.

For the nominal case, the satellite will be located at a distance from the Sun where the median value of 1336 W/m^2 is reached. This happens on the 5th of April of 2019 and the 2nd of October of 2019. For the first date, when the solar declination happens to be 5.8° and the Sun right ascension 13°, a beta angle of 62.7°, which gives the average eclipse time, happens for a RAAN of 80°. Take a look at figure 3.11 to visualize the selected cases.

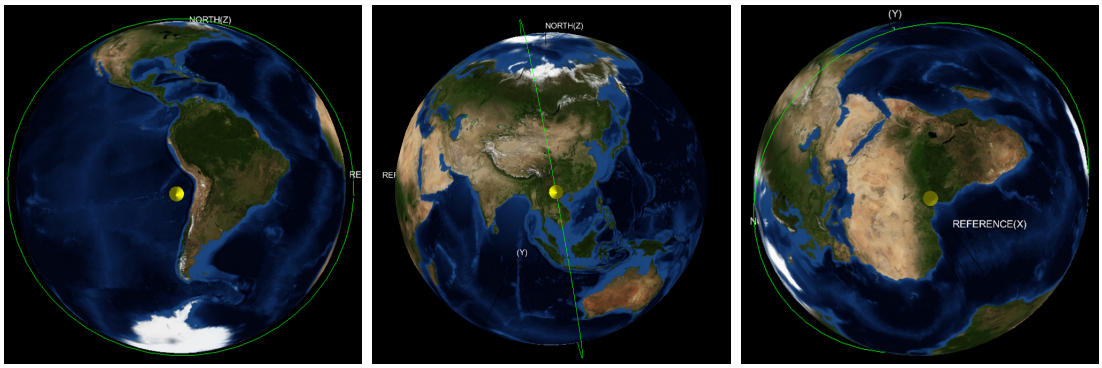

Figure 3.11: Orbits (as seen from the Sun) for hot case (left), cold case (center) and nominal case (right).

Please note that an inclination of 97° is considered in all cases and that the sun declination and right ascension are give by the date in each case.

3.5.2. Bond Albedo and IR radiation

The estimation of power input coming from Albedo and Earth IR are more difficult to estimate. One can use the Tables provided by Gilmore / NASA-STEM ([29], Table 2.2, page 27 and Table 2.3 page 28) which come from statistical data captured by sensors on-board spacecraft orbiting the Earth in low altitude orbits. Since the time constant of the satellite has been estimated in 9 minutes, the averaged values provided by Gilmore corresponding to 896 seconds have been used. This is 200 seconds higher than the actual time constant of the satellite but its much closer to the next value provided by Gilmore which is 128 seconds. Nominally the satellite will have a higher thermal mass which justifies the choice of this slightly higher value. The surface sensitivity is both to albedo and IR and the inclination in the range 60° to 90°. The values extracted which are used for the analysis are presented in Table 3.1. These values will only be exceeded 0.4% of the times. Corrections have been applied to produce extremes. The nominal values have been extracted by taking a look at the number of occurrences a pair of albedo / IR value happens, as shown in [29], Figure 2.4, page 31.

3.5.3. Summary and case definition

With all this information, the hot, cold and nominal cases for the environment can be defined. In the cold case, the altitude of the orbit is set to be the maximum, so the inputs from the Earth are the lowest ones. In the nominal case, the altitude is the nominal altitude. In the hot case, the altitude is the minimum possible, so the inputs from the Earth are the maximum. Remember that the energy radiated by an object is inversely proportional to the second power of the distance to the object. All the data used for each case is defined in Table 3.1.

Table 3.1: Orbital parameters for the cold, nominal and hot cases.

Parameter	Cold	Nom	Hot	Units
Date (year 2019)	5 Jul	5 Apr	3 Jan	
Sun distance	152.1	149.6	147.0	$km \times 10^6$
Sun power	1322	1336	1414	W/m^2
Solar declination	22.8°	5.76°	-22.8°	
Sun right ascension	103°	13°	283°	
Orbital precession:	-1.15×10^{-5}	-1.15×10^{-5}	-1.15×10^{-5}	deg/s
Albedo	0.15	0.17	0.59	
Planet IR	218	250	274	W/m^2
Planet temperature	261	265	270	K
Eccentricity	0	0	0	
Altitude	650	480	300	km
Period	5864	5492	5431	s
Inclination	97.21°	97.21°	97.21°	
RAAN	107°	80°	15°	
beta angle	0 °	62.7°	74°	
eclipse in	2250	2493	-	s
eclipse out	4372	3851	-	s
power generated (CV)	2.439 (0.12)	2.445 (0.12)	2.57 (0.12)	W

3.6. Dissipation

Devices and components inside the satellite release thermal energy as they operate. In other words, they dissipate heat. The origin of this thermal energy is electric power harvested from the cells or extracted from the battery. From a thermal point of view, most of the energy from the Sun that could have ended up as heat but is transformed into electrical power instead in the solar cells, will be anyways converted into heat later on inside the satellite.

Some components such as mechanical and electromagnetic ones are an exception. For example, a considerable part of the power that goes into the transceiver is sent to space in the form of electromagnetic energy. Reaction wheels and magnetorquers transform electrical energy into mechanical energy. Bur for most of the instruments, mainly processors, sensors, resistors, etc. all electrical energy they consume is transformed into heat. This could be advantageous as the energy that was prevented to derive into heat while the satellite was in sunlight (hot conditions) is released in form of heat while the satellite is in eclipse (cold conditions).

For the calculation of dissipation, it is important to first understand the way electrical power is managed in the satellite. Taking a look at figures A.1, A.2, A.3, A.4 it can be appreciated how the power flows through different devices. The power generated in the solar cells is directed to maximum power point trackers (MPPTs). These devices will extract the maximum power possible from the solar cell if full power is required. Otherwise they will shift the voltage/current point to output just the required amount of power. Therefore the efficiency of the solar cells decay and the residual heat stays at the cells (shown as the power excess feedback loop in the image). The power leaving the MPPT is then directed to an unregulated power bus. The battery is fed from the bus until is full. The same way the battery can provide energy to the bus when the demand surpasses the production of the solar cells (in eclipse time or when transmitting to Earth, for example). The different subsystems and payloads are fed as well from this unregulated bus.

Due to the operation of each subsystem, some power is lost in form of thermal energy. This power is represented in the figure with red arrows. The exact amount is determined by the efficiency of each component, (indicated inside the boxes in the figure).

The specific moment and location where this power is dissipated is relevant to accurately model the thermal behavior of the satellite and therefore is studied. This is why for the three different cases a number of phases have been defined to accurately represent the power dissipation of each component in time. The dissipation values have been inputed into the model as time-dependent boundary conditions for each case and assigned to the corresponding geometries.

The power required from the batteries have been computed so they are back to its full state at the end

of each orbit. For the computation of the energy produced by the solar cells during sunlight, an statistical analysis based on the Monte Carlo method has been run. Initializing 10.000 different cases with random initial attitudes for the satellite and selecting a random rotational axis, the power harvested by the solar cells is computed based on the geometry of the satellite and its properties. It has been found, as indicated in Table 3.1, that the amount of power generated by the solar cells, are similar for the three cases and around 2450 mW. This is in accordance with the predictions found in the documentation of the Delfi-PQ.

Schematics on power distribution with all the quantitative information used in the determination of power consumption could be found in Appendix A.

3.7. Pointing

The satellite is considered to be free tumbling, with an angular velocity of approx 5deg/s. For this reason a rotation along the axis [1,1,1] has been implemented in the model, which is considered to represent well enough a free tumbling movement in space, at least for obtaining some first results.

3.8. Solution Routines

The solution routines have been set to solve the transient problem in a cyclical way. This means that the solver will divide the orbit of the satellite in points equally spaced in time. The simulation starts with the satellite set to an initial temperature (guess). Then the program computes in each step the thermal inputs and outputs and based on the thermal inertia of the satellite and the time step considered computes the temperature of the satellite at that point for all its elements. The software continues doing the same until the temperature at all the points in the orbit are computed.

Once the orbit is complete, the program checks if the final temperatures are the same as the initial temperatures. If they are it means that the temperature profile in the satellite has reached its steady state and will repeat cyclically 'forever'. Otherwise, it means that the influence of the initial temperature conditions for the satellite are still influencing the solution. Therefore the satellite is in its transient state. We are interested in the nominal steady stabilized temperature cycle of the satellite as it better represents the satellite realistically. The initial temperature conditions are set in a random manner and therefore it is not interesting for the results to have it influencing the solution.

Therefore the software computes one transient orbit and compares the final and initial temperatures. If they do not match, the software repeats the computation of the transient orbit using now the final temperatures as new initial temperatures and in the end, it compares again. This is done a required number of times until both temperatures match. For the cases we are running it appears to be between 2 and 3 the number of cycles that need to be run to achieve a difference in temperature under 0.1K for all the +3000 elements of the model.

3.9. Verification

The following actions have been successfully completed in order to verify the model:

- Thermal network schematics produced by the package Therm NV has been reviewed to check the correct linear and radiative coupling among all the nodes of the model.
- The files generated by ESATAN TMS containing the model complete information have been reviewed.
- Property assignment has been visually checked with the ESATAN TMS display feature.
- Radiative results have been reviewed to ensure consistency with the reality to be simulated.
- Results generated are in accordance with spacecraft in similar conditions.

3.10. Satellite temperature profile

The results presented show the evolution of temperatures with time, along one orbit. These results are independent of the initial conditions of the model and so it is ensured that will repeat cyclically in each orbit as long as the assumptions for dissipation and orbital parameters remain the same. The results are divided in three groups: external elements (surfaces exposed to space, solar cells), internal elements (PCB boards, equipment, fixing elements) and battery.

3.10.1. External Temperatures

The temperature of the external elements of the satellite are presented in figure 3.12. In particular six sets of curves are shown, each of them belonging to one of the external surfaces of the prism. In each set of curves there is: 1) a red line, indicating the temperature of the external surface of the PCB panel; 2) a blue line, indicating the temperature of the internal surface of the PCB panel; and 3) a yellow line, indicating the temperature of the solar cells attached to the corresponding PCB panel. Please note that only four of the set of curves contain a yellow line as the +Z and -Z panels do not have solar cells attached.

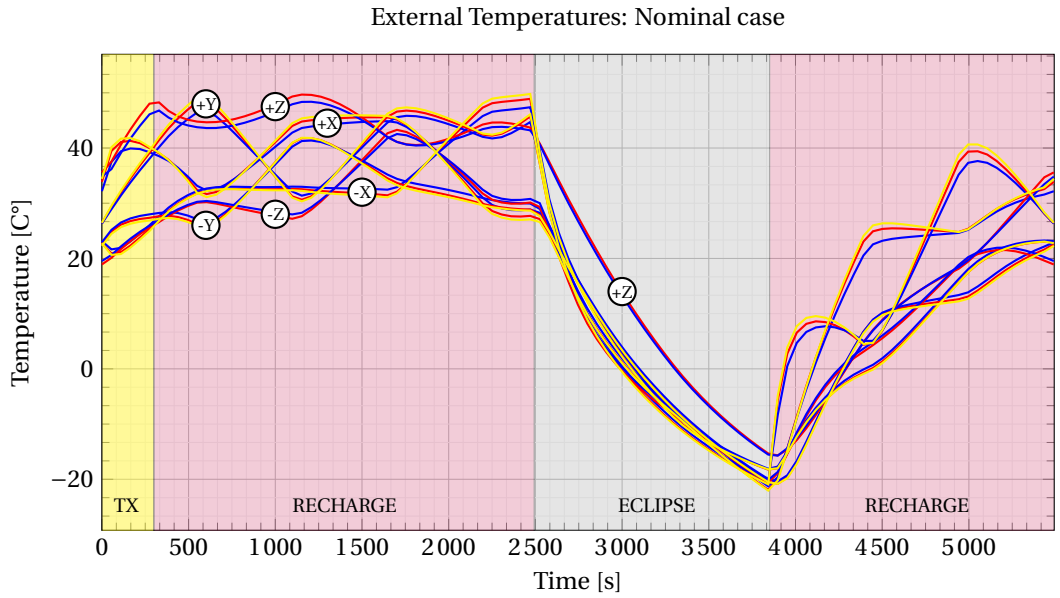

Figure 3.12: Computed external temperatures, nominal case.

Taking a look at each of the panels individually, the results show that the temperatures are, more or less, homogeneous (there are no great thermal gradients between solar cell, external and internal surface of the PCB) being the maximum temperature difference in the order of 5°C. It could be observed how the differences in temperature between external and internal surfaces of the PCB panels augment when the temperatures are higher. Take for example the +Y curves show in figure 3.12. At second 0, internal and external PCB surfaces are equal to each other in temperature and about 20°C. At second 600, the temperatures of the same surfaces are around 50°C but the top and bottom surface temperatures differ in about 4°C.

The temperatures of each one of the panels are different from each other in general. This could be explained by the fact that the satellite model has been computed as a free tumbling object. At a given instant, some surfaces are facing the Sun while others are not, some are facing the Earth while others not. Therefore the power inputs are different for each of them. Because of the geometrical configuration of the satellite, it is expected that, when a face reaches its highest temperature, the opposite is close to its coldest temperature. This behavior is clearly seen in the results. Take a look at figure 3.12 to see how the +/- pairs of faces are the top/bottom curves respectively.

During eclipse there is no Sun or Albedo inputs and so the thermal environment of all the surfaces are similar. Therefore the temperatures of all the surfaces seem to follow a similar path. There is a slight deviation in the +Z face. This could be explained because the mass of this board and thus its thermal capacity are greater than the other boards as it is connected to the antennas and electronic equipment as part of the communication system of the satellite. This higher thermal inertia creates a temperature offset with respect of the rest of the satellite.

The external surfaces of the satellite are thin, have a great surface area and are directly exposed to the Sun input. Therefore it could be seen how the temperatures raise almost immediately after the satellite leaves the shadow of the Earth at second 3851 in the simulation.

3.10.2. Internal Temperatures

Taking a look at the temperatures of the internal elements of the satellites (figure 3.13) it is possible to observe that most of them follow a similar trend along the orbit. The temperatures represented in the graph correspond to the following subsets:

(1) Board 1 - EPS
(2) Board 2 - Battery
(3) Board 3 - Dummy
(4) Board 4 - ADCS
(5) Board 5 - Dummy
(6) Board 6 - Dummy
(7) Board 7 - OBDH
(8) Board 8 - TTC
(9) Board 9 - TTC
(B) Battery
(S) Internal structure (average temperature of standoffs, spacers and rods)

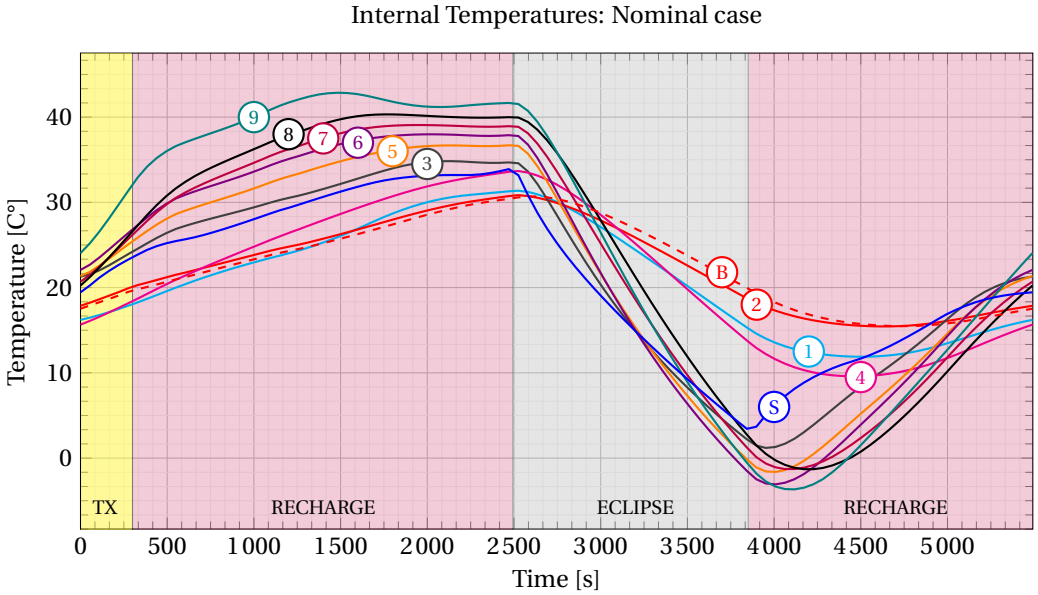

Figure 3.13: Computed internal temperatures, nominal case.

The boards with less mass (thermal capacity) experiment sudden changes in temperature while the ones with more mass, specifically board 1 (EPS), 2 (batteries) and 4 (ADCS), present smother temperature variations. This is particularly evident in the moment the spacecraft goes from eclipse to sunlight. Then the structural elements which are directly connected to the external structure and have low thermal mass start heating up with short delay. Lighter elements such as boards 3, 5, 6, 7, 8 and 9 present a short delay when heating up. More massive elements such as as boards 1, 2 and 4 take around 10 to 15 minutes to start heating up again.

It seems to be a thermal gradient in the internal structure as whole, from top to bottom. Board 9 is a couple of degrees hotter than board 8; board 8 a couple of degrees hotter than board 7 and so on. Please note that the counting of the boards is made from bottom to top like the floors of a building. Therefore board 1 is on the bottom and board 9 on the top. This thermal behavior could be easily explained by taking a look at figure 3.12. The +Z panel, on top of the satellite, is hotter than the bottom panel, on the bottom of the satellite, being the first one between 40°C and 50°C most of the time and the later one between 20°C and 40°C most of the time.

Overall, temperatures of all the boards are in the range [-5°C, 50°C]. Please note that this model intends to represent local peak temperatures caused by components such as the power amplifier used for communications. Nevertheless it does not accurately represent all the electronic components that might heat up over the temperatures presented. A deeper analysis shows that some structural elements reach temperatures down to -20°C at some point in time.

3.10.3. Battery

The temperature of the battery seem to be quite uniform (no thermal gradients) within the batteries. The thick line represents the average temperature of the batteries and the dashed lines the maximum and minimum temperatures found in the batteries.

It is interesting to observe how after the eclipse ends, it takes a while for the battery to start heating up. This is explained by the fact that all the elements surrounding the battery are colder than the temperature of the battery itself for a while after the eclipse. Therefore, the battery continues releasing heat to the elements around and lowering its temperature. This could be easily checked by taking a look at figures 3.12 and 3.13. It is approximately in the second 4750 of the simulation when the batteries start to heat-up again. At this moment the battery has a temperature of 14°C according to figure 3.14. Previous to this moment, most of the external panels of the satellite are below this temperature and afterwards above it (see figure 3.12). The same way, previous to this moment, most of the internal elements of the satellite are below this temperature and afterwards above it (see figure 3.13). On the other hands, the solar cells, which are directly exposed to sunlight, register an immediate increase in temperature when the satellite enters sunlight.

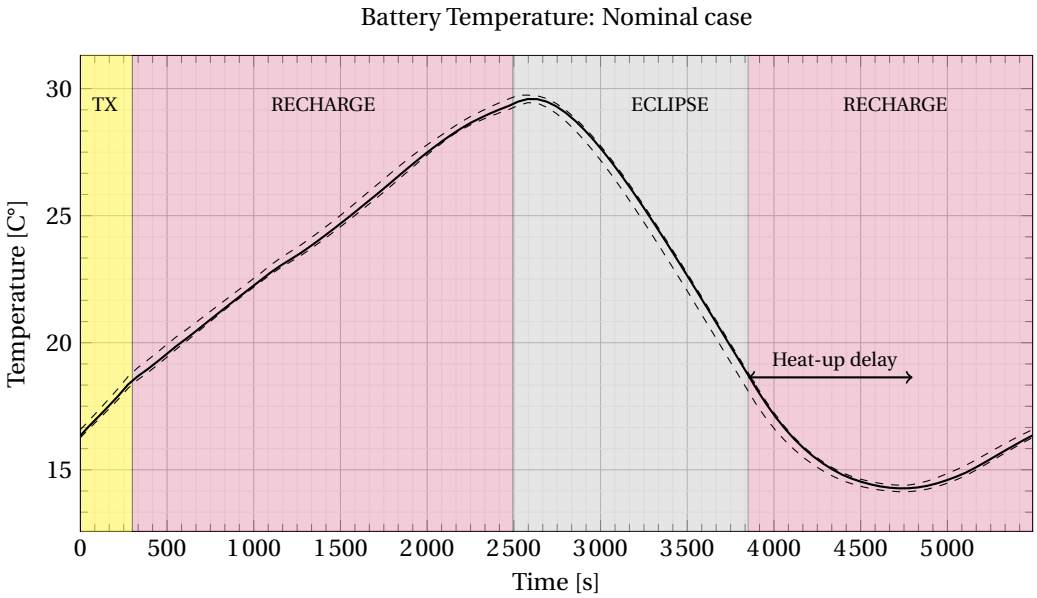

Figure 3.14: Computed average, minimum and maximum temperatures for the batteries on orbit. Nominal case.

3.11. Input for the sensitivity analysis

From the results obtained, a number of valuable outputs are extracted, to be taken into consideration when producing conclusions from the sensitivity analysis.

To begin with, expectable temperature ranges have been obtained for the nominal case.

- External component temperatures are in the range [-20°C, 50°C]
- Internal component temperatures are in the range [-5°C, 40°C]
- Battery temperatures are in the range [15°C, 30°C]

Summarizing, the results show that the internal components keep similar temperatures, suggesting that no important thermal gradients are expected to be found within the internal components and therefore they could be studied as a group. As well, figure 3.14 shows as well no temperature gradients, and therefore will be considered as another study group when extracting meaningful temperature data in Chapter 4. In a similar way, there are no important thermal gradients between the solar cells, internal and external surfaces of the shear panels.

The trend of temperatures along the orbit, how it plummets during the eclipse time and increases under sunlight conditions, being the different external panels at different temperatures as the satellite turns, serve as an important input to formulate conclusions on Chapters 4 and 5.

Further results, including hot and cold case computation can be found in Appendix C.

4

Temperature Sensitivity Analysis

The temperature sensitivity of PocketQubes to a number of design and environmental parameters is presented in this chapter. In particular, sensitivity to optical properties, orbital parameters, internal configuration, heat capacity and thermal conductivity is investigated. In order to do so, the temperatures along the orbit of a representative satellite are analyzed for several cases, each with different values of the aforementioned parameters. The DelfiPQ satellite in the nominal configuration described in chapter 3 has been chosen as a representative satellite.

Additional parameters described in previous chapters, such as external geometry, power management or pointing, were not included in the study due to time and practical constraints.

By exploring the impact that slight variations of design and environmental parameters have on the temperatures of different elements of the satellites it is possible to get an overview of which are the most relevant ones that influence temperatures and which are the ones that are not that important or even negligible. The idea behind is to produce quantitative data which allows to compare and rank these parameters, as a first approach to set a basis to standardized thermal design control.

Exploring which parameters influence the temperature of the satellite is the first step. Those parameters are then grouped into the aforementioned categories: from optical properties, to thermal conductivity. Then, limit values (minimum, maximum) of these parameters are investigated to determine the range of variation of each one. For example, the expected solar inputs PocketQubes may experience in the neighborhood of the Earth is estimated to be between 1322 and 1414 $\mathrm{W\,m^{-2}}$ (refer to table 4.9).

To understand the influence of each parameter on the temperatures, the same nominal simulations that were run with the help of the thermal model solver ESATAN, are recomputed with slight modifications. Tables of cases are generated with each parameter adopting different values within its range. Therefore each new simulation contains a slight modification of one and only one parameter. The rest of the parameters are kept equal to the nominal values.

Temperature data from all these parameters is extracted to later be compared and processed, allowing the researcher to get a better understanding on how this parameter is impacting the temperatures of the spacecraft. The process of modifying the models, solving them and managing all the data extraction is done through a Matlab interface which calls the ESATAN solver.

The result of each and every simulation is a large amount of temperature data. Therefore this data has to be processed in order to be understandable and meaningful. The model of the satellite consists in a couple of thousands of nodes. As well, the orbit of the satellite has been discretized in a dozen of positions, where the temperatures are computed. Therefore, at the end of a simulation, the result is a set of 12 times a couple of thousand temperatures corresponding to each node of the satellite at each position in orbit.

To reduce this data, first of all is divided into group averages. Data regarding average satellite temperature of the entire satellite, of only the external surfaces, of only the internal surfaces and of only the battery is produced. These four groups has been chosen for a reason. The first one gives a general idea of the temperature of the satellite. The second and third group represent elements which are subject to very different thermal environments, as the external ones are open to the cold space and thermal inputs such as as Albedo, OLR and

Sun Power whether the internal ones are at all times enclosed by the shear panels and therefore isolated from the exterior. Finally, the battery has been chosen as a particular group of special interest, given its narrow operational temperature range.

When referring to average temperatures, it consists on the average of the temperatures of all the nodes in the group, at all orbital positions. Therefore the output is a single number. In the same way, for the four groups, data on the maximum and minimum temperatures reached is extracted. This gives an idea of the amplitude of temperature swings in each case. When referring to maximum temperature, it consists on the maximum of the maximum of all the nodes in the group of every position in orbit. The same way the minimum of the minimum is computed. This process yields a single value for maximum and a single value for minimum. All this temperature data is then compiled into a graph and a side table like the one showed in 4.1 for better interpretation of the results.

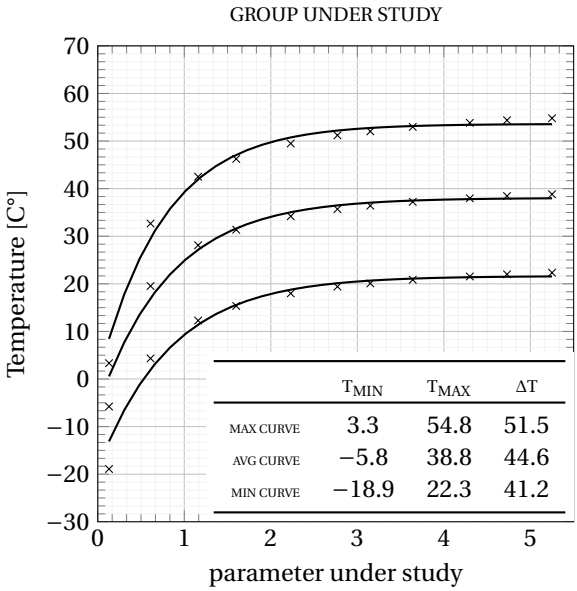

Figure 4.1: Example of temperature sensitivity data plot.

The group under study is indicated on top of the graph, in this case, the data corresponds to the battery group. For each value of the parameter under study (horizontal axis), Figure 4.1 shows three data points on the vertical axis, corresponding to the minimum, average and maximum temperatures obtained for the satellite in that case. Results from several cases along the range of variation of the parameter under study are shown. Trend lines of the maximum, average and minimum temperatures for all these different cases are drawn.

Therefore these lines give an idea on how the maximum, average and minimum temperatures shift when the parameter under study changes. This enables the researcher to draw conclusions, for example, on how by setting the value of a particular design parameter the expected satellite temperatures are not expected to surpass certain maximum or drop below certain minimum. Along with this intuitive visual interpretation of the sensitivity of temperature to a certain parameter, a summary table is shown on the right bottom corner. It shows, for each of the three trend lines (max curve, avg curve and min curve), its minimum and its maximum, and the difference between them.

This gives a quantitative value on temperature change linked to variation of a parameter. For example, regarding figure 4.1, it is possible to affirm that a change in the value of the parameter under study from 0 to 5, has shifted the average temperatures of the study group of the satellite from -5.8 [C°] to 38.8 [C°], a total change of 44.6 [C°]. Therefore the impact of these parameter on average temperatures of the study group of the satellites, on its range of variation could be associated with the figure 44.6 [C°].

By comparing this values with the ones extracted from analysis of variation of other parameters it is possible to quantitatively rank them and therefore understand which of them have most influence in the temperatures of the satellite.

4.1. Optical Properties

Optical properties refer to the ability of materials to absorb and emit energy in form of radiation. These properties do not depend on the composition of the material itself, but on its external appearance. By coating or covering any material with a specific substance its optical properties are modified. Two parameters are commonly used to define the optical properties of an object: emissivity, ε, and absorptivity, α. While the first one is related to energy emission and absorption in the infrared range, the later one is related to energy emission and absorption in the visible range.

Optical properties directly impact the temperatures of the satellite as they determine: 1) the amount of radiation absorbed from external sources (Sun, Earth), 2) the amount of energy evacuated to space and 3) the thermal couplings among the internal components of the satellite. The optical analysis could be divided in a external and an internal subproblem.

The external subproblem refers to the surfaces exposed to space (external surface area of shear panels, solar cells, deployables, etc.) These surfaces are subject to absorb energy from the Sun and Earth and, at the same time, work as radiators evacuating energy to space. Therefore both ε and α have an important role on these surfaces. Usually the ratio α/ε is used as the main parameter to define the optical properties of these external surfaces. The optical properties of shear panels and deployables are easily modifiable by coating or covering them. On the other hand, the optical properties of solar cells, which represent a notable amount of the external surface area of PocketQubes, are difficult to modify.

The internal subproblem refers to all the components inside of the satellite as well as the internal surfaces of the shear panels. The internal components of the satellite are enclosed by the shear panels and thus cannot receive external environmental inputs or radiate energy to space. This is the main difference with the external subproblem. Therefore, ε is the only parameter playing a role in this case. The higher this value, the better the different elements of the satellites are thermally coupled to each other. Therefore the more uniform the temperatures are expected to be among the internal components of the satellite.

Satellites such as the Unicorn-2 of Alba-Orbital have perforated shear panels, allowing internal components to receive energy from the environment and to directly radiate energy to space. In this case the analysis is more complex as α might play an important role when determining the temperatures of the internal components.

Based on the information presented, variation in four optical properties are studied: o_1 the α/ε of the external surface area of the shear panels, o_2 the ε of the internal surface area of the shear panels, o_3 the ε of the internal boards and o_4 the ε of the battery. The summary of the optical properties is presented in table 4.1. These values have been chosen based on materials that are commonly used for small satellites.

Table 4.1: Summary of optical properties of PocketQubes.

Category	ID	Parameter	Minimum	Nominal	Maximum
Optical	o_1	α/ε shear panels external	0.13 (White Paint)	1.12 (Black Paint)	5.25 (Aluminum Tape)
	o_2	ε shear panels internal	0.04 (Aluminum Tape)	0.85 (Black Paint)	0.90 (White Paint)
	o_2	ε PCB boards	0.04 (Aluminum Tape)	0.85 (Black Paint)	0.90 (White Paint)
	o_4	ε battery	0.04 (Aluminum Tape)	0.85 (Black Paint)	0.90 (White Paint)

To study the temperature influence of the variation of the α/ε ratio, a material with high α/ε ratio, aluminum tape (α/ε =5.25), and a material with low α/ε ratio, white paint (α/ε =0.13), has been chosen. By combining these two materials any desired value for the α/ε ratio in the range 0.13 to 5.25 can be achieved. The cases defined to study the influence of this parameter on the temperatures are presented in table 4.2. Coatings with higher and lower α/ε than the ones of the materials chosen for setting the boundaries, such as polished beryllium (α/ε =44) or optical solar reflectors (α/ε =0.09) exists. Nevertheless is considered unlikely that those materials will be implemented in PocketQubes in general, as they are costly and reserved

to specific applications. Aluminum tape and white paint are cheap and easy-to-implement coatings in PocketQubes and therefore likely to be used in these missions. Black coating has been considered as nominal case, as the Delfi-PQ carries this coating on the external surface of its shear panels.

Table 4.2: Variation of α/ε ratio based on white paint and aluminum tape combinations.

ID	Coating	White paint	Aluminum tape	α	ε	α/ε
o_1	0	100%	0%	0.120	0.900	**0.13**
o_1	1	30%	70%	0.183	0.298	**0.61**
o_1	2	15%	85%	0.197	0.169	**1.16**
o_1	3	10%	90%	0.201	0.126	**1.60**
o_1	4	6.0%	94%	0.205	0.092	**2.23**
o_1	5	4.0%	96%	0.206	0.074	**2.77**
o_1	6	3.0%	97%	0.207	0.066	**3.15**
o_1	7	2.0%	98%	0.208	0.057	**3.64**
o_1	8	1.0%	99%	0.209	0.049	**4.30**
o_1	9	0.5%	99.5%	0.210	0.044	**4.73**
o_1	10	0%	100%	0.210	0.040	**5.25**

To study the temperature influence of the variation of the ε, a material with low ε, aluminum tape (ε =0.04) and a material with high ε, white paint (ε =0.90) has been chosen. By combining these two materials any desired value for the α/ε ratio in the range 0.04 to 0.90 can be achieved. The cases defined to study the influence of this parameter on the temperatures are presented in table 4.3. Black coating has been considered as nominal case, as the Delfi-PQ carries this coating on the internal surface of its shear panels, boards and battery.

Table 4.3: Variation of ε based on aluminum tape and white paint combinations.

ID	Coating	Aluminum Tape	White Paint	α	ε	α/ε
o_2,o_3,o_4	0	100%	0%	0.21	**0.04**	05.25
o_2,o_3,o_4	1	90%	10%	0.20	**0.13**	1.60
o_2,o_3,o_4	2	80%	20%	0.19	**0.21**	0.91
o_2,o_3,o_4	3	70%	30%	0.18	**0.30**	0.61
o_2,o_3,o_4	4	60%	40%	0.17	**0.38**	0.45
o_2,o_3,o_4	5	50%	50%	0.17	**0.47**	0.35
o_2,o_3,o_4	6	40%	60%	0.16	**0.56**	0.28
o_2,o_3,o_4	7	30%	70%	0.15	**0.64**	0.23
o_2,o_3,o_4	8	20%	80%	0.14	**0.73**	0.19
o_2,o_3,o_4	9	10%	90%	0.13	**0.81**	0.16
o_2,o_3,o_4	10	0%	100%	0.12	**0.90**	0.13

The optical properties of the solar cells, although unmodifiable, play an important role in the optical problem as they cover in general most of the external surface area and deployables of PocketQubes. The optical properties of the solar cells carried by DelfiPQ are used as nominal and considered similar for other kind of solar cells. They are advanced triple junction solar cells manufactured by AzurSpace.

These solar cells have an absorptivity of 0.91 or less according to the data sheet (see [18]) assuming a CMX 100 AR coverglass is applied. Qioptiq, manufacturer of this covers, which are made of oxides of titanium and aluminum, states a minimum emittance of 0.88 for them (see [28]). When the solar cells are producing electric power, the absorptivity value decays as much as the efficiency of the solar cell which is, according once again to the data sheet of the manufacturer, 30%, so a minimum value of 0.71 for the absorptivity of the solar cells could be reached. Nevertheless the model considers a constant absorptivity of 0.71 for the solar

cells (cells producing maximum power). Corresponding additional heat is inputed manually in the solar cells when the cells are under the Sun and not producing maximum power.

The optical properties of other components of the satellite such as the antennas can be checked in appendix A.

Sensitivity results on optical properties

The following figures show the impact on temperature of varying the optical properties of the external and internal surfaces of the shear panels, the ones of the boards and the ones of the battery, according to the values presented earlier.

Sensitivity to α/ε ratio of the external surface of shear panels.
The variation of the optical properties of the external surfaces of the satellite have a notable impact in all the temperature indicators measured, as shown in Figure 4.2.

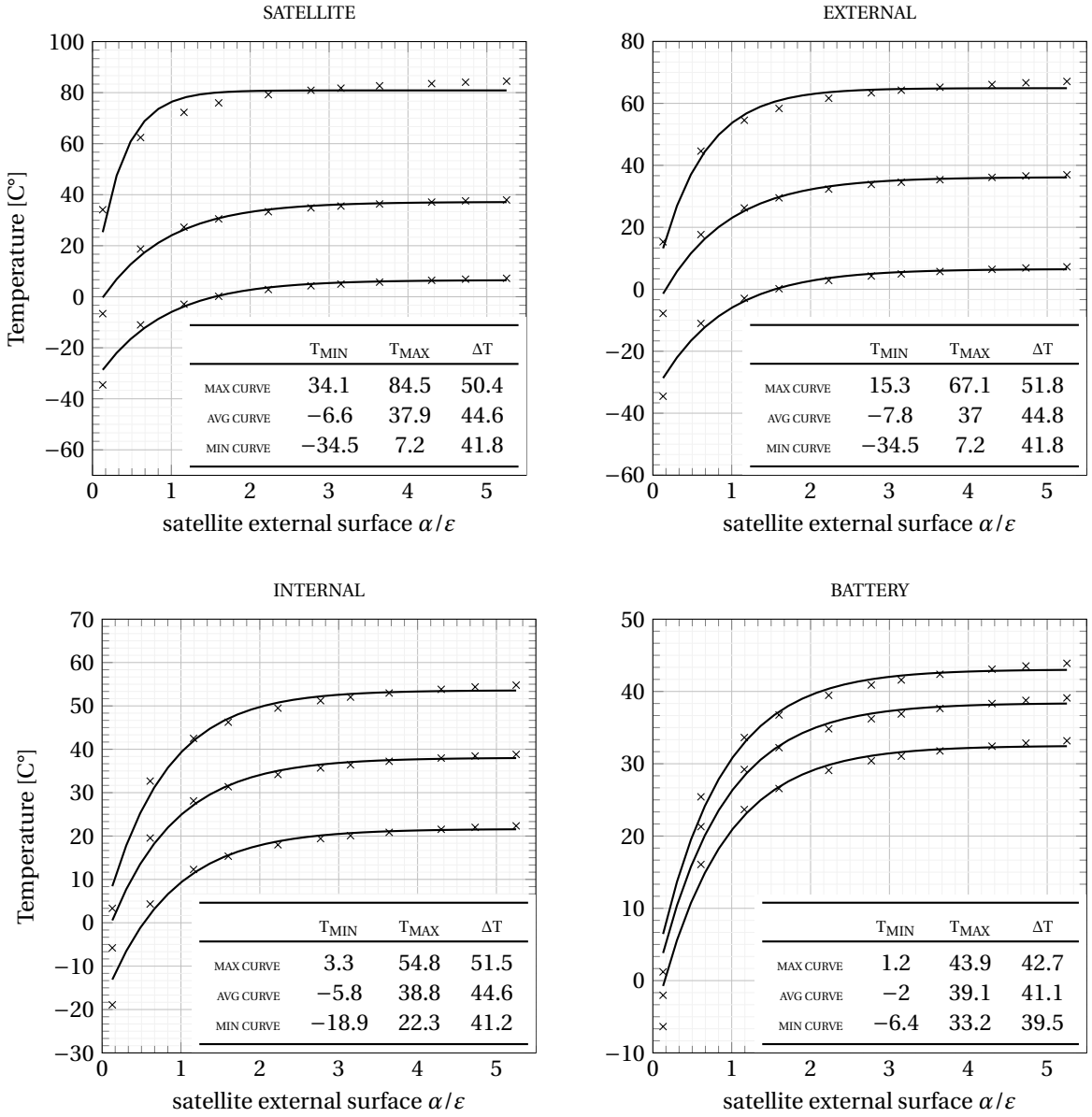

Figure 4.2: Temperature sensitivity to optical properties of the external surface of the satellite.

The four trends seem to follow a similar path, where the maximum rate of variation in temperatures happens in the range $\alpha/\varepsilon \approx [0,1]$. This means that ratios higher than 1 on the external surfaces of the satellite have

a small impact on the temperatures. Given that black paint have a α/ε of 1.12, just by generating combinations of white and black paint on the external surface of the satellite, expectable in-orbit temperatures ranges could be shifted. For example, peak temperatures of the satellite could be reduced in up to 50K just by switching from black paint to white paint. At the same time, battery average temperature could be accommodated in the range of -2 to 39 C° by modifying the coating of the external surfaces of the satellite.

Summing-up, the alteration of the optical properties of the external side of the shear panels of a PocketQube such as the DelfiPQ affects maximum, minimum and average temperatures of all the subsets of the satellite. This makes the external coating a useful means of achieving thermal control.

Sensitivity to ε of the internal surface of shear panels.
In this case, the variation of the optical properties of the internal surface of the shear panels seems to have a little impact on the temperatures of the shear panels itself. On the other hand, it plays a role for internal components and board, in particular for the battery.

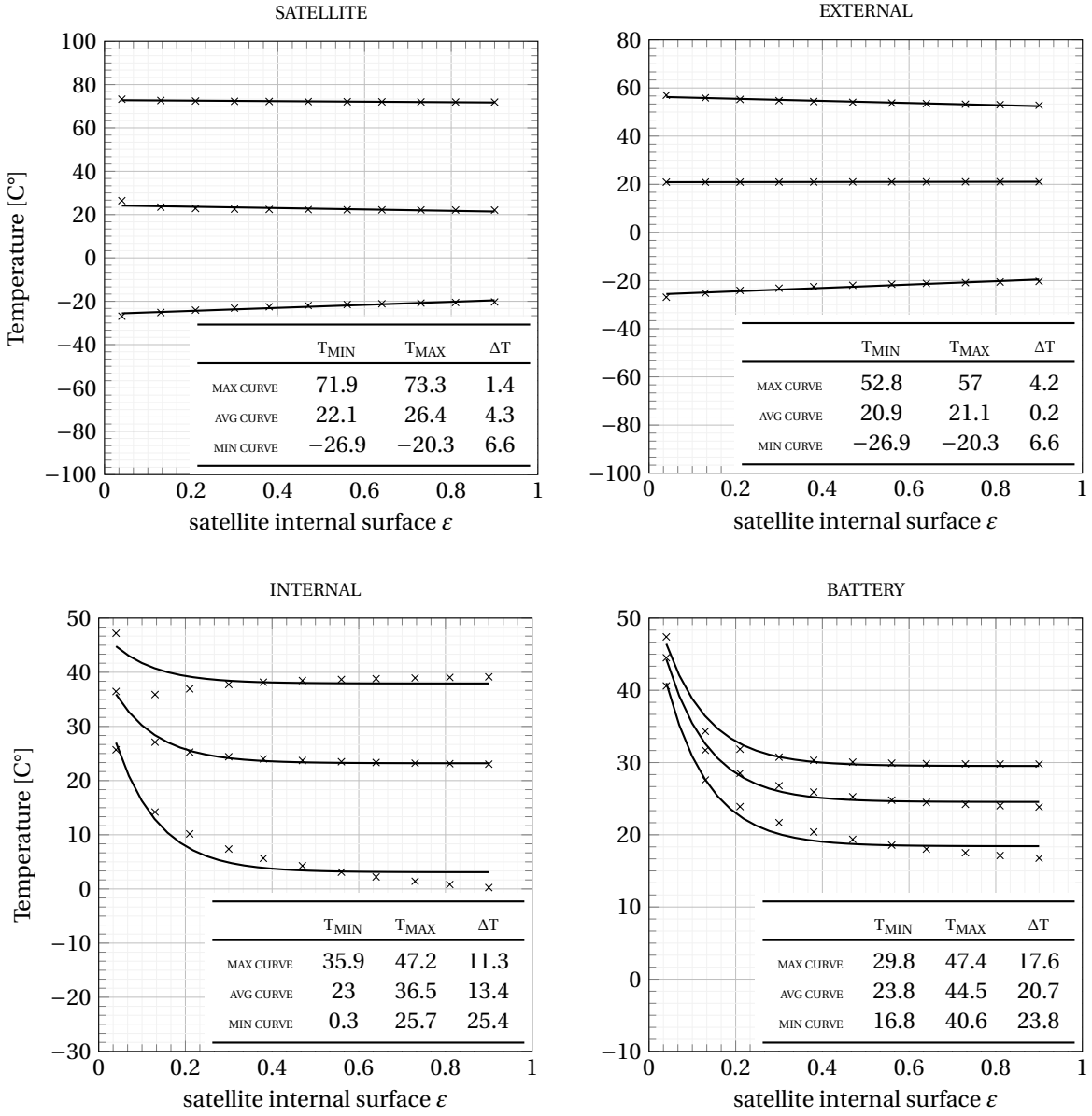

Figure 4.3: Temperature sensitivity to the optical properties of the internal surfaces of the shear panel of the satellite.

According to figure 4.3, the higher the emissivity of the internal surfaces, the lower the temperatures of the battery and internal components. Given that these components are surrounded by the shear panels, and

that they emit in the infrared range, an increase on emissivity makes the thermal coupling to the shear panels stronger. These shear panels, when pointing towards space, act as a radiator then, absorbing energy from the internal components and radiating it to space. Therefore the more coupled the internal components are to the shear panels the lower the temperature they experiment.

Quantitatively, the impact in temperature change of varying the optical properties of the internal surface of the shear panels is around 3 times weaker for the average temperature of internal components and 2 times weaker for the average temperatures of the batteries, when compared to varying the optical properties of the external surfaces. In any case, the change is still important and so changing this optical property could be used for thermal control of the spacecraft.

Sensitivity to ε of the boards.
As shown in the results, the impact of modifying the optical properties of the internal boards is limited.

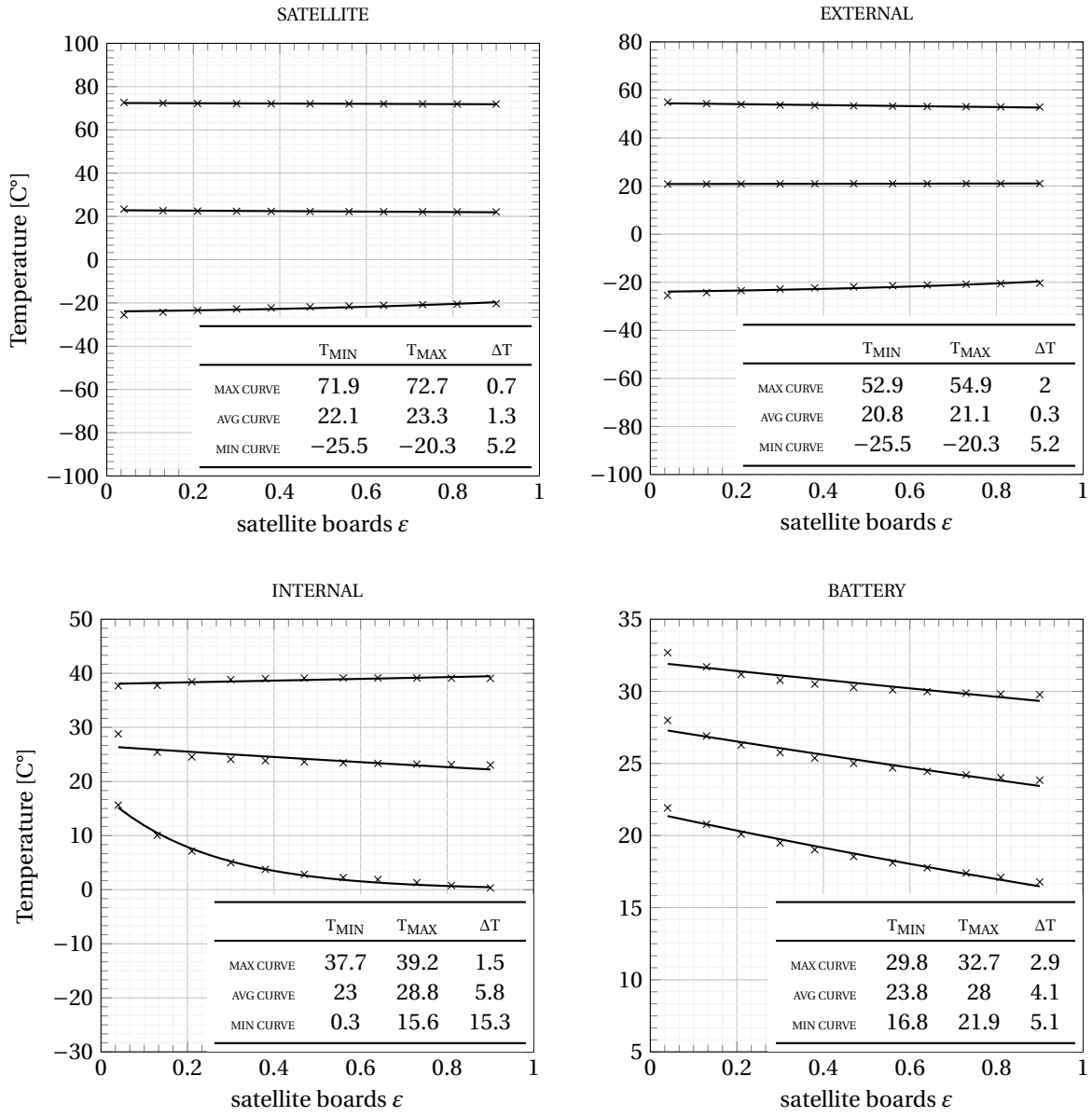

Figure 4.4: Temperature sensitivity to the optical properties of the internal elements of the satellite.

The most relevant impact on temperatures is the minimum ones of the boards itself. Similarly to the situation explained earlier, an increase in the emissivity of the boards increases the coupling to the side panels

which actuate as radiators, therefore decreasing the temperatures of the internal elements of the satellite. As shown in the results, this could decrease minimum temperatures from 15 C° down to 0 C°.

Sensitivity to ε of the battery.
The change in the coating of the battery has to have almost no impact on none of the elements of the satellite, including the battery itself.

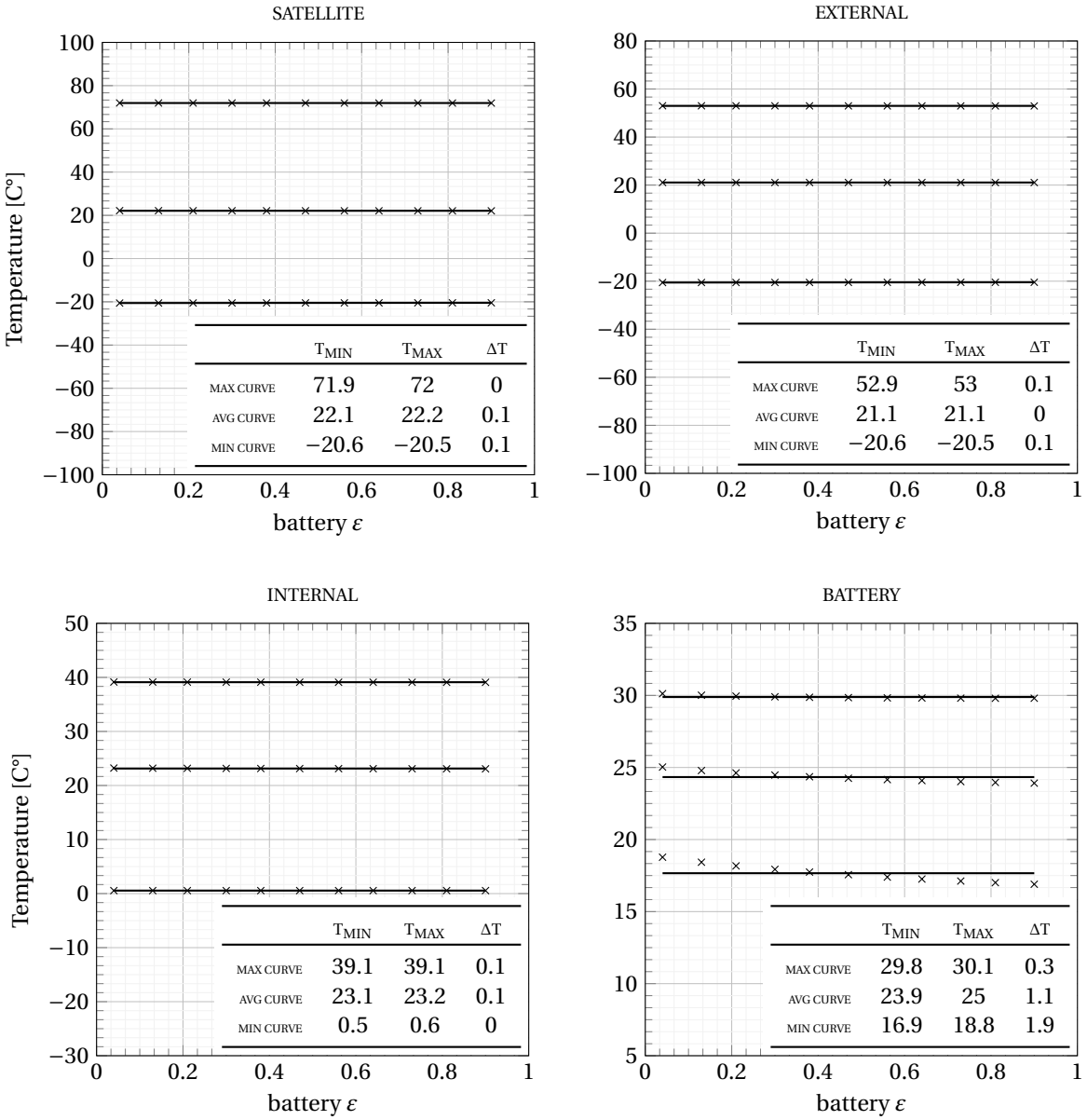

Figure 4.5: Temperature sensitivity to the optical properties of the battery.

The results show a negligible impact on temperatures of the satellite in general, external and internal components. This is expectable as surface of the batteries represent a small surface when compared to the total surface areas of the entire satellite. On the other hand, it might seem counterintuitive that a change in emissivity of the battery has such a low impact on the temperatures of the battery itself. This could be explained by the fact that the temperature of the battery is kept quite constant and similar to its environment along the orbit, as shown by the thermal analysis of chapter 3. Refer to figure 3.13. Therefore, radiative coupling does not play an important role on heat exchange. Summing-up, under the constraints of the study, changing the coating of the battery has a little impact on its temperatures, and therefore, might not be the best approach to achieve proper thermal control.

4.2. Thermal Environment

The thermal inputs coming from the environment are mainly defined by the orbit in which a spacecraft is injected. Therefore, it is fundamental for this study to investigate which are the characteristics of the most common orbits PocketQubes will be using. The prediction of the orbits is based on limiting factors, literature survey and an analysis of the orbits of CubeSats.

Few picosatellites have been launched into space. Contrarily, more than a thousand nanosatellites have been successfully placed in orbit. Being those the most similar ones to PocketQubes in applications and features, a statistical study of the orbits used by nanosatellites is used to infer which are the preferred orbits.

Data from a total number of 2207 nanosatellite missions was extracted in August 2018 from the nanosatellite database [2]. According to it, 860 were not launched, 179 were canceled and 48 failed to launch. For the remaining 1120 satellites, the orbits could be classified as presented in Figure 4.6. The vast majority of nanosatellites are injected in low Earth orbits (LEO) and just a few of them were sent (or are planned to be send) further away; to GEO, heliocentric, lunar or interplanetary orbits.

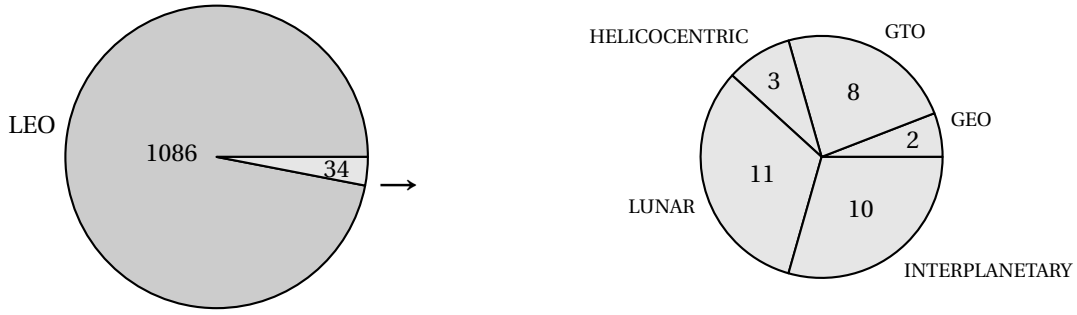

Figure 4.6: Distribution of orbits for nanosatellites, based on [2].

According to Bouwmeester et al, who analyzed the conditions and application domains for PocketQubes [3], picosatellites are expected to be placed at low altitudes, in the neighborhood of the Earth. Most of them could be forming vast constellations in LEO.

Spaceworks announced in its last version (2017) of the nano/microsatellite forecast [30] that Earth and remote sensing would be the preferred mission for these spacecraft, increasing from a previous mark of 43% to 64% for the coming years of the missions devoted to EO.

Based on the forecasts and historical data it can be assumed with a certain degree of confidence that the main domain for future PocketQube missions will be low altitude orbits in the neighborhood of our planet.

The three main thermal inputs: solar radiation, Bond albedo and infrared power coming from the planet are estimated providing expected values as well as upper and lower boundaries.

4.2.1. Orbital parameters

Before starting to define the orbits of PocketQubes and the corresponding environmental inputs with more detail, it is convenient to understand how orbits are defined. Refer to appendix B for background information on this topic. The parameters under study are the orbital altitude, the inclination and the local time of the ascending node. The nominal and boundary values for these parameters were introduced in Table 3.1.

Eccentricity

Sensitivity to orbital eccentricity is not investigated as PocketQubes are unlikely to be injected in elliptical orbits, being circular orbits the most common ones for LEO. This is corroborated by orbital data from the nanosatellite database corresponding to the 1086 nanosatellites analyzed that were injected in low Earth orbits. A total of 976 out of the 1086 satellites are reported to have an eccentricity lower than 0.005. Few nanosatellites have a higher eccentricity, being the highest one found 0.12.

Therefore, for simplification purposes and without loosing generality, the value of eccentricity can be considered null. Slightly eccentric orbits could be associated to inaccuracies in orbital injection or the effects of gravitational perturbations. This implies that all orbits considered in this study are circular.

Altitude
The altitude in which PocketQubes might be injected depends on limiting factors such as reentry regulations, orbital occupation, observability by radar, mission constrains (EO), and communication/power restrictions. All these parameters will be analyzed in the following paragraphs.

Because of the reduced external surface area of PocketQubes and the lack of space on board for de-orbit mechanisms, they are usually bound to the aerobreaking effect of the atmosphere to reentry. In order to comply with space debris regulations, the maximum possible altitude for these satellites should fall between 630 and 760 km depending on their mass and external surface area, therefore ensuring reentry in 25 years time or less since the moment of injection into orbit (refer to [3], Figure 3, page 4). This data contemplates all different type of PocketQubes considered in the study as stated in previous sections. However, this lifetime limit might be revised in the future and so a more realistic one of 5 years is suggested in the aforementioned paper, for which the maximum altitude would then be 480 km.

Taking a look at the count of objects as a function of the altitude in LEO orbits (see figure 4.7, gray columns, right axis), one can observe that the gross is located in the region of 600 to 1100 km, with two peaks around 800 km altitude. The first peak is due to the debris generated after the collision of the Cosmos-2251 (950 kg) satellite with the Iridium-33 (560 kg) satellite. They collided in February 2009, at an altitude of 789 km and a velocity of 42120 km/h. The second peak relates to the destruction of the FY-1C (750 kg) satellite as part of an anti-satellite missile test carried by China in January 2007 at an altitude of 865 km.

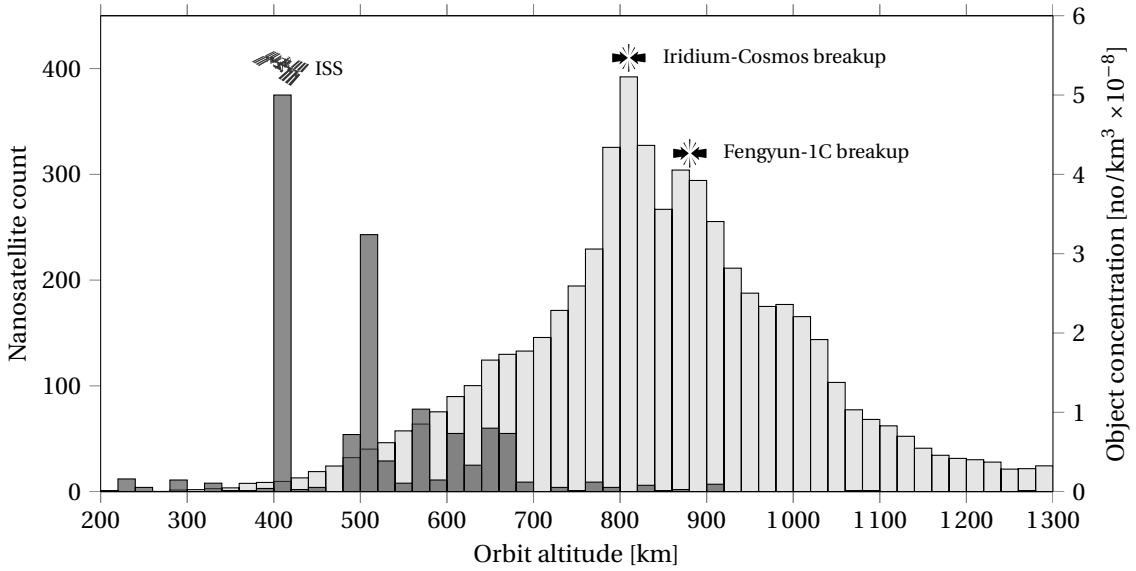

Figure 4.7: Nanosatellite orbital occupation according to [2].

Based on the orbital occupation of LEO orbits by altitude, Bouwmeester et al. propose the range 300 to 400 km as ideal for PocketQubes. Nevertheless, according to [3], all PocketQubes located at an altitude of 300 km are expected to reenter in less than half a year, most likely less than two months, due to the aerobreaking effect of the atmosphere, which is a reduced lifetime in spacecraft terms.

Most of the already launched nanosatellites, according to SpaceWorks Nano/Microsatellite forecast, are deployed either from the ISS or injected in a Sun-synchronous polar orbit (SSO). This is corroborated by orbital data from the nanosatellite database corresponding to the 1086 nanosatellites in LEO (see figure 4.7, blue columns, left axis). The most popular altitude for nanosatellites, with almost 400 deployments, is around 400 km which correspond to injections from the ISS orbiting the Earth at the same altitude. The second most popular altitude used is around 500 km, with a count of circa 300 spacecraft. There are few nanosatellites injected at altitudes higher than 700 km.

Observability by radars is another important issue. The reflected radar signal is inversely proportional to the power 4 of the distance, which could be another argument in favor of using lower orbits for picosatellites. Nonetheless, PocketQubes at 600 km altitude have been already tracked successfully by radars.

In the same direction communications and mission-related constraints are found. Being the most popular mission expected for these spacecraft Earth Observation, and taking into account the reduced volume for the optical instrumentation on-board, the closer the satellites to the surface of the Earth the better the resolution they might be able to achieve. Regarding communications, these spacecraft are expected to have restricted power budgets meaning that the further away from the ground station, the less the information that can be down linked.

Considering that the international space station lacks deployers for picosatellites, and with an expected decay in popularity of ISS deployments of nanosatellites from a current 61% to just a 15% of the injections during the coming years according to SpaceWorks [30], this option is discarded as favorite or nominal. This argument is as well supported by the numerous companies developing dedicated launchers for PocketQubes and CubeSats that have been flourishing in the latest years.

Table 4.4: Sensitivity cases for orbital altitude.

ID	Case	Altitude [km]
t_1	0	300
t_1	1	346
t_1	2	392
t_1	3	438
t_1	4	484
t_1	5	530
t_1	6	576
t_1	7	622
t_1	8	668
t_1	9	714
t_1	10	760

To keep the research constraints wide, a maximum orbital altitude of 760 km (to comply with deorbiting regulations and due to the lack of nanosatellites injected in higher orbits) and a minimum of 300 km (as for lower altitudes lifetime will range from few months to few days) are considered in this study. A nominal altitude for these satellites is chosen as 480 km as it ensures a lifetime ranging from a couple of months up to 5 years depending on the type of PocketQube and it seems to be the preferred altitude for nanosatellites.

The altitude of the orbit plays an important role in the determination of the environmental inputs. More specifically the ones coming from the planet. Table 4.4 contains the cases generated for the analysis of sensitivity to altitude.

Inclination

Taking a look at the statistical data of the LEO satellites from the nanosatellite database (figure 4.8), it comes clear that there are two preferred inclinations. The firs one, 52° with more than 400 satellites correspond to the missions deployed from the International Space Station, which shares the same inclination. The second one, around 97°, correspond to the specific inclination needed to achieve a sun-synchronous orbit (SSO).

Sun-synchronous orbits have potential advantages for EO satellites, as they always encounter the same illumination conditions when passing over a point of interest of the Earth. As well, because the inclination required is close to 90°, the orbit is nearly polar allowing the satellite to inspect all latitudes of the Earth. Alba Orbital aims to launch to SSO polar orbits at an altitude between 350 to 550 km. Unisat-5 with the only four PocketQube launched into space was set into an orbit of 600 km altitude, 97.5 degrees inclinations, SSO, polar.

Taking into account the aforementioned reasons which predict a decay in launches from the ISS, it is assumed, that most of the future PocketQubes will be injected in SSO orbits. Therefore, the nominal value for orbital inclination is set to ≈97°. For sensitivity purposes all the range from 0° to 180° is explored. Because having a retrograde orbit does not impact the thermal results, studying half of the range (0° to 90°) is enough to characterize the sensitivity to orbital inclination. Table 4.5 contains the different analysis cases. Note that for each case, the Albedo and planet infrared emissions (OLR, planet temperature) vary. This has been taking into account into the simulations. The data pertaining Albedo and OLR has been extracted from [29].

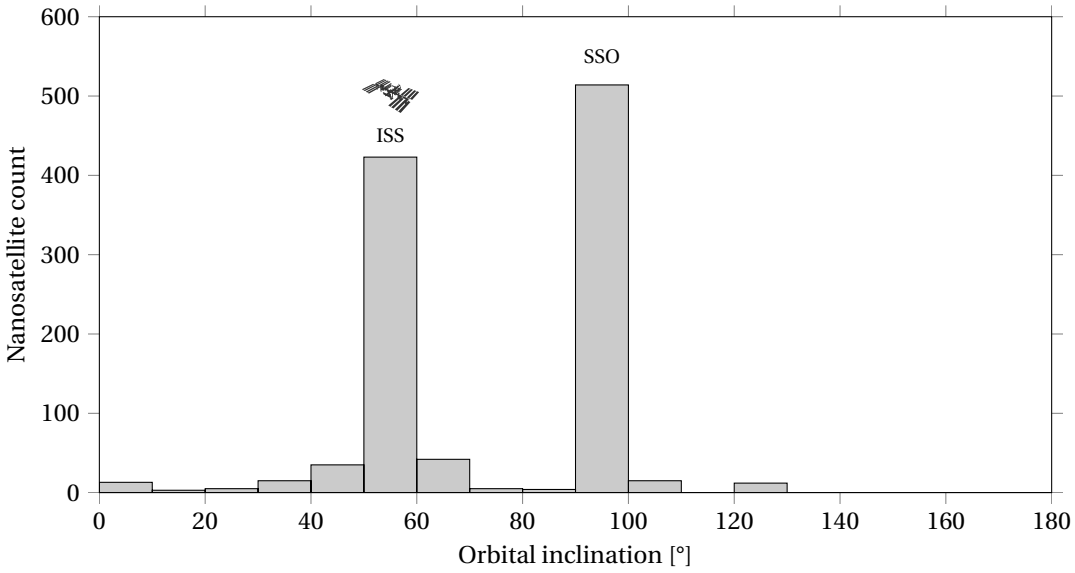

Figure 4.8: Orbital inclination distribution for successfully launched nanosatellites.

Table 4.5: Sensitivity cases for orbital inclination.

ID	Case	Inclination	Albedo	OLR	Planet T
t_2	0	0	0.18	246	266 K
t_2	1	10	0.18	246	266 K
t_2	2	20	0.18	246	266 K
t_2	3	30	0.22	235	263 K
t_2	4	40	0.22	235	263 K
t_2	5	50	0.22	235	263 K
t_2	6	60	0.23	233	262 K
t_2	7	70	0.23	233	262 K
t_2	8	80	0.23	233	262 K
t_2	9	90	0.23	233	262 K

Local Time of the Ascending Node

The local time of the ascending node has a direct impact on the determination of the eclipse duration, as explained in section 3.5.1. Table 4.6 summarizes the cases to be investigated, and the associated beta angle and percentage of the orbit in eclipse.

Table 4.6: Sensitivity cases for local time of the ascending node.

ID	Case	RAAN	β-angle	eclipse
t_3	0	0	65.9°	14.3%
t_3	1	30	16.4°	37.4%
t_3	2	45	31.3°	35.8%
t_3	3	60	46.2°	32.1%
t_3	4	90	75.4°	0%
t_3	5	120	72.4°	0%
t_3	6	135	57.9°	25.4%
t_3	7	150	43.1°	33.1%
t_3	8	180	13.4°	37.7%

Sensitivity results on orbital parameters

The following figures show the impact on temperature of varying the orbital parameters of the external and internal surfaces of the shear panels, the ones of the boards and the ones of the battery, according to the values presented.

Sensitivity to altitude.
The impact of the orbital altitude on the temperatures of the satellite seem to be important, specially for the minimum values registered.

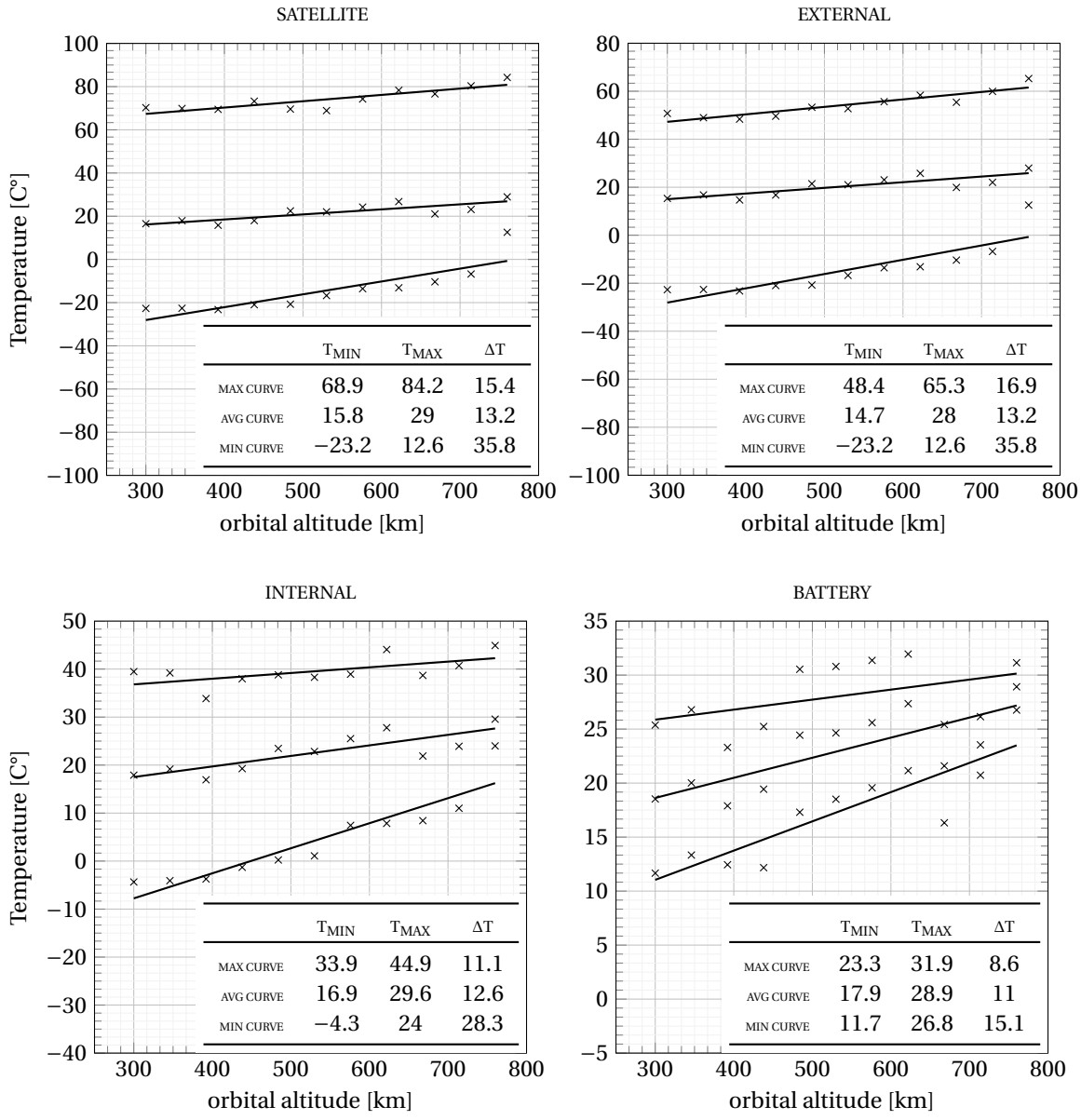

Figure 4.9: Temperature sensitivity to orbital altitude.

For the external surfaces of the satellite, as well as for the temperatures of the satellite in general, the results show a trend, where temperatures tend to increase for higher values of altitude. The increase in average temperature in both cases is 13 C°. The minimum temperatures on the other hand climb almost three times more, up to 35.8C°. One could think this is due to a reduction of the eclipse time, which goes from 1311 seconds for the orbit of 300 km altitude to 1293 seconds for the orbit of 760 km altitude. The difference is only of 20 seconds longer eclipse. According to the thermal time constant and the trends observed in the results presented in Chapter 3, the increase in temperatures due to the eclipse reduction should be in the order of 1

C°.

There is no clear correlation between altitude and internal temperatures.

Sensitivity to orbital inclination

On the other hand, there is a clear correlation for the temperature of all subsets of the satellite and the inclination. The higher the inclination, the higher the average and minimum temperatures, with increases around the 20 C°. The maximum temperatures seem to be less affected by inclination.

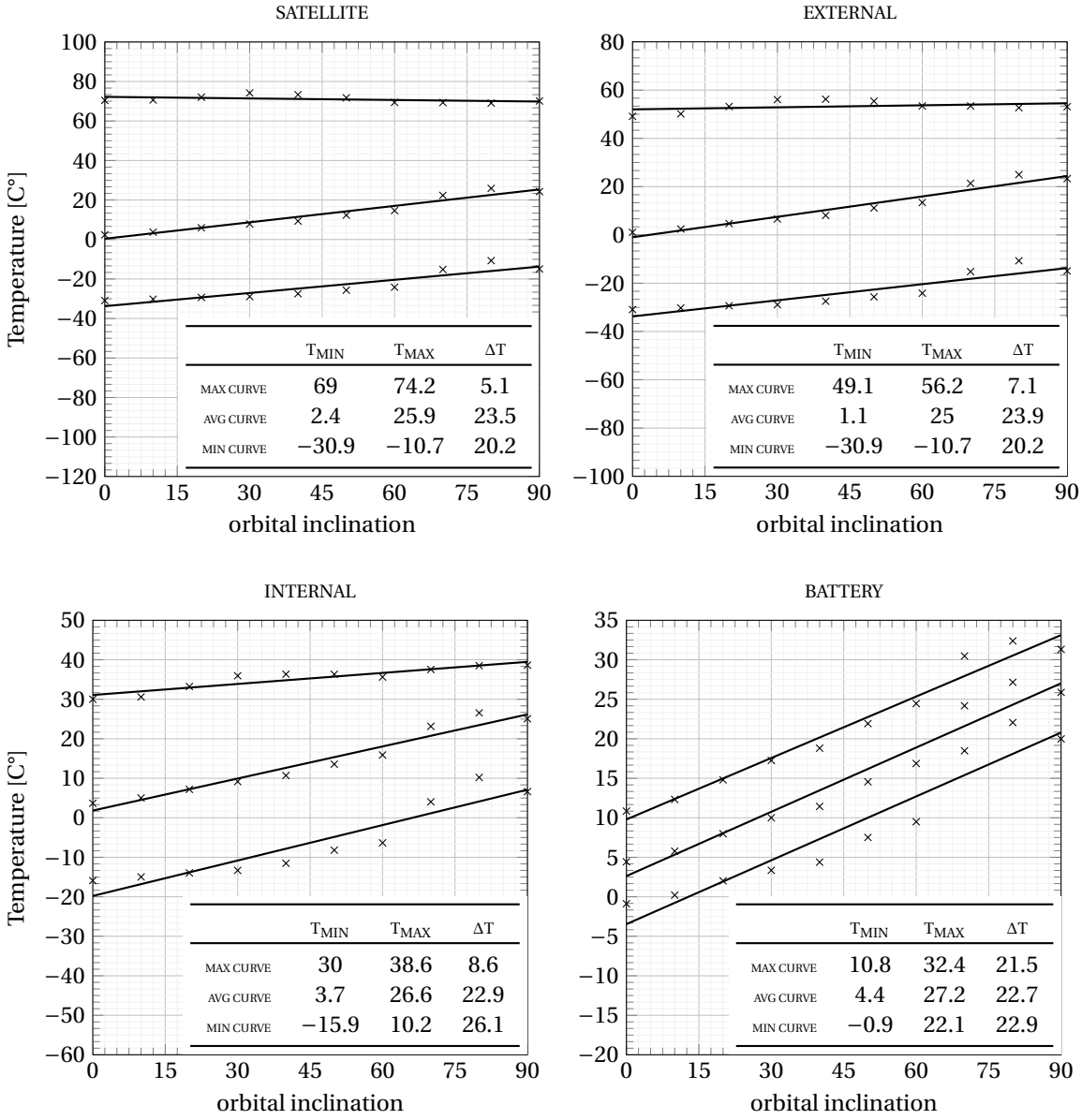

Figure 4.10: Temperature sensitivity to orbital inclination.

According to table 4.5, the higher the inclination the stronger the Albedo (as the satellite orbit the poles of the Earth). On the contrary the OLR from the planet seems to decrease. But the true reason for this increase in temperature with inclination is that the eclipse time vastly changes, from 2281 seconds for an equatorial orbit to only 810 seconds, for a polar orbit. This is a difference of 24 minutes of eclipse.

In summary, inclination is not the only contributor to temperature change as shown in the charts. The eclipse, which effect couldn't be isolated, plays an much important role.

Sensitivity to RAAN.

The results show a trend that is clearly correlated with the eclipse duration. The percentage of orbit under eclipse has been plotted as a red line to highlight this correlation.

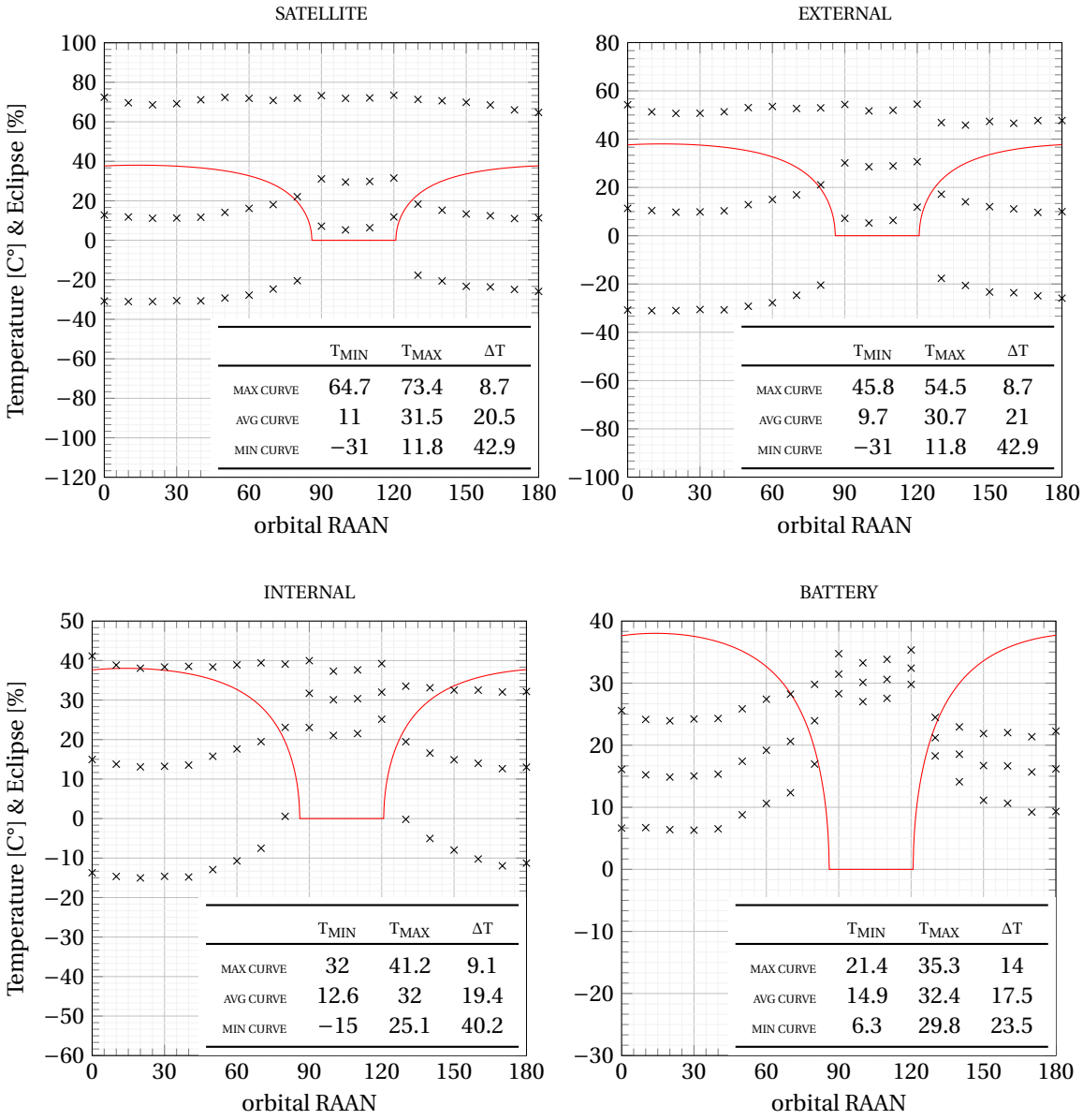

Figure 4.11: Temperature sensitivity to right ascension of the ascending node.

In this case the change in temperature is mostly caused by the effect of the eclipse duration, as other parameters do not vary in this case such as altitude, inclination, Albedo or OLR (being those the nominal ones). The results show that there is no clear trend or correlation of maximum temperatures and RAAN (eclipse time). On the other hand, the average temperatures drop for all elements of the satellite around 20 C° from a situation of no eclipse to the one in which is eclipse is maximum. The effect is even more intense for the minimum temperatures, in the order of 40 C°. The batteries are an exception, with temperatures dropping only 20 C° from a situation of no eclipse to the one of full eclipse lenght.

This results are in accordance to the ones presented in Chapter 3. Temperatures on the satellite keep doping since the moment it enters the eclipse. The longer the eclipse, the more the temperatures will drop.

4.2.2. Bond Albedo and IR radiation

A conservative method to asses the power input coming from Albedo and Earth IR sources is to use statistical data captured by sensors on-board satellites orbiting the Earth at low altitude orbits. The data used, which has been extracted from [29] comes in function of the inclination of the orbit and the average time. The smaller the period of time, the higher the variation. This period of time could be linked to the thermal constant of the satellite. For a 3p pocketqube such as the Delfi-PQ in its first configurtion, the thermal constant is estimated to be around 560s. For the smallest possible configuration of Pocketqubes, the 1p, the thermal constant could be assumed to be approximately a third of the one of the DPQ, lets say 180s. The tables show data for either 128 or 896 seconds average. The 128 seconds average is chosen for determining this data.

For the nominal case, a high inclination and an average time of 128 seconds is chosen, leading to an average albedo of 0.23, and an average Earth IR of 233 W/m2 (Planet Temperature = 262.5K).

For the cold case, mission-critical data is chosen, 128 seconds and high inclinations. The combined extreme is an albedo of 0.31 and an Earth IR of 262 W/m2 For the hot case, mission-critical data is chosen, 128 seconds and high inclinations. The combined extreme is an albedo of 0.16 and an Earth IR of 212 W/m2.

For studying of variation in Albedo, a minimum value of 0.06 (273 IR) and a maximum of 0.49 (128 IR) is found. For studying of variation in IR, a minimum value of 111 (Albedo 0.38) and a maximum of 331 (Albedo 0.22) is found.

Table 4.7: Sensitivity cases for Albedo.

ID	Case	Albedo	OLR	Planet T
t_4	0	0.06	273	273
t_4	1	0.108	257	269
t_4	2	0.156	241	264
t_4	3	0.203	225	260
t_4	4	0.251	209	255
t_4	5	0.299	192	250
t_4	6	0.347	176	245
t_4	7	0.394	160	239
t_4	8	0.442	144	233
t_4	9	0.490	128	226

Table 4.8: Sensitivity cases for Earth IR power.

ID	Case	OLR	Albedo	Planet T
t_5	0	111	0.380	218
t_5	1	135	0.362	229
t_5	2	160	0.344	239
t_5	3	184	0.327	247
t_5	4	209	0.309	256
t_5	5	233	0.291	263
t_5	6	258	0.273	269
t_5	7	282	0.256	275
t_5	8	307	0.238	281
t_5	9	331	0.220	287

Sensitivity results on Albedo and OLR

Sensitivity to Albedo.
The results show little correlation between Albedo and temperature changes.

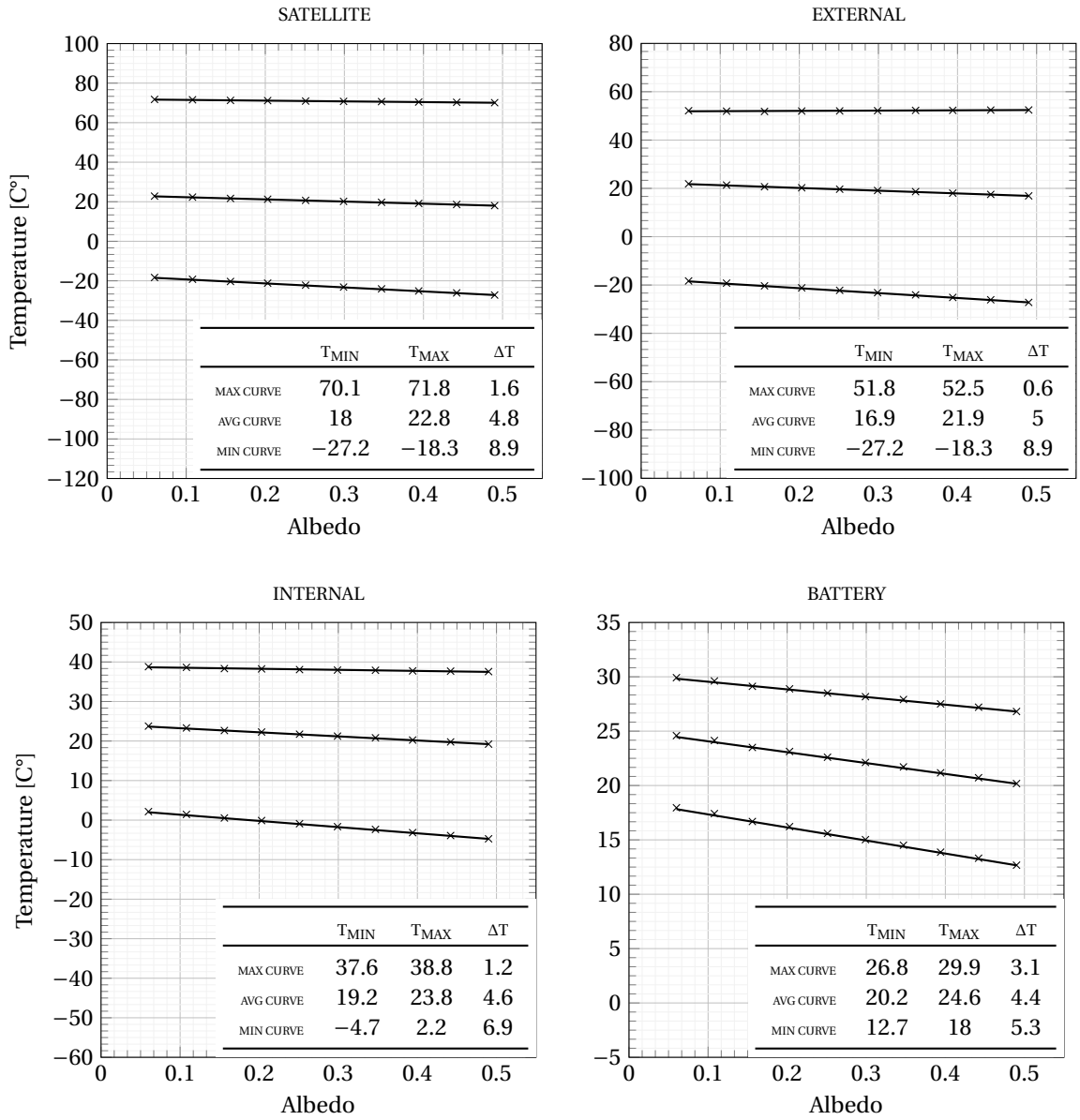

Figure 4.12: Temperature sensitivity to Earth Albedo.

The maximum temperatures are practically unaltered with changes in Albedo. On the other hand, average, and specially minimum temperatures seem to be slightly influenced by Albedo, in the order of 5C° to 9C°. The trend indicates that the higher the Albedo, the lower the temperatures. Although it may seem counter-intuitive, the fact that the OLR drops with increases in Albedo, as indicated in table 4.7, could be the reason behind this trend.

Sensitivity to OLR.
Outgoing longwave radiation have a stronger impact on satellite temperature, although still limited.

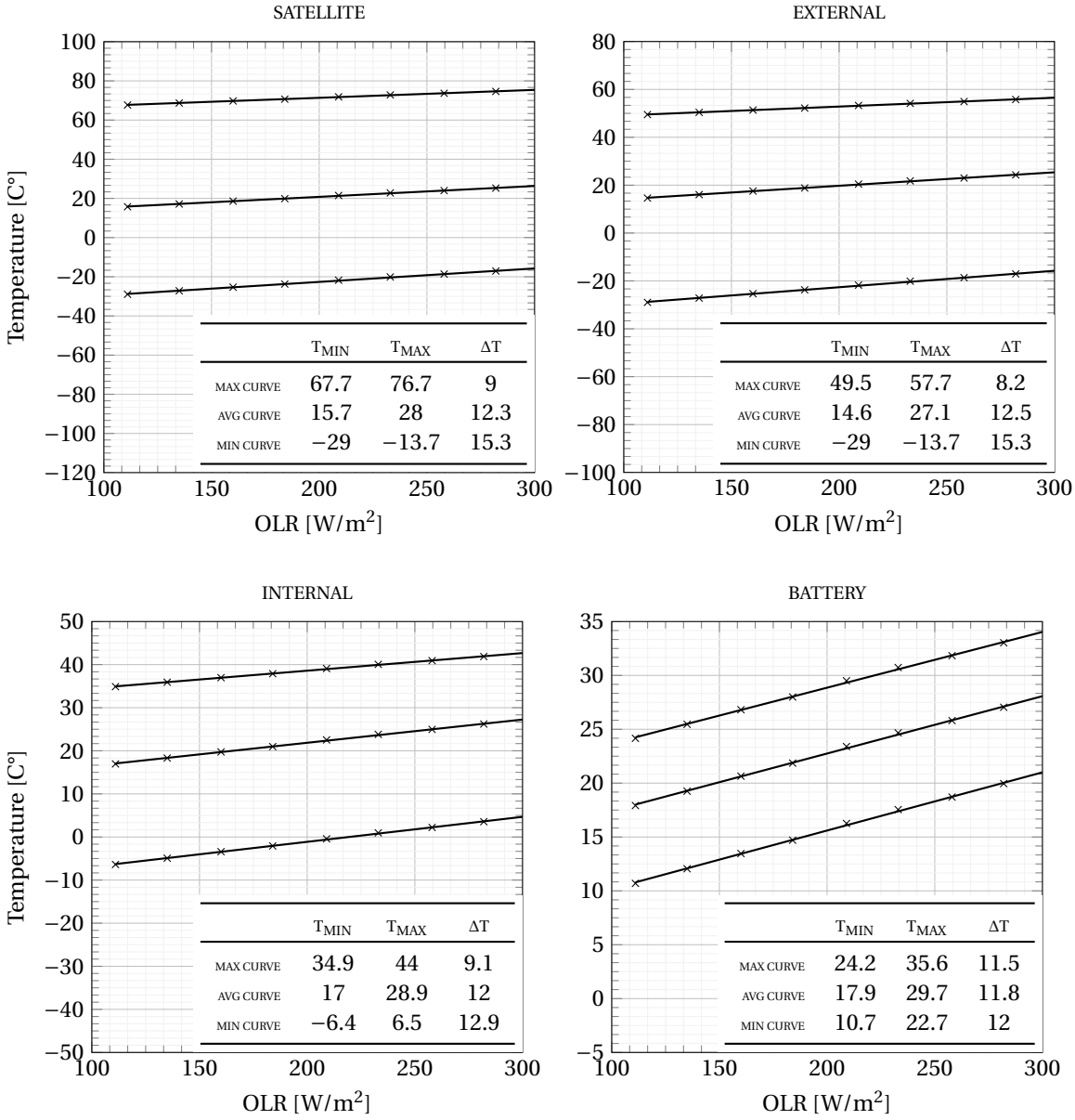

Figure 4.13: Temperature sensitivity to Earth IR Radiation.

The trends indicate that the more the infrared energy radiated by planet Earth, the higher the temperatures (maximum, average and minimum) for all subsets of the satellite. The change is similar for all the categories, around 10 C° increase in temperature from the case with minimum OLR to the one with maximum OLR.

4.2.3. Solar radiation

According to the conclusions drawn on section 3.5.1, the intensity of solar power in the vicinity of the Earth varies from 1322 to 1414 Wm^{-2}. Table 4.9 reflects the cases investigated.

Sensitivity to solar radiation.
The results show a clear trend indicating that an increase in solar power increases the temperature of all elements of the satellite, having a slightly higher impact on the maximum temperatures. The magnitude of this impact nevertheless is quite reduced, around 4 C°.

Table 4.9: Sensitivity cases for solar power in W/m^2.

ID	Case	Sun Power
t_6	0	1322
t_6	1	1332
t_6	2	1342
t_6	3	1353
t_6	4	1363
t_6	5	1373
t_6	6	1383
t_6	7	1394
t_6	8	1404
t_6	9	1414

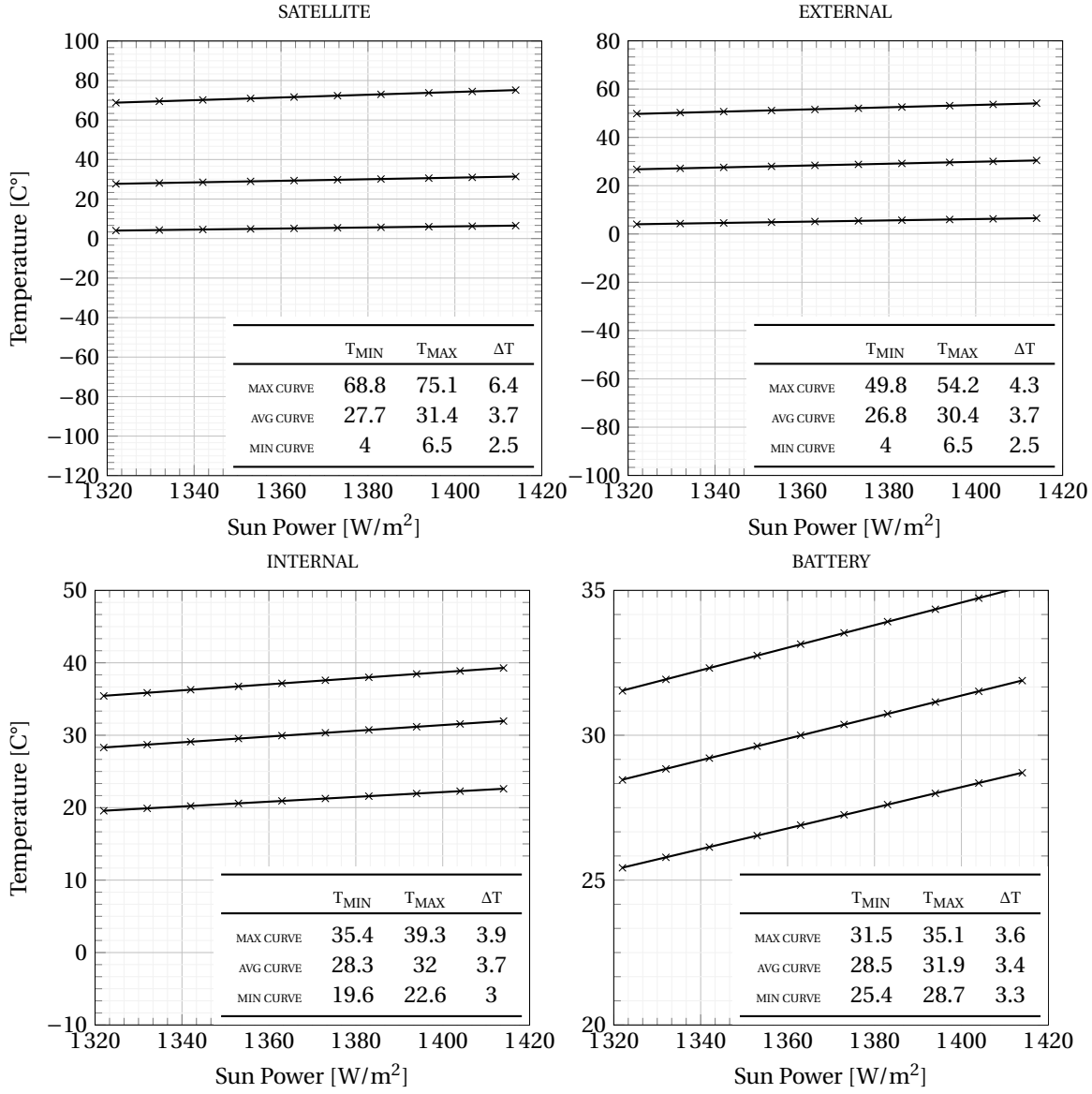

Figure 4.14: Temperature sensitivity to Sun Power.

4.3. Thermal Capacity

The thermal capacity of the entire satellite as a system and its components in particular plays a role in determining the amplitude of temperature fluctuations along the orbit.

The thermal capacity of a material or element is measured in [J K^{-1}] and indicates how much thermal energy has to be inputed or extracted from the system to induce a change in temperature of 1K in it. Qualitatively, materials with high thermal capacity absorb large quantities of energy with small increases of temperature. They act as a thermal energy storage and help reducing the amplitude of temperature swings.

The thermal capacity of a geometry is usually derived from its equivalent intensive property, specific heat C_{sp} [J kg^{-1} K^{-1}], and other model parameters such as the density of the material ρ, its thickness t, physical dimensions (width l_1 and length l_2) and the number of nodes in the geometry N. The finite element software requires as input all the aforementioned properties but in the end only uses the thermal capacity of each node C_N for the computation of temperatures. The way in which the software computes the thermal capacity of each node is presented in equation 4.1. This formula assumes all the nodes of the geometry have equal dimensions.

$$C_N = \left(\frac{l_1 \cdot l_2}{N} \cdot\right)\left(t \cdot \rho \cdot C_{sp}\right) \tag{4.1}$$

Therefore the thermal capacity of the nodes which represent the satellite are affected by geometrical and meshing factors (which stay constant once the geometry of the satellite is defined) as well as by the product of thickness, density and specific heat, which value is altered to study sensitivity on temperatures. This product depends on three variables which can be chosen independently. In order to facilitate the analysis, the thickness and density of the geometries are kept constant in the model for each geometry (t_{model}, ρ_{model}), and the specific heat C^*_{sp} is used as varying parameter, including possible changes for thickness and density (see equation 4.2 for clarification).

$$C^*_{sp} = \frac{t \cdot \rho \cdot C_{sp}}{t_{\text{model}} \cdot \rho_{\text{model}}} \tag{4.2}$$

The gross composition of a PocketQube counting towards the thermal capacity of it lies in the materials of its internal printed circuit boards, shear panels, deployable wings, electronics, payloads, battery and structural elements.

Printed Circuit Boards

Printed circuit boards are the elements which structurally support and electrically connect electronic components. They are comprised of several layers of non-conductive substrate and copper and commonly manufactured as thin 2D surfaces. The most common material used as non-conductive substrate is FR4 (glass-reinforced epoxy laminate). Two different types of copper layers can be distinguished being those ground layers and signal layers. The first ones consists of full planes of copper and are used to provide power to the electronic components. The latter ones consists on traces (copper paths) carrying electrical signals among electronic components.

The number of copper layers in a PCB vary from a single one up to tens of them. PCB providers usually offer standard pool PCB with up to 8 layers, and non-pooled with up to 16. The thickness of a single copper layer can vary from 12 micrometers (1/3 oz.) to up to 105 micrometers (3 oz.), being the usual thickness 35 micrometers (1 oz.). Common PCB thickness is 1.55 mm but can vary from as low as 0.20 mm up to 3.2 mm. Copper has a density of 8960 kg/m^3 and thermal capacity of 385 J/kg K while FR4 is known to have a density around 1850 kg/m^3 and a thermal capacity of 950 J/kg K, being FR4 comprised of woven fiberglass (≈700 kg/m^3) embedded in epoxy resin (≈1000 kg/m^3). With this information extreme cases as well as a nominal case for the heat capacity of PCB are computed. Reference: Eurocircuits.

In the lower boundary, a PCB with two copper layers of 12 micrometers each, and a total thickness of 0.2 mm is considered. In this case, the proportion of copper over FR-4 is equivalent to 14%. Therefore, the average density of the material would be 2820 kg m^3 and its specific heat 571 J/kg K (see properties in table 4.10). In the nominal case, a total number of eight, 35-micrometer copper layers, are considered for a PCB with a total thickness of 1.55 mm. In this case the proportion of copper in the material is 22%, the average density 3418 kg/m^3 and the specific heat 553 J/kg K (see properties in table 4.11). In the upper boundary a PCB with 16 copper layers with a thickness of 105 micrometers and a total thickness for the material of 3.2 mm is considered. For this case the average density of the material is equivalent to 2091 kg/m^3 and its specific heat to 593 J/kg K. The copper to FR4 ratio is only 4% in this case (see properties in table 4.15).

Table 4.10: Lower boundary for heat capacity of PCB.

Property	Units	Cu	FR4	PCB
t	µm	24	176	200
ρ	kg m^{-3}	8960	1850	2820
C_{sp}	J kg^{-1} K^{-1}	385	950	873
$t \cdot \rho \cdot C_{sp}$	J kg^{-1} K^{-1} m^{-2}			492
t_{model}	µm			1550
ρ_{model}	kg m^{-3}			3418
C^*_{sp}	J kg^{-1} K^{-1}			**93**

Table 4.11: Nominal value for heat capacity of PCB.

Property	Units	Cu	FR4	PCB
t	µm	280	1270	1550
ρ	kg m^{-3}	8960	1850	3418
C_{sp}	J kg^{-1} K^{-1}	385	950	825
$t \cdot \rho \cdot C_{sp}$	J kg^{-1} K^{-1} m^{-2}			4372
t_{model}	µm			1550
ρ_{model}	kg m^{-3}			3418
C^*_{sp}	J kg^{-1} K^{-1}			**825**

Table 4.12: Upper boundary for heat capacity of PCB.

Property	Units	Cu	FR4	PCB
t	µm	105	3095	3200
ρ	kg m^{-3}	8960	1850	2091
C_{sp}	J kg^{-1} K^{-1}	385	950	931
$t \cdot \rho \cdot C_{sp}$	J kg^{-1} K^{-1} m^{-2}			6229
t_{model}	µm			1550
ρ_{model}	kg m^{-3}			3418
C^*_{sp}	J kg^{-1} K^{-1}			**1176**

Shear Panels & Deployable Wings

The shear panels are part of the external structure of the satellite, serving as a support for the solar cells and absorbing shear loads during launch phase. The most common materials they could be manufactured in are FR-4, aluminum alloys or some kind of CFRP. As well, 3D printed plastic panels could be considered as a cheaper solution. In the first case, the panels itself are already used as PCB for installing the solar cells and part of the electronics for power harvesting. This is the case for example of the QubeScout-S1. In the later cases, an additional PCB board is usually added on top of the metal, composite or plastic panels to provide electrical connections for the solar cells, like in the case of the Eagle-1.

The deployable wings are assumed to be manufactured in a similar fashion as the shear panels. Both shear panels and deployable wings could be manufactured as full panels or include openings for lowering the total mass. In the extreme case the panel is reduced to a frame.

The shear panels and the wings are described as double-layer elements in the finite element model. In case the shear panels are only comprised of PCB, then, both layers are set with the properties of PCB described in the previous section and a thickness for each layer equivalent to half of the nominal. In the case the shear panels are comprised of a PCB support for the cells and an the additional structural element manufactured in aluminum, CFRP or plastic, the external layer is set with the properties of PCB and nominal thickness and the inner layer with the properties of the material to be used and nominal thickness.

Most common aluminum alloys used in aerospace applications are AA2014-T6, AA2219-T62, AA2024-T4, AA7050-T74 and AA7075-T6, with similar densities around 2800 kg m^{-}3 and specific heats close to 870 J kg^{-1} K^{-1}. Composite materials are more diverse in properties, with densities varying from 1600 kg m^{-}3 to 2000 kg m^{-}3 and specific close to 1000 J kg^{-1} K^{-1}. Plastic materials for 3D printers are ABS, polyamides (nylon) or resin (epoxy). Densities in this case range from 900 to 1300 kg m^{-}3 and specific heats from 1000 to 1600 J kg^{-1} K^{-1}.

Table 4.13: Lower boundary for heat capacity of shear panels.

Property	Units	A	CFRP	Epoxy
t	µm	500	500	500
ρ	kg m^{-3}	2800	1600	1250
C_{sp}	J kg^{-1} K^{-1}	870	1000	1000
$t \cdot \rho \cdot C_{sp}$	J kg^{-1} K^{-1} m^{-2}	1218	800	625
t_{model}	µm	1000	1000	1000
ρ_{model}	kg m^{-3}	2800	1800	900
C^*_{sp}	J kg^{-1} K^{-1}	**435**	**444**	**694**

Table 4.14: Nominal values for heat capacity of shear panels.

Property	Units	A	CFRP	ABS
t	µm	1000	1000	1000
ρ	kg m^{-3}	2800	1800	900
C_{sp}	J kg^{-1} K^{-1}	870	1000	1420
$t \cdot \rho \cdot C_{sp}$	J kg^{-1} K^{-1} m^{-2}	2436	1800	1278
t_{model}	µm	1000	1000	1000
ρ_{model}	kg m^{-3}	2800	1800	900
C^*_{sp}	J kg^{-1} K^{-1}	**870**	**1000**	**1420**

Table 4.15: Upper boundary for heat capacity of shear panels.

Property	Units	A	CFRP	Nylon
t	µm	2000	2000	2000
ρ	kg m^{-3}	2800	2000	1150
C_{sp}	J kg^{-1} K^{-1}	870	1000	1600
$t \cdot \rho \cdot C_{sp}$	J kg^{-1} K^{-1} m^{-2}	4872	4000	3680
t_{model}	µm	1000	1000	1000
ρ_{model}	kg m^{-3}	2800	1800	900
C^*_{sp}	J kg^{-1} K^{-1}	**1740**	**2222**	**4089**

Table 4.16 enumerates the sensitivity cases to be studied. The data presented in Chapter 3 has been used for the battery, electronic components and structural elements.

Sensitivity to thermal capacity

Out of the six sensitivity analysis on thermal capacity, in this section, only the first two ones are presented. Cases c_3 to c_6 are presented in Appendix D. The thermal capacity, in the later cases, have negligible impact on the maximum and average temperatures of the satellite. On the other hand, the minimum temperatures are lifted around 10 C°, when increasing the thermal capacity of the internal PCB boards or the thermal capacity of the structural elements. Nevertheless is still a moderate to low impact on temperatures.

Contrary to intuition, the results show that increasing the thermal capacity of the battery within its defined range, do not make a notable impact on the temperature of the batteries itself.

Sensitivity to shear panels composition (PCB based)
Increasing the thermal mass of the shear panels have a little impact on average and maximum temperatures. On the contrary, the impact is moderate in minimum temperatures. The coldest points of the satellite could be shifted up to a total 22 C° for the external elements and 15 C° for internal ones.

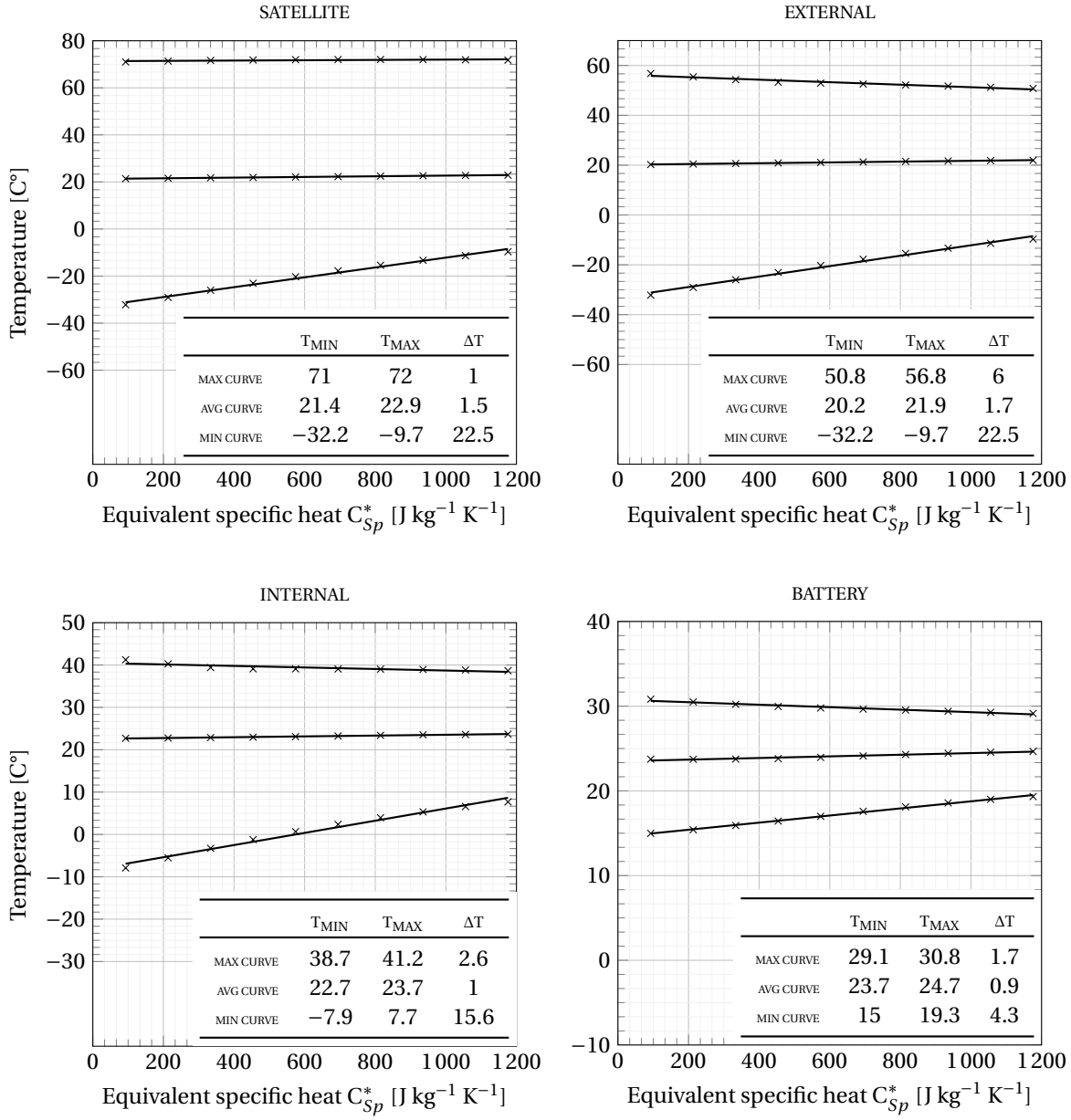

Figure 4.15: Temperature sensitivity to shear panel heat capacity, single material.

Sensitivity to shear panels composition (PCB + **Aluminum**, **Composite** or **Plastic**).
The results show that using substrates of aluminum, composite or plastic, have almost no impact on the temperatures of the satellite. By using composite substrates, higher values of thermal capacity could be achieved, although the impact in temperatures is medium to low: minimum temperatures could be lifted around 8 C° for the external surfaces of the satellite.

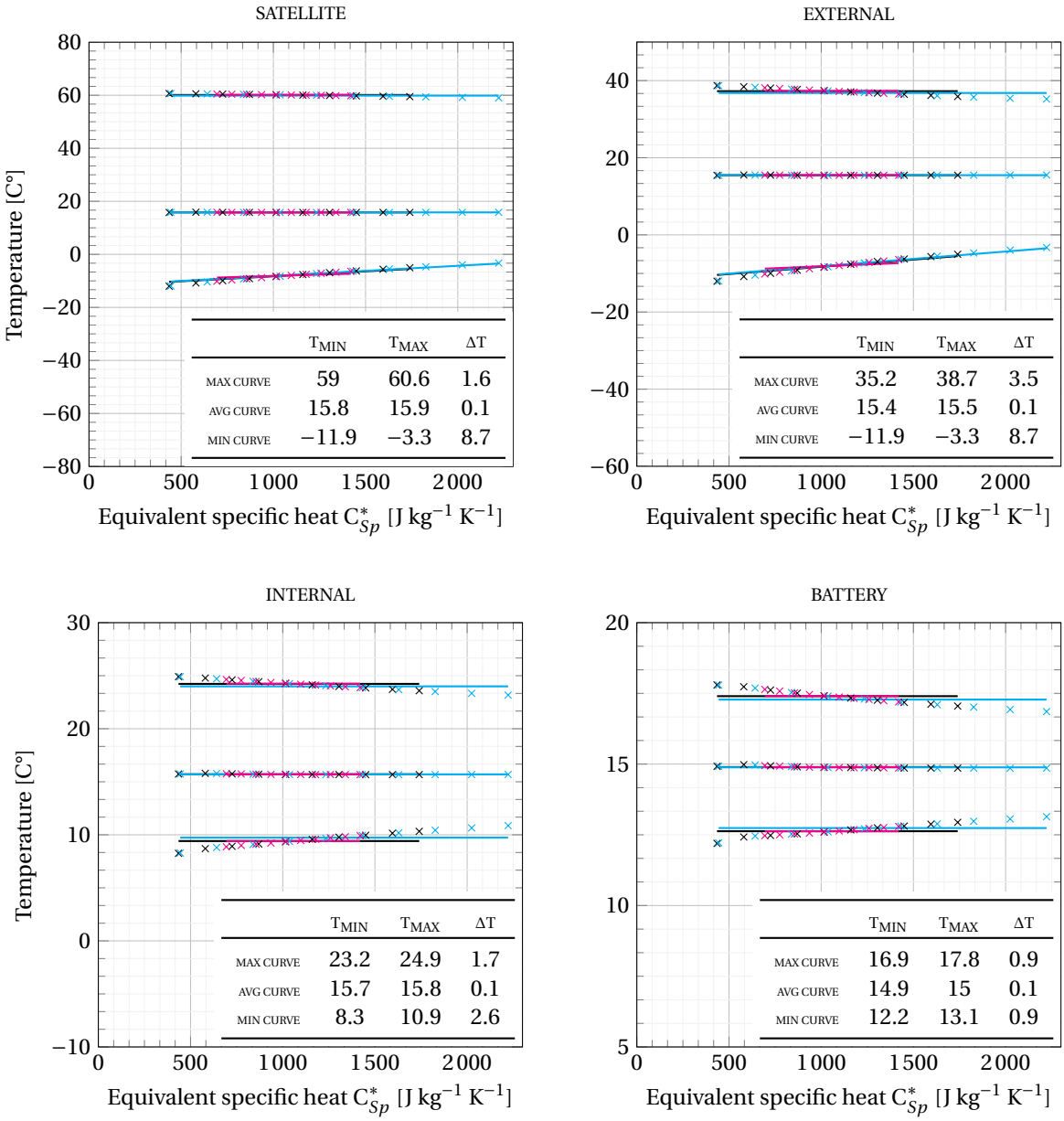

Figure 4.16: Temperature sensitivity to shear panel heat capacity, multiple materials.

Table 4.16: Equivalent specific heat values for heat capacity testing [J kg^{-1} K^{-1}].

ID	Subset	Min	Max	Nom	Units
c_1	Shear panels (PCB)	93	1176	825	J kg^{-1} K^{-1}
c_2	Shear panels (Alu)	435	1740	870	J kg^{-1} K^{-1}
c_2	Shear panels (Composite)	444	2222	1000	J kg^{-1} K^{-1}
c_2	Shear panels (Plastic)	694	1420	4089	J kg^{-1} K^{-1}
c_3	Internal Boards	93	1176	825	J kg^{-1} K^{-1}
c_4	Battery	693	930	1197	J kg^{-1} K^{-1}
c_5	Electronic components	10	18	100	J K^{-1}
c_6	Structural elements	0	0.5	10	J K^{-1}

4.4. Conductivity

The minimum, nominal and maximum values presented in Chapter 3 have been compiled in table 4.17. Six cases for conductivity are studied. Given that the the minimum, average and maximum values of conductances through spacers, standoffs, and connections of battery and electronic components to boards found are small and close together, the range has been extended in order to broaden the study (the minimum values have been reduced to 0 and the maximum increased to 10W/K.)

Table 4.17: Equivalent conductivity [W/K].

ID	Subset	Min	Nom	Max	Unit
k_1	Conductivity of PCBs	18	51	55	W/m K
k_2	Conductance board to board via spacers	0	0.24	10	mW/K
k_3	Conductance internal to external structure via standoffs	0	0.031	10	W/K
k_4	Conductance battery to board	0	0.15	10	W/K
k_5	Conductance soldered or attached components to board	0	0.90	10	W/K
k_6	Conductance solar cells to shear panels	2000	4000	15000	W/m^2 K

The results are quite uniform for all the six cases. Therefore only the first one is presented in this section (see 4.17). To check the rest refer to Appendix D.

The impact on temperatures of conductivities, within its possible range of variation, is negligible. Therefore, from a general perspective, modifying the conductive properties of materials such as PCBs or enhancing/blocking conductive paths by, for example, adding thermal straps in the first case or using thermal washers in the second, should not have a notable impact on the temperatures of the satellite.

This affirmation should be understood within the context of the research. Enhancing conductivity of PCBs could be very useful for avoiding localized thermal spots in reduced size, highly dissipating components. As well thermal washers could be useful to isolate a surface constantly pointing to the Sun or a thermal strap for connecting a highly dissipating payload to a radiator. Nevertheless, for satellites such as the Delfi-PQ in its nominal configuration and similar, the results show that conductivity is not a relevant parameter.

Sensitivity to conductivity of the PCB material.

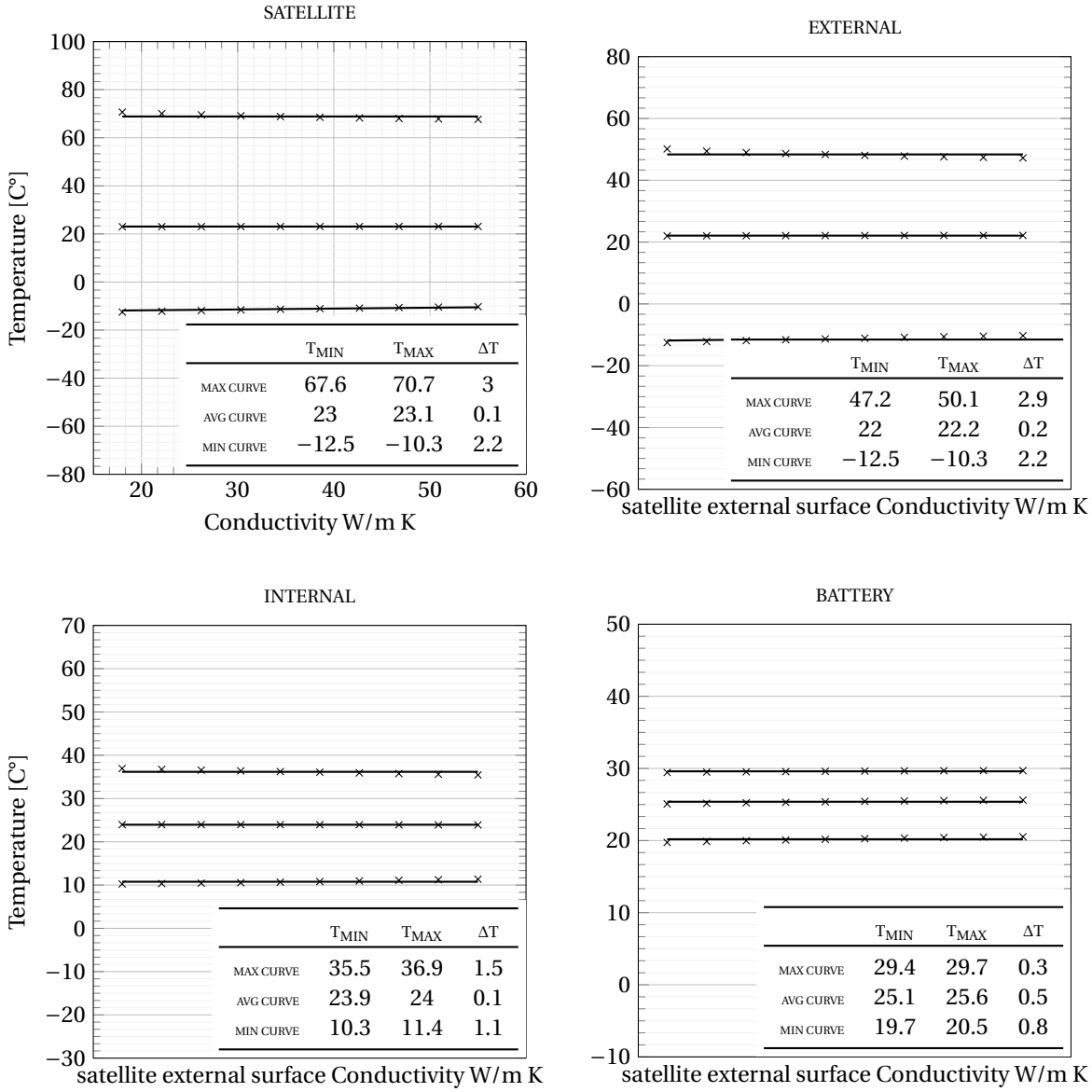

Figure 4.17: Temperature sensitivity to conductivity of PCBs.

4.5. Internal configuration

The internal configuration of the satellite plays as well a roll in the distributions of temperatures, mainly inside the satellite. The internal structure and configuration of small satellites such as PocketQubes and CubeSats is similar: most of them opt for stacking the PCBs, which are kept in position thanks to four corner rods which traverse them (see figure 4.18). A set of spacers, standoffs, bolts, nuts and other fixating elements keep the boards in place.

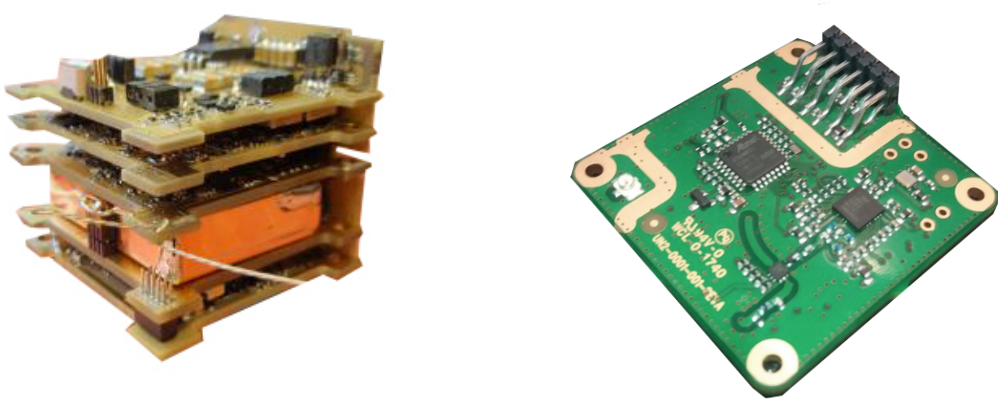

Figure 4.18: Typical internal configuration of a PocketQube (left) and detail of a PCB (right).

Besides payloads with specific geometries, small satellites internal space is mostly comprised of PCB boards. These PCB boards could be stacked in a single column or several. For example, in the case of the Delfi-PQ, two approaches for stacking the boards are on the table: single and triple. The single one (nominal) consists on a single column of PCBs situated perpendicularly to the longitudinal axis of the satellite. The tripe approach consist in three columns of stacked PCBS, perpendicular to the transverse axis of the satellite, one next to each other.

Other geometrical elements such as the battery can change in geometry. For example, the designer could opt for using cylindrical power cells or pouch (rectangular) ones. This might have as well an impact on the temperatures of the satellite.

Studying the impact of the internal configuration on the temperatures of the satellite is not trivial, as a wide variety of different payloads and arrangements could be proposed. This research limits the study of internal configuration to three different cases:

- **g1** Single stack, cylindrical battery, current configuration.
- **g2** Single stack, cylindrical battery, reversed order of the stack.
- **g3** 3-stack solution, pouch battery.

Sensitivity to internal distribution.

The variation of internal distribution of the subsystems have a moderate impact on temperatures, as shown in Figure 4.19. Average and maximum temperatures of internal and external components might vary from 6C° to 11C°. The sensitivity of the battery temperatures to its geometry seems to be important. When opting for pouch power cells the minimum temperatures registered on the battery can drop up to 31C°, which is very notable. In a similar way, when using pouch power cells, the maximum temperatures could scale up 27 C°. Therefore, from a thermal perspective and based on the results obtained, it is preferable to use cylindrical power cells to limit the amplitude of temperature swings on the battery.

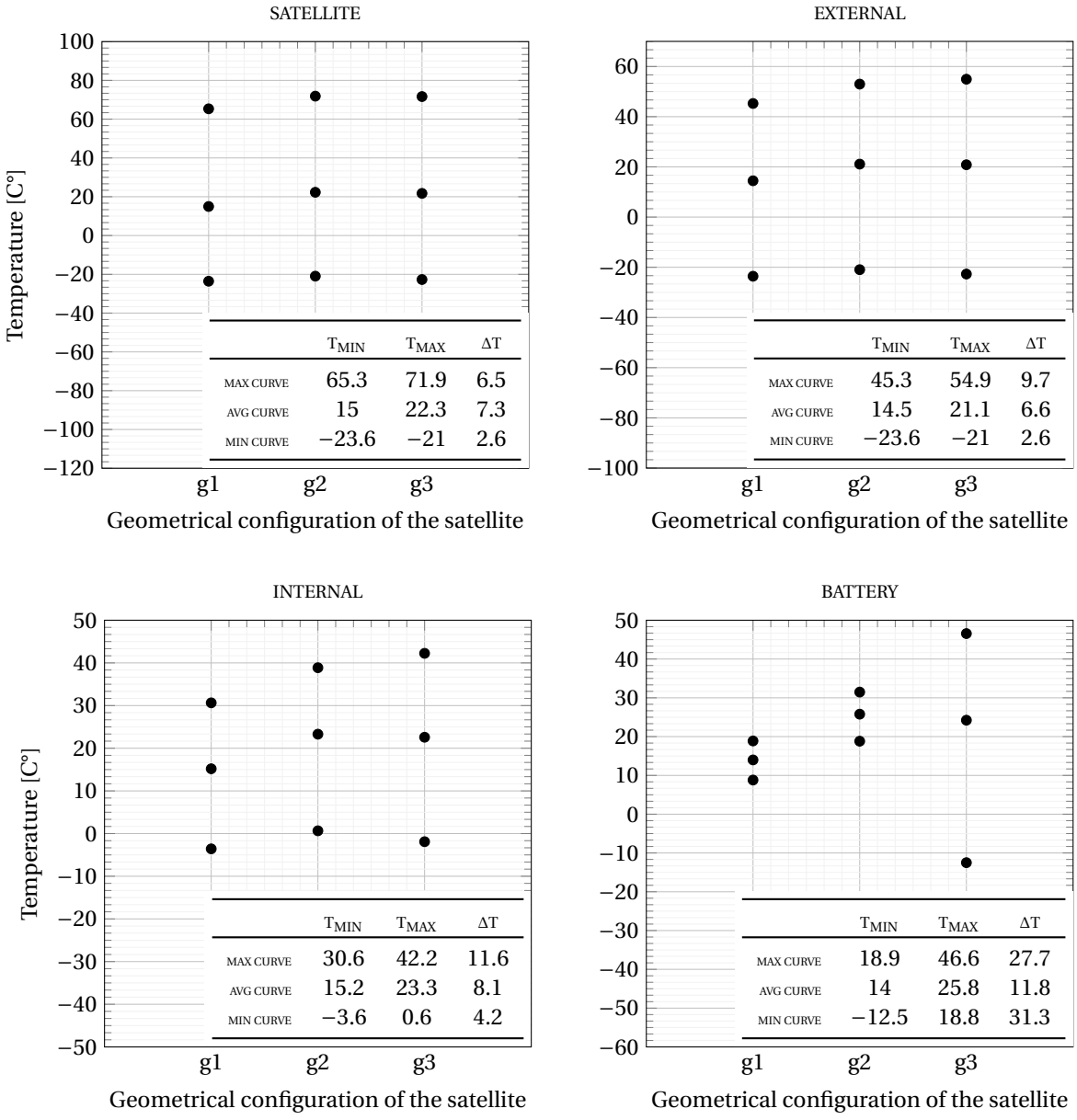

Figure 4.19: Temperature sensitivity to internal configuration.

5

Analysis of Results

Chapter 4 introduced a large amount of quantitative data on temperature sensitivity to multiple design and environmental parameters. In this section this data is processed to provide a general understanding of the most relevant parameters from a thermal control perspective on PocketQubes such as as the Delfi-PQ. The following figures show how much, by varying different design and environmental parameters, certain key temperatures change. More specifically, it indicates the maximum possible change in temperatures achievable [ΔK] when varying the aforementioned parameters from its minimum possible value to its maximum one, as specified in Chapters 3 and 4.

The approach for comparing data consists in generating ranks for key temperatures, such as the satellite and battery maximum, average and minimum ones. This input is relevant for the thermal designer when deciding which thermal control method or approach could be more effective and which design parameters won't have that much contribution to the thermal behavior of the PocketQube.

5.1. Satellite average temperature sensitivity

The results on average temperatures of the satellite show (see figure 5.1), in general lines, a clear influence on optical properties, a moderate influence on orbital parameters and a very low influence on material properties.

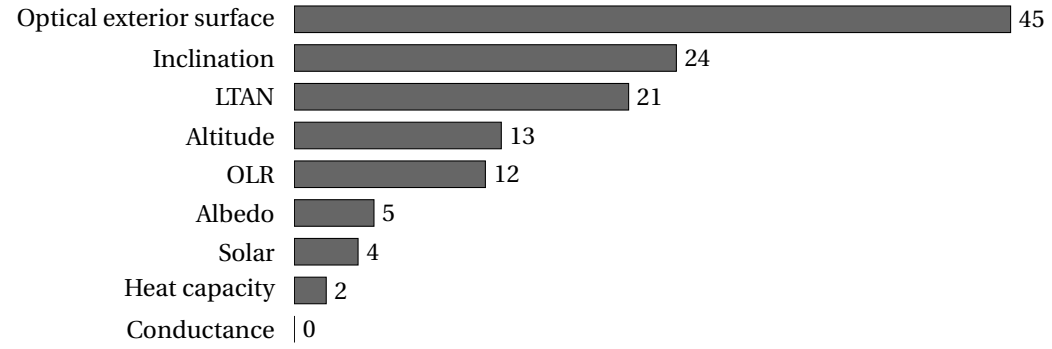

Figure 5.1: Satellite average temperature sensitivity [ΔK].

Although the DelfiPQ, satellite chosen as baseline, is covered on up to 65% of its external surfaces by solar cells, which optical properties could not be modified, just by varying the absorptivity to emissivity ratio of the reminder available surface, the impact on average satellite temperatures is notable, up to 45 °C.

Therefore, the thermal engineer, should choose carefully the optical properties of the external surface of the satellite. At the same time this can be used as a cheap and easy-to-implement passive means of temperature control. The difference in temperatures of up to 45 °C could be achieved only by combining black and white paint in different ratios, as explained in section 4.1.

Orbital parameters seem to have a moderate impact, being orbital inclination the most relevant one within this group. Nevertheless is not inclination itself, but the duration of the eclipse which really is impacting the temperature of the satellite (refer to section 4.2 for a detailed explanation). Therefore, both orbital inclination and LTAN, which are directly related to eclipse duration, could have an impact in the order of 20 °C of change in temperature.

The duration of the eclipse could be defined by setting the satellite on a sun-synchronous orbit and selecting the desired LTAN. In this way, from orbits without eclipses up to orbits with maximum eclipses could be set up. In any case, mission requirements might prevent the thermal designer to choose on the LTAN.

Fluctuations on environmental inputs such as Earth OLR and Albedo as well as solar input have a reduced impact on temperatures.

Lastly, heat capacity and conductive properties have a negligible impact on the average temperatures of the satellite. Based on the results, modifying these parameters won't be a useful action when aiming to adjust the average temperatures of a PocketQube.

5.2. Satellite minimum temperature sensitivity

The results of the thermal analysis of the DelfiPQ summarized in section 3.10 showed how fast temperatures plummeted during eclipse. Therefore, the longer the eclipse, the lower the temperatures reached. When observing the factors which most influence the minimum temperatures of the satellite (see figure 5.2), is not surprising to find the LTAN (eclipse duration) in first position. Reducing the eclipse time of the orbit from its maximum duration to no eclipse at all, lifts the minimum temperatures reached on the satellite by 43 °C.

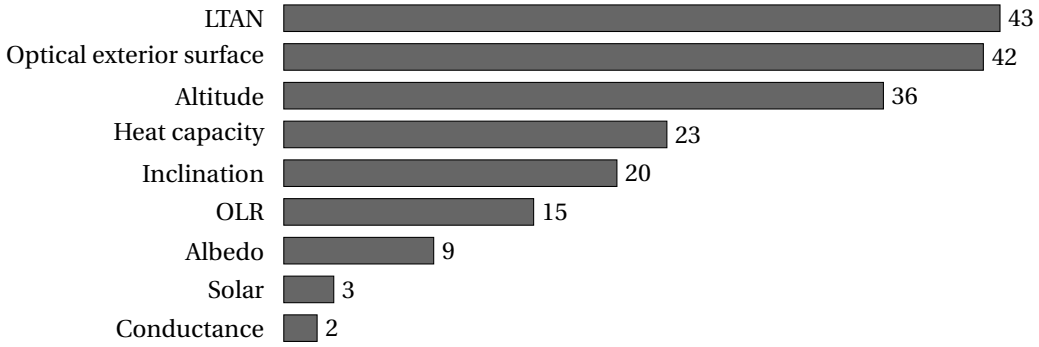

Figure 5.2: Satellite minimum temperature sensitivity [ΔK].

Optical properties still plays an important role in minimum temperatures, with an impact of up to 42 °C difference. Other orbital parameters and environmental factors such as orbital altitude, inclination and OLR have a medium to high impact on temperatures as well.

Which is interesting is to see how thermal capacity now has a moderate impact on temperatures of around 25 °C, ×25 higher than the influence it had on the average temperatures. This result confirms that increasing thermal capacity is useful for preventing minimum temperatures dropping, without having any impact on the average temperatures of the satellite.

5.3. Satellite maximum temperature sensitivity

When dealing with maximum temperatures of the satellite, once again, the optical properties of the external surface is the most influential factor, by far (see figure 5.3). Environmental and orbital parameters such as the inclination, orbital altitude, LTAN and Albedo have a moderate-to-low impact and material properties such as thermal conductance and heat capacity are almost negligible regarding maximum temperatures. While it is possible to influence average and minimum satellite temperatures by modifying different parameters, in the case of maximum satellite temperatures, optical properties of the external surfaces seem to be the most effective way to do so.

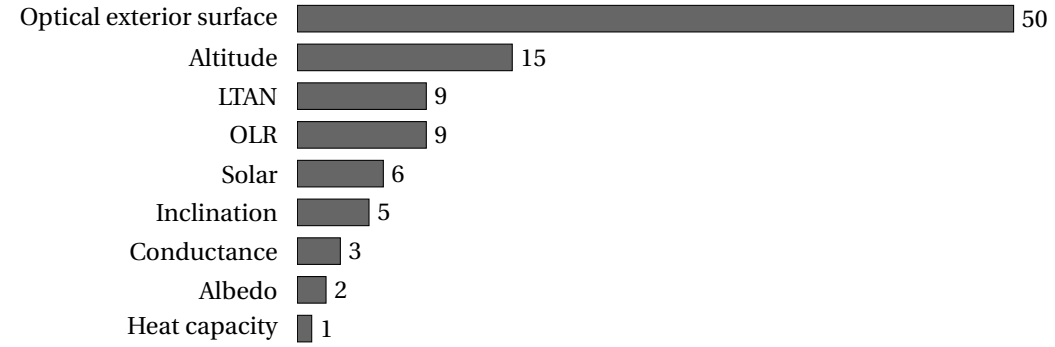

Figure 5.3: Satellite maximum temperature sensitivity [ΔK].

5.4. Battery average temperature sensitivity

Given that the batteries in general have a reduced operational temperature range, there is an special interest in analyzing which are the factors that affect it the most.

The results for battery average temperatures is presented in figure 5.4. Optical properties, once more, rank the first. The coating of the external surface of the satellite has not only an important impact on satellite average temperatures but as well on the battery in particular. The emissivity of the internal surfaces of the satellite has as well a moderate impact, getting a third place in the rank, inducing battery average temperature differences of up to 21°C. As explained in section 4.1, an increase in emissivity of the internal walls of the satellite, enhances the radiative coupling among the equipment inside the satellite and the external walls, which might act as a radiator. It is remarkable that the emissivity and heat capacity of the battery itself, rank low among the parameters that affect the temperature of the battery. The optical properties of the elements around the battery are more relevant for its average temperature than the properties of the battery itself.

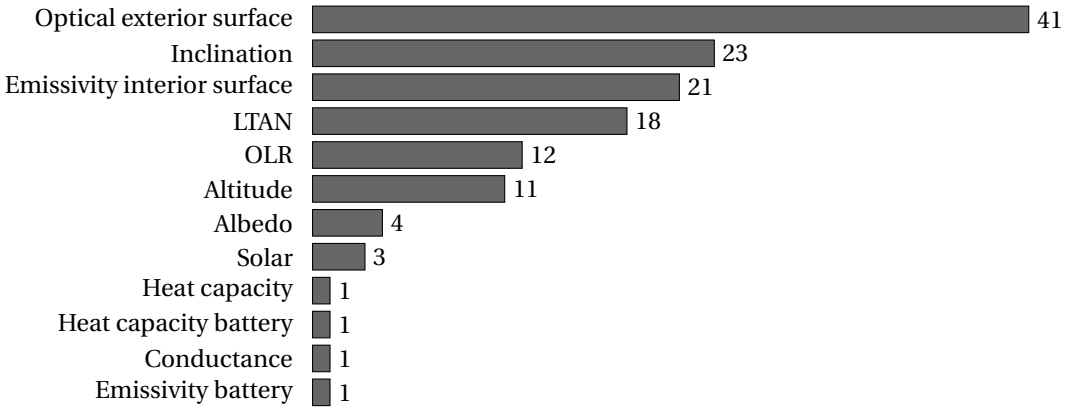

Figure 5.4: Battery average temperature sensitivity [ΔK].

5.5. Battery minimum temperature sensitivity

Similar results are obtained for the battery minimum temperatures, as presented in Figure 5.5. Optical properties of the external surfaces of the satellite are the most influential parameter, followed by the optical properties of the internal surfaces. Eclipse duration given by LTAN and inclination values, are the second most important parameters influencing minimum temperatures. Once again, it seems that the properties of the battery have a residual influence on the temperature of the battery itself.

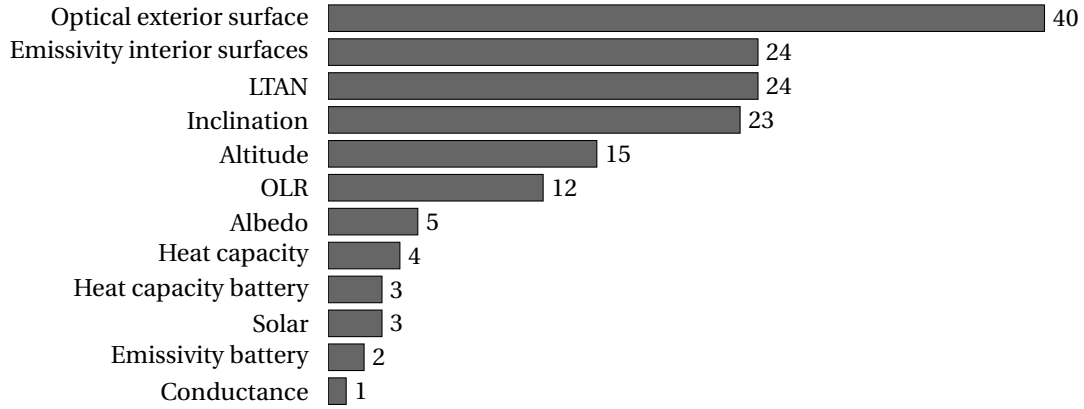

Figure 5.5: Battery minimum temperature sensitivity [ΔK].

5.6. Battery maximum temperature sensitivity

Contrary to the results obtained for the maximum temperatures of the satellite, in the case of the battery, there are multiple influential parameters (see Figure 5.6). Nevertheless, the orders of magnitude of the influence of the different parameters are very similar to the previous cases presented for the battery.

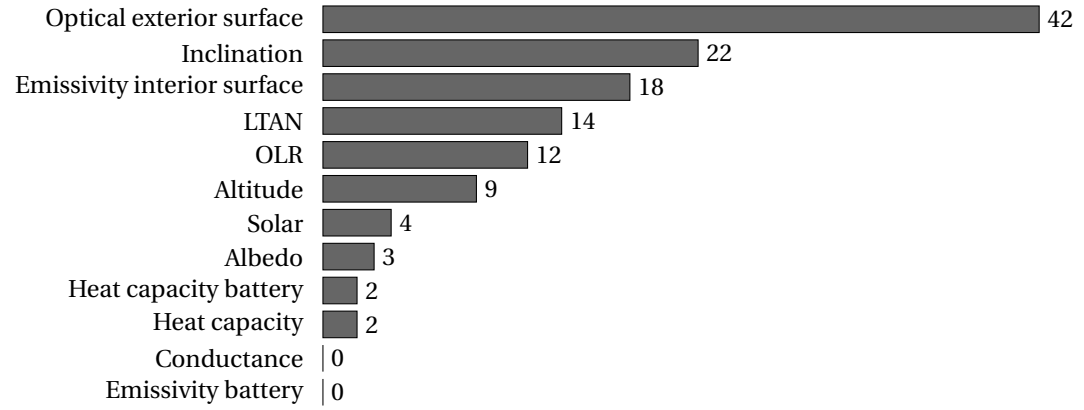

Figure 5.6: Battery maximum temperature sensitivity [ΔK].

6

Conclusions & Recommendations

The general trends and conclusions described in Chapters 4 and 5 could be applied in future thermal analysis and design solutions for PocketQubes in the ways described in the following paragraphs, answering to the research questions proposed in section 1.4.1 on how standardized thermal analysis and design solutions could be applied to PocketQubes to ensure thermal control.

Regarding thermal analysis of future PocketQube missions, and based on the sensitivity results obtained in section 4.4, conductive couplings seem to play a minimum role in its thermal behavior. Therefore, time could be saved by not including them in thermal models or just reducing its level of detail. In line with the analysis performed by Ruhl [31], most of the thermal energy exchanged between internal elements on compact structures such as PocketQubes is done via radiative couplings (up to 80%).

Similarly, the material properties (thermal conductivity, density, mass, thermal capacity), have a limited role on the temperature behavior of PocketQubes. According to the results presented in section 4.3, they do not impact the average temperatures of the satellite notably (within the range of variation proposed). Neither the maximum temperatures. On the other hand, they could be useful when the objective is to lift minimum temperatures.

From a thermal analysis point of view, once again, determining with high accuracy the thermal capacities of the satellite is not of importance from a global perspective. Representation of structural elements such as bolts, nuts, standoffs, rods, washers, could be avoided or greatly simplified. Increasing the thermal capacity of PCB boards or elements is proven to be a good method for lifting minimum temperatures.

The thermal environment has a moderate impact on the temperatures to be experimented by PocketQubes. Solar radiation, Albedo and OLR fluctuations could influence temperatures in up to 10 °C according to the results presented in Chapter 5, being the IR radiation from the planet the most influential one. From a thermal analysis point of view, investing time in accurately determining the values of this heat inputs is discouraged.

On the other hand, duration of the eclipse is an important parameter to take into account as it influences not only minimum temperatures but also satellite average temperatures, affecting as well the temperature of internal critical components such as the battery. Therefore, from an analysis point of view, setting the correct beta angle in the simulations is important. Temperatures might shift between 20 °C and 45 °C due to changes in eclipse duration.

If not constrained by satellite mission objectives, when designing for thermal control, it is recommendable to conveniently decide on the local time of the ascending node as it will determine the duration of the eclipse. For sun-synchronous orbits, eclipse duration will remain the same as long as the satellite stays in it.

Optical properties are the most influential parameter on the temperatures of PocketQubes. Thermal analysis should consider them carefully. They could be easily modified for thermal control purposes. Section 4.1 demonstrated how, by using combinations of simple coatings such as white and black paint, the temperatures of the satellite could be regulated in a range of 45 °C. Even when a large part of the external surface is covered by other elements, the optical properties have a high impact on satellite temperatures.

Furthermore, the optical coatings of the surfaces in the inside of the satellite are relevant for thermal control. As mentioned earlier, and according to the results presented in Chapter 5, radiative coupling plays a much more important role in heat transport than conduction. Therefore increasing the emissivity of the internal surfaces of the satellite creates an stronger coupling of the elements inside, which effectively extract thermal energy from the internal elements to the panels and from there to space, cooling down the interior.

Defining the emissivity of the internal surfaces effectively determines the thermal environment inside the satellite, which impact the temperatures of the internal equipment including the battery, up to the point that this is more relevant for the temperature of the battery than changing properties on the battery itself.

6.1. Further Steps

Further steps towards better understanding the thermal behavior of PocketQubes from a general perspective could be taken in the direction of analyzing the sensitivity of satellite temperatures to parameters such as the external geometry, dissipation, power management or pointing. This will provide the PocketQube community with a broader understanding on the topic. Due to time constraints, proper results on the effects of these parameters on temperatures couldn't be obtained and incorporated in this document.

Furthermore, the effects of varying several parameters at the same time could be studied (co-dependence). This study was limited to correlate changes in temperature with changes in design and environmental parameters and therefore their effects have been isolated from the rest. Nevertheless, when dealing with different versions and types of PocketQubes, is not only one parameter which changes from one to another design, but several.

Afterwards, a n-dimensional matrix containing expected temperature ranges and thermal behavior of PocketQubes based on the values of their different design and environmental parameters could be produced. From this, a simplified map, schematic, guide, or even software could be developed, allowing to obtain temperature information and general design guidelines for several different types of PocketQubes without the need of developing a tailored thermal model.

Bibliography

[1] S. Lee; A. Hutputanasin; A. Toorian; W. Lan; R Munakata; J. Carnahan; D. Pignatelli; A. Mehrparvar. CubeSat design specification Rev. 13. 2014. The CubeSat Program, Cal Poly SLO.

[2] E. Kulu. Nanosatellite launches with forecasts. Nanosats.eu, Retrieved in May 2018. URL `https://www.nanosats.eu`.

[3] J Bouwmeester; S. Radu; M.S. Uludag; N. Chronas; S.Speretta; A. Menicucci; E.K.A. Gill. Conditions and application domains for PocketQubes. Delft University of Technology.

[4] I. de Pater; J.J. Lissauer. Fundamental Planetary Science: Physics, Chemistry and Habitability. 2010. ISBN: 052161855X.

[5] E. Escobar; M. Diaz; J.C. Zagal. Evolutionary design of a satellite thermal control system: Real experiments for a CubeSat mission. 2016. Applied Thermal Engineering. 105 (2016) 490-500.

[6] E. Agasid; R. Burton; R. Carlino; G. Defow; A. Dono Perez; A. G. Karacalioglu; B. Klamm; A. Rademacher; J. Schalkwyck; R. Shimmin; J. Tilles; S. Weston. Small Spacecraft Technology State of the Art. 2015. Mission Design Division. Ames Research Center, Moffett Field, California. NASA/TP-2015-216648/Rev. 1.

[7] G.C. Birur; T.P. O'Donnell. Advanced Thermal Control Technologies for Space Science missions at Jet Propulsion Laboratory. 2001. Jet Propulsion Laboratory, California Institute of Technology, Pasadena, California 91109. (818) 354-4762.

[8] V. Baturkin. Micro-satellites thermal control - concepts and components. 2005. National Technical University of Ukraine, Kyiv Polytechnic Institute. Acta Astronautica. 56 (2005) 161-170.

[9] M. Barton; J. Miller Thermal Design for Spacecraft Modules. 2006. US Patent: US20060038082A1. AeroAstro Inc.

[10] R.J. Twiggs; J.G. Jernigan; L.R. Cominsky; L.R. Malphrus; B.K. Silvermans; B.S. Zack; K. McNeil; S. Roach-Barret; W. and the T-LogoQube Team. 2014. California State Polytechnic University. US Patent: CubeSat Workshop.

[11] S. Radu; M.S. Uludag; S. Speretta; J. Bouwmeester; A. Dunn; T. Walkinshaw; P.L. Kaled Da Cas; C. Cappelletti. 2018. The PocketQube Standard. Issue 1. Alba Orbital; TU Delft; Gauss SRL.

[12] C. Macco. 2014. Design and Verification of the Delfi-n3Xt Thermal Control Subsystem. Master of Science Thesis. TU Delft Space Systems Engineering.

[13] AW 16340 ICR123 750mAh. 2016. Test of AW 16340 ICR123 750mAh battery. *Nanosats.eu*, Retrieved in May 2018. Retrieved from the Internet in June 2018. URL `https://lygte-info.dk/review/batteries2012/AW%2016340%20ICR123%20750mAh%20%28Black%29%202016%20UK.html`.

[14] H. Maleki; S. Al Hallaj; J. Robert Selman; R. B. Dinwiddie; H. Wang. 1999. Thermal Properties of Lithium-Ion Battery and Components. Journal of Electrochemical Society. 146 (3) 947-954 (1999).

[15] M. Muratori; Y. Guezennec; M. Canova. 2010. A Model Order Reduction Method for the Temperature Estimation in a Cylindrical Li-Ion Battery Cell. Conference paper. DOI: 10.1115/DSCC2010-42000.

[16] T. van Boxtel. 2015. Thermal modelling and design of the DelFFi satellites. Master of Science Thesis. TU Delft Space Systems Engineering.

[17] M. Muratori. 2009. Thermal characterization of lithium-ion battery cell. Corso di Laurea in Ingegneria energetica. Politecnico di Milano. Facolta di Ingegneria Industriale.

[18] 30% Triple Junction GaAs Solar Cell. Type TJ Solar Cell 3G30C - Advanced 80 micrometers. Data sheet. AzurSpace. Solar Power GMBH.

[19] M. Graziosi. Delfi-C3 Thermal Control Subsytem: Design, assembly, integration and verification. Master of Science Thesis. TU Delft Space Systems Engineering.

[20] L. Jacques. Thermal Design of the Oufti-1 Nanosatellite. 2009. Master of Science Thesis. Unviersity of Liege. Applied Sciences Faculty. Centre Spatial de Liege.

[21] L. Pasqualetto. Internship Report. 2016. ESA/ESTEC TEC-MTT European Space Research and Technology Centre. European Space Agency.

[22] K. Azar; J.E. Graebner. Experimental Determination of Thermal Conductivity of Printed Wiring Boards. 2016. Twelfth IEEE SEMI-THERM Symposium. 0-7803-31 39-7/96 01 996 IEEE.

[23] T. Flecht Thermal modelling of the PICSAT nanosatellite platform and synergetic prestudies of the CIRCUS nanosatellite. 2016. Master of Science Thesis. Lulea University of Technology. Department of Computer Science, Electrical and Space Engineering.

[24] C.G. Justus; G.W. Batts; B.J. Anderson; B.F. James. Simple Thermal Environmental model (STEM) User Guide. 2001. Computer Sciences Corporation. Marshall Space Flight Center. NASA/TM-2001-211222

[25] M.M. Finckensor and R.F. Coker. Optical Properties of Nanosatellite Hardware. 2014. Marshall Space Flight Center. NASA/TM-2014-218195

[26] P. Fortescue; J. Stark; G. Swinerd. Spacecraft Systems Engineering. Third Edition. 2003. Wiley editorial. ISBN 0471619515.

[27] J. Nicolics; M. Mundlein; G. Hanreich; A. Zluc; H. Stahr; M. Franz. Thermal Analysis of Multilayer Printed Circuit Boards with Embedded Carbon Black-Polymer Resistors. 2007. 30th ISSE. 1-4244-1218-8/07/ 2007 IEEE.

[28] Solar Cell Coverglasses. Data sheet. QiOptiq.

[29] D.G. Gilmore. Spacecraft Thermal Control Handbook. Volume I: Fundamental Technologies. Second Edition. 2002. The Aerospace Press. El Segundo, California. American Institute of Aeronautics and Astronautics, Inc. ISBN 1-884989-11-X

[30] B. Doncaster; C. Williams; J. Shulman. Nano/Microsatellite Market Forecast. 2017. SpaceWorks Enterprises, Inc.

[31] T. Ruhl Effective Thermal Testing and Potential Design Solutions for PocketQube Subsystems. 2018. Master of Science Thesis. TU Delft Space Systems Engineering.

A

Finite Element Model Data

Table A.1: List of geometries of the model and properties assigned.

Category	ID	Reference	Geometry	Material	Optical	Thickness
battery	01	battery_1	cylinder	battery	battery	N/A
	02	battery_2				
	03	battery_case_bottom	surface, double sided	plastic	plastic_int, plastic_ext	plastic
	04	battery_case_x_neg				
	05	battery_case_x_pos				
	06	battery_case_y_neg				
	07	battery_case_y_pos				
boards	08	board_01_EPS	surface, double sided	pcb	board_top, board_bottom	pcb
	09	board_02_battery				
	10	board_03_dummy_1				
	11	board_04_ADCS				
	12	board_05_dummy_2				
	13	board_06_dummy_3				
	14	board_07_OBDH				
	15	board_08_TTC_1				
	16	board_09_TTC_2				
components	17	antenna_x_neg	surface, single sided	antenna	antenna	antenna
	18	antenna_x_pos				
	19	antenna_y_neg				
	20	antenna_y_pos				
panels	21-70	panel_x_neg	surface, double sided	pcb	panels_int, panels_ext	pcb
	71-120	panel_x_pos				
	121-270	panel_y_neg				
	271-368	panel_y_pos				
	369-389	panel_z_neg				
	390-410	panel_z_pos				

List of geometries of the model and properties assigned (continued).

solar	411	cell_x_neg_A1	surface, single sided	cell	solar_cell_int, solar_cell_ext	cell
	412	cell_x_neg_A2				
	413	cell_x_neg_B1				
	414	cell_x_neg_B2				
	415	cell_x_pos_A1				
	416	cell_x_pos_A2				
	417	cell_x_pos_B1				
	418	cell_x_pos_B2				
	419	cell_y_neg_A1				
	420	cell_y_neg_A2				
	421	cell_y_neg_B1				
	422	cell_y_neg_B2				
	423	cell_y_pos_A1				
	424	cell_y_pos_A2				
	425	cell_y_pos_B1				
	426	cell_y_pos_B2				

Table A.2: List of geometries of the model (NGTN) and properties assigned.

Category	ID	Reference	Geometry	Thermal Capacity
structure	427	Spacer_1_A	NGTN	spacer_cap
	428	Spacer_1_B		
	429	Spacer_1_C		
	430	Spacer_1_D		
	431	Spacer_2_A		
	432	Spacer_2_B		
	433	Spacer_2_C		
	434	Spacer_2_D		
	435	Spacer_3_A		
	436	Spacer_3_B		
	437	Spacer_3_C		
	438	Spacer_3_D		
	439	Spacer_4_A		
	440	Spacer_4_B		
	441	Spacer_4_C		
	442	Spacer_4_D		
	443	standoff_bottom_A	NGTN	standoff_cap
	444	standoff_bottom_B		
	445	standoff_bottom_C		
	446	standoff_bottom_D		
	447	standoff_center_A		
	448	standoff_center_B		
	449	standoff_center_C		
	450	standoff_center_D		
	451	standoff_top_A		
	452	standoff_top_B		
	453	standoff_top_C		
	454	standoff_top_D		
components	455	ADCS_comp	NGTN	ADCS_comp_cap
	456	EPS_comp		EPS_comp_cap
	457	antenna_comp		antenna_comp_cap

Table A.3: Thickness of surfaces and assigned to the model.

Reference	Real Value	Model Input	Units
antenna	0.00050	0.00050	m
cell	0.00008	0.00008	m
pcb	0.00160	0.00080	m
plastic	0.00150	0.00075	m

Table A.4: Capacitances assigned to the NGTN of the model.

		Mass				Heat Capacity			
Parameter	Nodes	Min	Nom	Max	Units	Min	Nom	Max	Units
ADCS_comp_cap	x1	-	0.022	-	kg	8	17	-	J/K
EPS_comp_cap	x1	-	0.015	-	kg	10	18	-	J/K
antenna_comp_cap	x1	-	0.015	-	kg	10	18	-	J/K
spacers_cap	x16	-	0.001	-	kg	-	0.5	-	J/K
standoff_cap	x12	-	0.001	-	kg	-	0.8	-	J/K

Table A.5: Materials densities assigned to the model.

Material	Min	Nom	Max	Units
antenna	8730	8730	8730	kg/m^3
battery	1824	2416	2780	kg/m^3
cell	5316	6520	6520	kg/m^3
pcb	2161	2783	2783	kg/m^3
plastic	1200	1200	1222	kg/m^3

Table A.6: Material specific heat assigned to the model.

Material	Min	Nom	Max	Units
antenna	380	380	380	J/kg K
battery	825	930	1040	J/kg K
cell	493	325	700	J/kg K
pcb	567	567	1440	J/kg K
plastic	1200	1200	3000	J/kg K

Table A.7: Material conductivities assigned to the model.

	In-plane			Through-plane			
Material	Min	Nom	Max	Min	Nom	Max	Units
antenna	109	109	109	-	-	-	W/m K
battery	20	28	74	0.5	3.4	3.4	W/m K
cell	50	57	100	-	-	-	W/m K
pcb	17.7	51.4	55	0.30	0.30	0.36	W/m K
plastic	0.19	0.20	0.22	-	-	-	W/m K

Table A.8: Model geometries mass and capacitance.

Category	#	Geometry	Density	Volume	Mass	Sp. Heat	Capacity
Batteries	01	battery_1	2416	7.040×10^{-6}	0.01700	930	15.8
	02	battery_2	2416	7.040×10^{-6}	0.01700	930	15.8
	03	battery_case_bottom	1200	2.650×10^{-6}	0.00317	0.2	0.0
	04	battery_case_x_neg	1200	1.130×10^{-6}	0.00136	0.2	0.0
	05	battery_case_x_pos	1200	1.130×10^{-6}	0.00136	0.2	0.0
	06	battery_case_y_neg	1200	1.130×10^{-6}	0.00136	0.2	0.0
	07	battery_case_y_pos	1200	1.130×10^{-6}	0.00136	0.2	0.0
Boards	08	board_01_EPS	2783	2.822×10^{-6}	0.00785	567	4.5
	09	board_02_battery	2783	2.822×10^{-6}	0.00785	567	4.5
	10	board_03_dummy_1	2783	2.822×10^{-6}	0.00785	567	4.5
	11	board_04_ADCS	2783	2.822×10^{-6}	0.00785	567	4.5
	12	board_05_dummy_2	2783	2.822×10^{-6}	0.00785	567	4.5
	13	board_06_dummy_3	2783	2.822×10^{-6}	0.00785	567	4.5
	14	board_07_OBDH	2783	2.822×10^{-6}	0.00785	567	4.5
	15	board_08_TTC_1	2783	2.822×10^{-6}	0.00785	567	4.5
	16	board_09_TTC_2	2783	2.822×10^{-6}	0.00785	567	4.5
Cells	17	cell_x_neg_A1	6520	2.4142×10^{-7}	0.00157	325	0.5
	18	cell_x_neg_A2					
	19	cell_x_neg_B1	6520	2.4142×10^{-7}	0.00157	325	0.5
	20	cell_x_neg_B2					
	21	cell_x_pos_A1	6520	2.4142×10^{-7}	0.00157	325	0.5
	22	cell_x_pos_A2					
	23	cell_x_pos_B1	6520	2.4142×10^{-7}	0.00157	325	0.5
	24	cell_x_pos_B2					
	25	cell_y_neg_A1	6520	2.4142×10^{-7}	0.00157	325	0.5
	26	cell_y_neg_A2					
	27	cell_y_neg_B1	6520	2.4142×10^{-7}	0.00157	325	0.5
	28	cell_y_neg_B2					
	29	cell_y_pos_A1	6520	2.4142×10^{-7}	0.00157	325	0.5
	20	cell_y_pos_A2					
	31	cell_y_pos_B1	6520	2.4142×10^{-7}	0.00157	325	0.5
	32	cell_y_pos_B2					
Panels	33	panel_x_neg	2783	1.424×10^{-5}	0.03963	567	22.5
	34	panel_x_pos	2783	1.424×10^{-5}	0.03963	567	22.5
	35	panel_y_neg	2783	1.424×10^{-5}	0.03963	567	22.5
	36	panel_y_pos	2783	1.720×10^{-5}	0.04788	567	27.1
	37	panel_z_neg	2783	4.000×10^{-6}	0.01113	567	6.3
	38	panel_z_pos	2783	4.000×10^{-6}	0.01113	567	6.3

Table A.9: Model NGTN mass and capacitance.

Category	#	Reference	Mass	Capacity
components	39	ADCS_comp	0.022	17
	40	EPS_comp	0.015	18
	41	antenna_comp	0.015	18
	42	antenna_A	0.006	9
	43	antenna_B	0.006	9
	44	antenna_C	0.006	9
	45	antenna_D	0.006	9
structure	46	Spacer_1_A	0.001	0.5
	47	Spacer_1_B	0.001	0.5
	48	Spacer_1_C	0.001	0.5
	49	Spacer_1_D	0.001	0.5
	50	Spacer_2_A	0.001	0.5
	51	Spacer_2_B	0.001	0.5
	52	Spacer_2_C	0.001	0.5
	53	Spacer_2_D	0.001	0.5
	54	Spacer_3_A	0.001	0.5
	55	Spacer_3_B	0.001	0.5
	56	Spacer_3_C	0.001	0.5
	57	Spacer_3_D	0.001	0.5
	58	Spacer_4_A	0.001	0.5
	59	Spacer_4_B	0.001	0.5
	60	Spacer_4_C	0.001	0.5
	61	Spacer_4_D	0.001	0.5
	62	standoff_bottom_A	0.001	0.8
	63	standoff_bottom_B	0.001	0.8
	64	standoff_bottom_C	0.001	0.8
	65	standoff_bottom_D	0.001	0.8
	66	standoff_center_A	0.001	0.8
	67	standoff_center_B	0.001	0.8
	68	standoff_center_C	0.001	0.8
	69	standoff_center_D	0.001	0.8
	70	standoff_top_A	0.001	0.8
	71	standoff_top_B	0.001	0.8
	72	standoff_top_C	0.001	0.8
	73	standoff_top_D	0.001	0.8

Table A.10: Model mass and capacitance

Totals	Mass Budget CBE	Model Mass	Difference	Model Capacity
Structure (4 side panels, structure)	0.205	0.179	87%	112.2
Solar Arrays	0.030	0.013	43%	4.0
Antenna Board Up	0.012	0.011	92%	4.5
Antenna Board Bottom	0.025	0.026	104%	2.5
COMMs	0.015	0.016	106%	9.0
EPS (Boards 01 & 02, Batteries)	0.075	0.073	97%	58.6
ADCS	0.030	0.030	100%	21.5
Antennae	0.022	0.024	109%	36.0
Dummy Boards	0.000	0.023	-	13.5
Satellite	0.424	0.395	93%	290

Table A.11: Optical sets assigned to the model.

	Emissivity			Absorptivity		
Optical set	Min	Nom	Max	Min	Nom	Max
antenna	0.02	0.02	0.02	0.25	0.25	0.25
battery	0.05	0.85	0.92	-	-	-
solar_cell_ext	0.80	0.88	-	0.71	0.91	0.93
solar_cell_int	0	0	0	0	0	0
panels_ext	0.04[1]	0.89	0.40[2]	0.21[1]	0.95	0.63[2]
panels_int	0.05	0.89	0.98	0.05	0.95	0.98
board_top	0.05	0.89	0.98	0.05	0.95	0.98
board_bottom	0.05	0.89	0.98	0.05	0.95	0.98
plastic	0.05	0.92	0.97	-	-	-

[1] These are the values that, used together, provided the minimum α/ε ratio.
[2] These are the values that, used together, provided the maximum α/ε ratio.

Table A.12: Model conductive couplings.

Coupling	Reference	Min	Nom	Max	Units
	plastic_case_to_board	2000	4000	15000	W/ m2 K
Conductive interface	external_panels	0	500	4000	W/ m2 K
Contact zone	cells_to_panels	2000	4000	15000	W/ m2 K
	spacers*	0.000069	0.00024	0.00024	W/ K
	pins*	-	-	-	W/ K
User defined conductors	battery*	0.010	0.150	2.200	W/ K
	standoffs*	0.009	0.031	0.065	W/ K
	components*	0.25	0.9	4.6	W/ K

* Value per individual coupling (single node to single node).

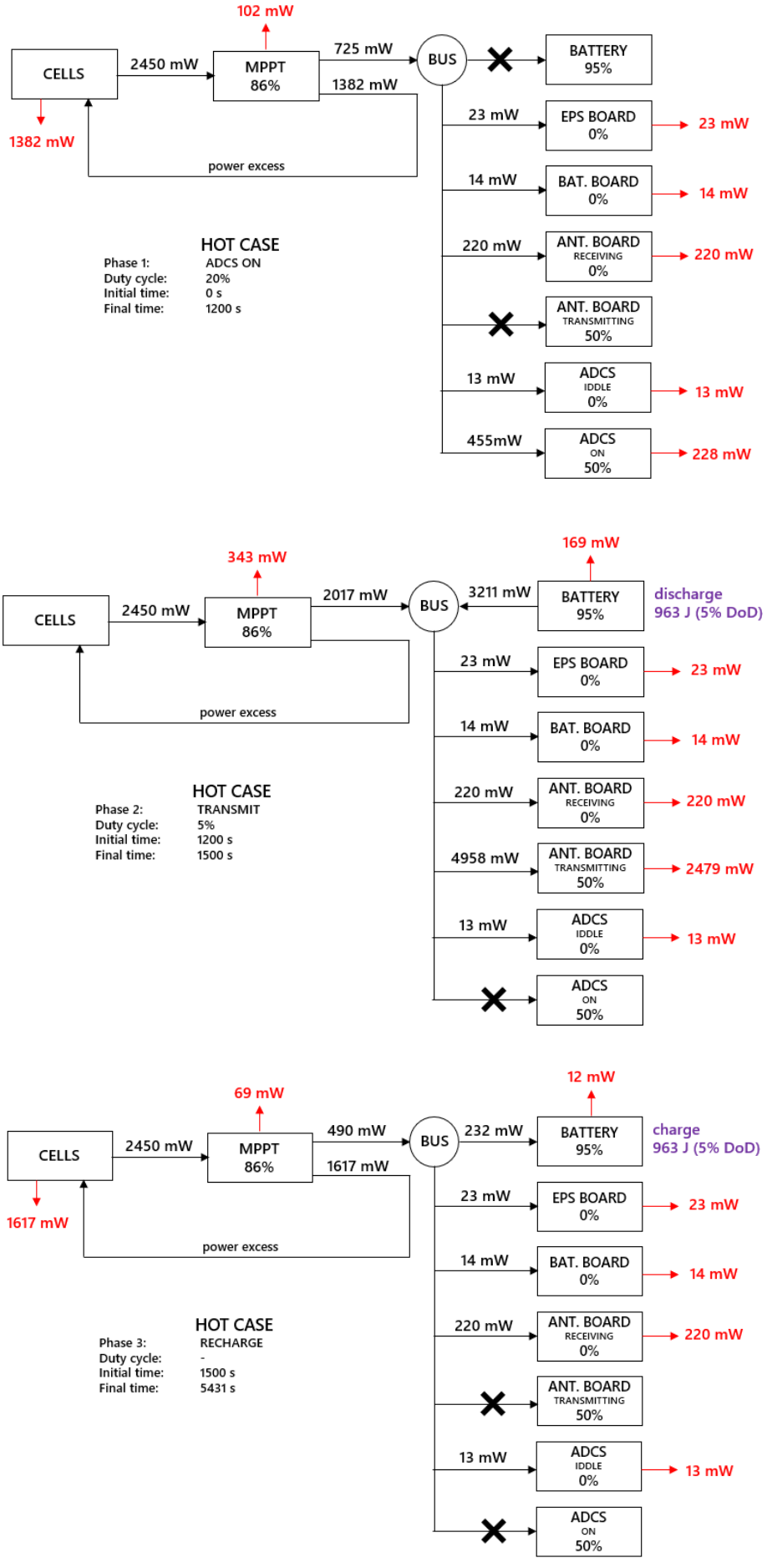

Figure A.1: Power distribution for the hot case, three phases.

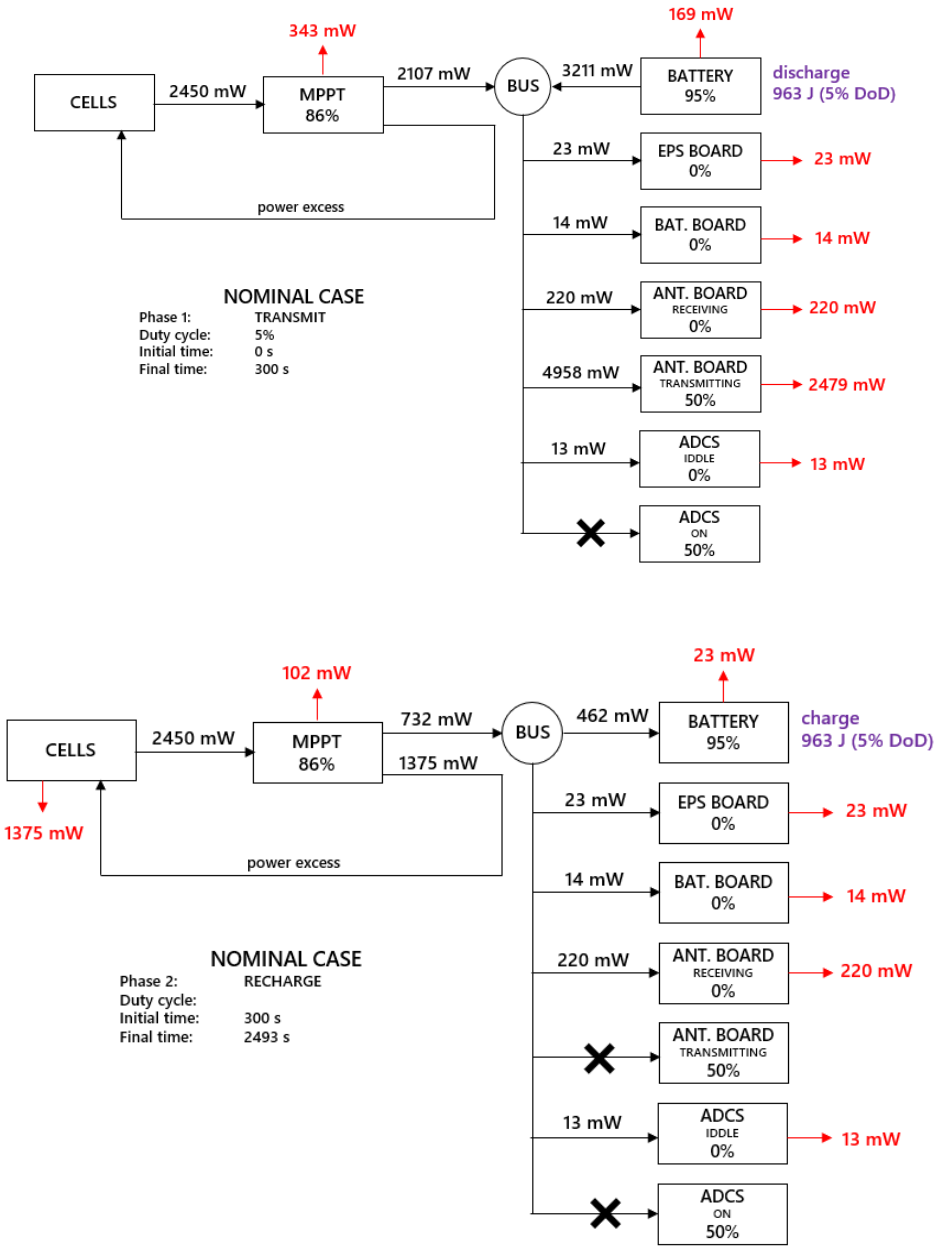

Figure A.2: Power distribution for the nominal case, four phases (Part A).

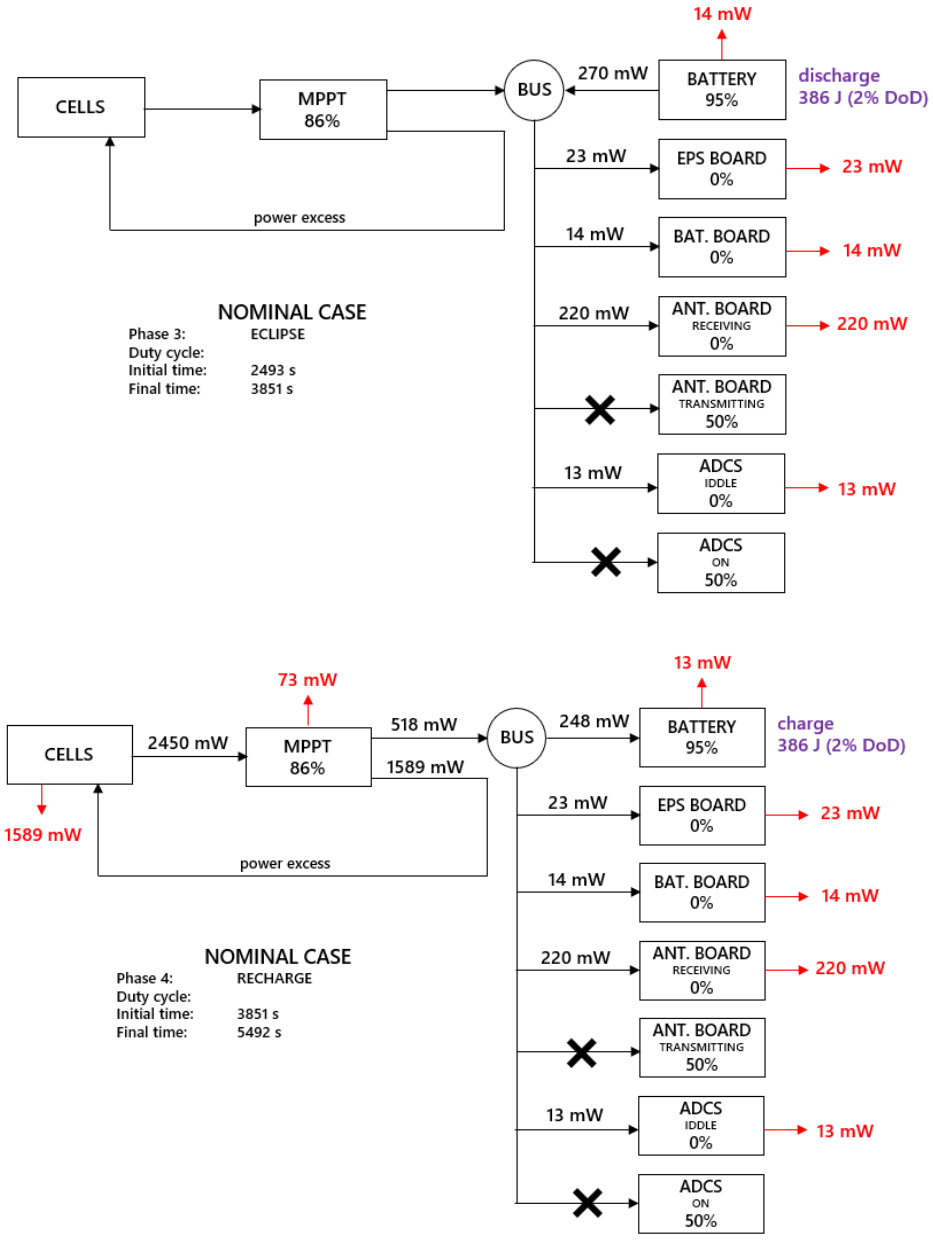

Figure A.3: Power distribution for the nominal case, four phases (Part B).

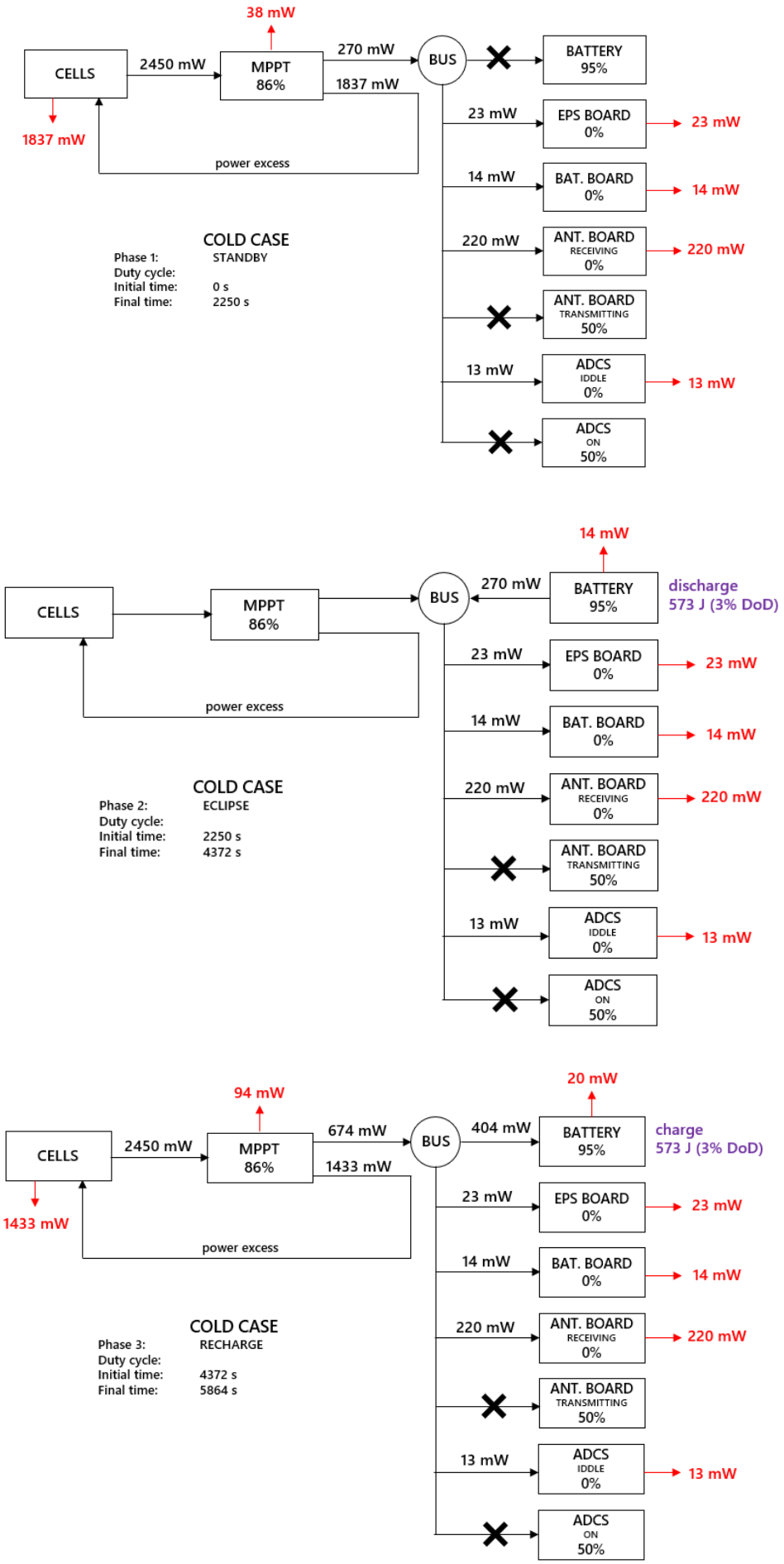

Figure A.4: Power distribution for the cold case, three phases.

B

Orbital Mechanics Extended

A classical orbit is characterized by six parameters, named orbital elements, which are semimajor axis (a), eccentricity (e), inclination (i), right ascension of the ascending node (Ω), argument of periapsis (ω) and true anomaly (ν).

Size and shape
The semimajor axis (a) and eccentricity (e) define the size and shape of the orbit respectively. Closed orbits are either elliptical or circular. In the first case, the semimajor axis indicates the distance between the center of the ellipse (O) and its furthest points (see figure B.1 for reference). The central body (which for the satellites being considered is the Earth), is located at one of the focal points of the ellipse (F, F').

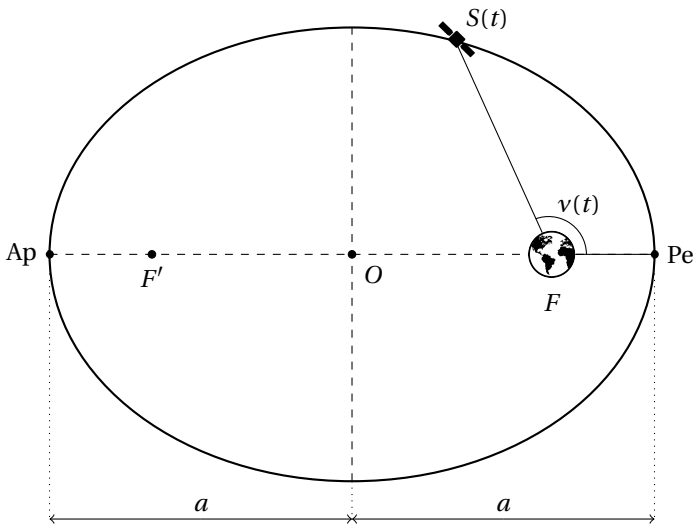

Figure B.1: Shape of a closed orbit and main points of interest.

The point of the orbit where the satellite is closest to the central body (F) is named periapsis (Pe) and the one where the satellite is furthest is named apoapsis (Ap). The distance from the apses and the central body can be computed by equation B.1 as a function of the semi-major axis and the eccentricity.

$$\text{Pe} = (1-e)\,a \qquad \text{Ap} = (1+e)\,a \tag{B.1}$$

The true anomaly ($\nu(t)$) determines the position of the satellite within the orbit ($S(t)$). It is defined by the angle formed between the segment central body-to-perigee $\overline{F\text{Pe}}$ and central body-to-satellite $\overline{FS}$ (see figure B.1 for reference). It ranges from 0 to 360° and varies with time as the satellite moves along the orbit .

The shape of the orbit is given by its eccentricity, which might vary in the range [0, 1). According to equation B.1, when the eccentricity is 0, both perigee and apogee are located at the same distance from the center. This is the case of the circular orbit and then the semimajor axis becomes the radius of the circle. The higher the eccentricity, the more elliptical the orbit, the closer the perigee to the central body and the further away the apogee. On the limit, when the eccentricity reaches a value of 1, the orbit opens at the apogee degenerating into a parabolic shape.

Orientation

The orbit of a satellite as shown in figure B.1 is contained in a plane, which receives the name of orbital plane. Two angles are used to locate this plane with respect an inertial frame of reference (O, x, y, z) which are the inclination ($0° \leq i \leq 180°$) and right ascension of the ascending node ($0° \leq \Omega \leq 360°$) see figure B.2 for reference.

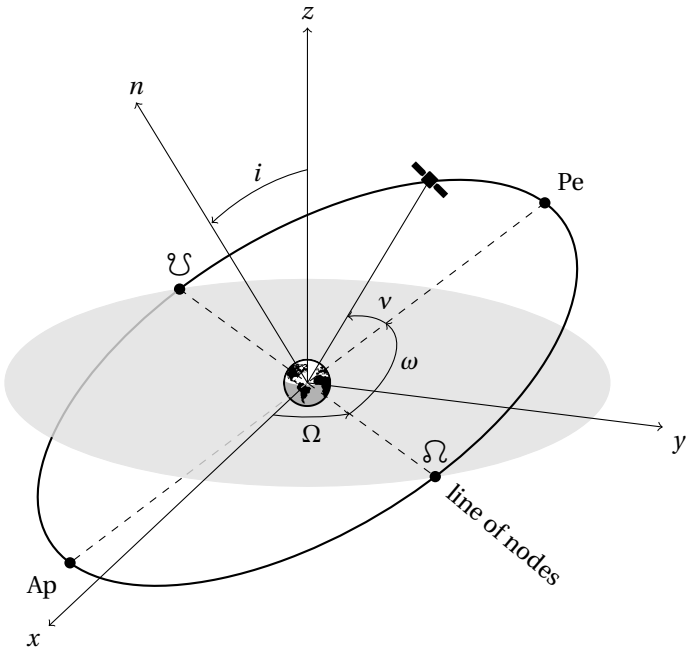

Figure B.2: Orientation of a closed orbit and main point of interest.

The inclination defines the angle between the equatorial plane of the orbiting body and the plane of the orbit. Figure B.2 shows the equatorial plane in gray and the inclination as the angle formed between the normal vector of the equatorial plane (z) and the normal vector of the orbital plane (n).

The spacecraft moves counterclockwise for orbits with inclinations ranging from 0° to 90° and clockwise with inclinations ranging from 90° to 180° commonly known as retrograde orbits. When the orbit inclination is 90° or close, the satellite passes above the poles of the planet (North, South) and therefore the orbit is called polar. When the inclination is equal to 0° or 180°, the equatorial and the orbital plane coincide and the orbit is then called equatorial.

Except in the 0° or 180° cases, the two planes intersect along a line which receives the name of line of nodes (see figure B.2). The point where the satellite passes from below the equatorial plane to above is known as ascending node (☊). The point where the satellite passes from above the equatorial plane to below is known as descending node (☋).

The orientation of the line of nodes with respect to the inertial frame of reference is given by the right ascension of the ascending node (Ω). The position of the periapsis with respect to the line of nodes is given by the argument of periapsis (ω). Note that this last parameter becomes undefined for circular orbits as the periapsis is undefined as well. Both inclination and right ascension of the ascending node or RAAN for short, play a crucial role in determining the environmental inputs.

An inclination equal to 0° (equatorial), means that the satellite is never able to visit regions with higher latitudes. The higher the inclination, the higher the latitudes the satellite is able to observe. This combined

with the fact that the Earth rotates along the axis passing by the South and North poles, means that an orbit with inclination of 90° (polar) allows the satellite to visit every point in the surface of the planet. This is why polar or nearly-polar orbits are more interesting for LEO satellites that are commonly dedicated to Earth observation. This phenomenon can be clearly observed by taking a look at the traces left by LEO satellites at different inclinations (figure B.3).

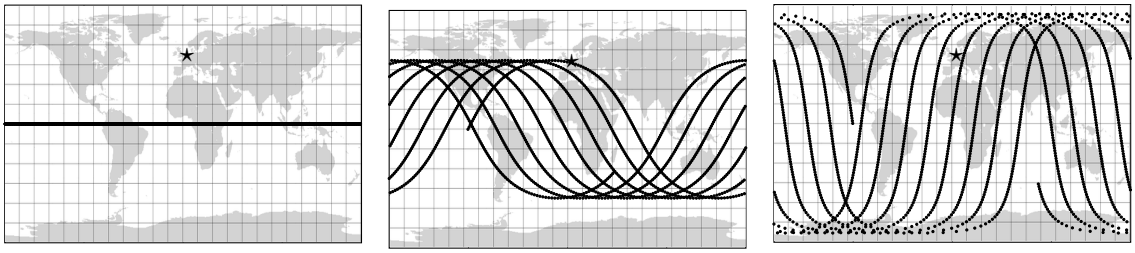

0 ° inclination (equatorial) 52 ° inclination 97 ° inclination (nearly polar)

Figure B.3: Traces left by LEO satellites with different inclinations. TU Delft ground station marked with a star.

Sun-synchronous orbits are those in which the angle of the orbital plane with respect to the direction of the Sun (known as beta angle) is always kept constant.

The higher the altitude, the fainter the radiation received from Earth.

The altitude of the orbit is relevant as it determines the power input from coming from the Earth (Albedo and IR radiation). At the same time the altitude determines the period of the orbit and thus the frequency of eclipses. The satellite is to be set in a nearly-circular orbit 350 to 650 km altitude, according to specifications, to comply with debris regulation and ensure a minimum life for the satellite. Based on this information and the third Law of Kepler (see [29], equation 2,3, page 39), where R is the planet radius (taken as 6378 km), h is the orbit altitude and μ the standard gravitational parameter of the Earth (3.98603×10^{14} m^3 s^{-2}) the period of the orbit is estimated to be within 5492s (91.5 minutes) and 5677s (94.6 minutes).

Because the orbit is considered to be nearly polar, sun-synchronous, with undetermined RAAN, eclipse duration is in principle undetermined as well. The minimum eclipse time would be 0 seconds, which happens for orbit beta angles greater than the critical. For the 350 km altitude orbit the critical beta angle is 67.5 degrees and for the 650 km one, is 62.3 according to equation 3.14 (see [29], equation 2.8, page 41).

Because the orbiting body will be the Earth, the semimajor axis could then be expressed as the sum of the Earth radius, $R_{\oplus}$, and the orbital altitude, h, which are constant. Another consideration of circular orbits is that the apses (perigee, apogee) become undefined, as all the points of the orbit are at the same distance from the central body, which is located at the center of the circle. As well, the true anomaly varies linearly with time, and the angular velocity of the spacecraft is constant which greatly simplifies the problem.

C

DPQ Thermal Analysis Extended Results

C.1. External Temperatures

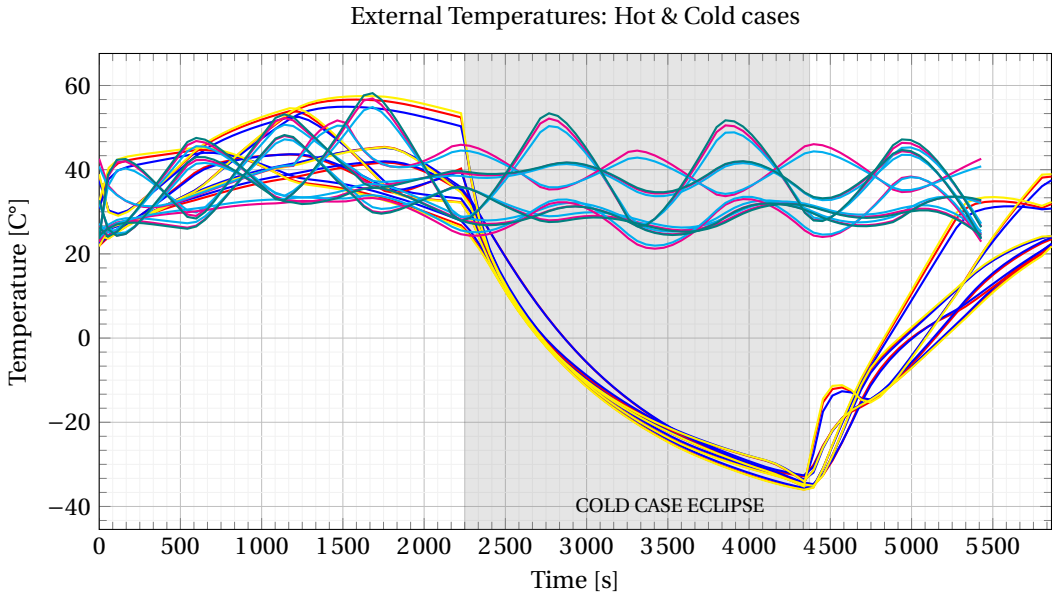

Figure C.1: External temperatures, Cold and Hot Cases.

The temperatures of the external elements of the satellite for the hot and cold cases are presented in Figure C.1. For the cold case, red lines represent the temperature of the external surface of the lateral panels of the satellite, blue lines the ones of the internal surface of the side panels of the satellite and yellow lines the temperature of the solar cells. For the hot case, magenta lines are associated with the temperature of the external surface of the lateral panels of the satellite, cyan lines with the internal surface of the side panels of the satellite and green lines with the temperature of the solar cells.

It is remarkable to see how the average temperatures of the +X panel in the cold case reach same values as other panels in the hot case. It seems that, due to the random nature of the rotation of the satellite set in the simulation, this panel has been oriented towards the Sun for a longer period of time than others. In any case, the temperatures of the side panels do not differ that much in the cold or hot cases while they are under the influence of the Sun. It is as well very similar to the nominal case. The main differences occurs during the eclipse. In the hot case, eclipses won't happen therefore the temperatures remain fluctuating within a range comprised between 20°C and 55°C. On the other hand, the cold case has the longest eclipse possible of all the orbits considered and the temperature drops down to -35°C.

Once more it looks like there are not noticeable thermal gradients among the solar cells, the external and the internal surfaces of the side panels of the satellite. The difference is only noticeable (and small) when the

temperatures come close to 50°C.

Note that the solution is cyclical in all cases, meaning this that, although the temperatures swing along the orbit, they repeat in a cycle with each orbit. The solution obtained can be considered 'stationary' in the sense that there is no influence from initial temperatures set for starting the simulation. The can be checked by comparing the values of the elements at the end of the orbit and at the beginning, which must be the same in order to consider the solution is cyclical. This condition is inputed in the solver on purpose. Also note that, in figure C.1, the data for the hot case does not reach the end of the graph. This is due to the fact that the hot case considers a slightly shorter orbit than the cold case. Therefore the presented data stops there.

C.2. Internal Temperatures

(1) Board 1 - EPS

(2) Board 2 - Battery

(3) Board 3 - Dummy

(4) Board 4 - ADCS

(5) Board 5 - Dummy

(6) Board 6 - Dummy

(7) Board 7 - OBDH

(8) Board 8 - TTC

(9) Board 9 - TTC

(B) Battery

(S) Internal structure (average temperature of standoffs, spacers and rods)

The comparison of temperature between hot and cold cases for the internal components is shown in figure C.2. For the hot case, the temperatures seem to be quite homogeneous. This could be explained by the more stable thermal environment, without eclipses. For the cold case, the temperatures drop down further than the nominal case, up to -20°C.

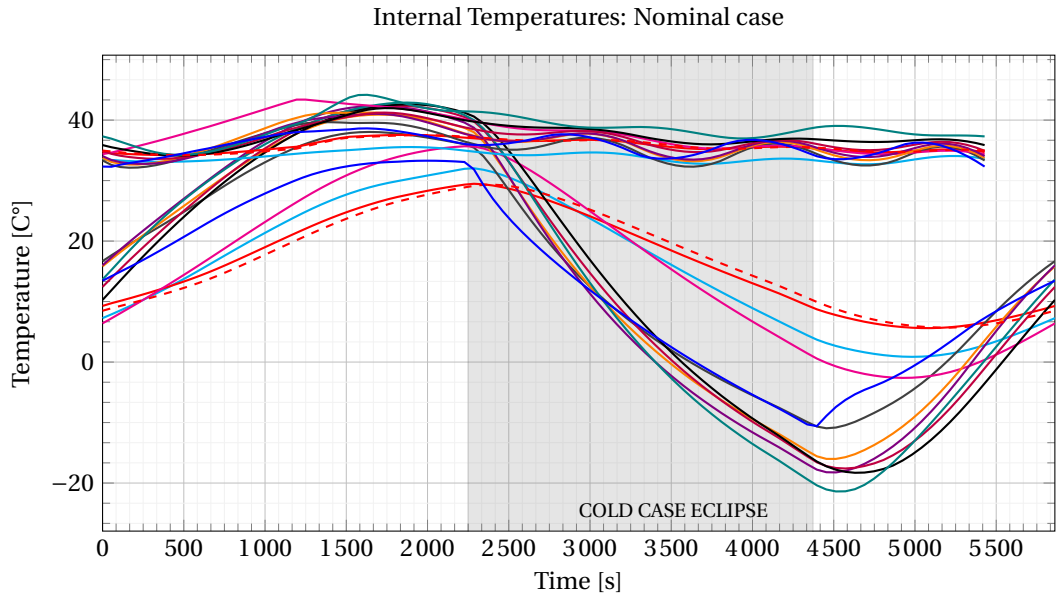

Figure C.2: Internal temperatures, nominal case.

C.3. Battery Temperatures

In time, the temperature of the battery varies more for the nominal and cold cases, due to the influence of the eclipse (shadowed region) on the temperatures of the satellite. In all three cases, the temperatures seem to be tolerable and a little bit on the hot side.

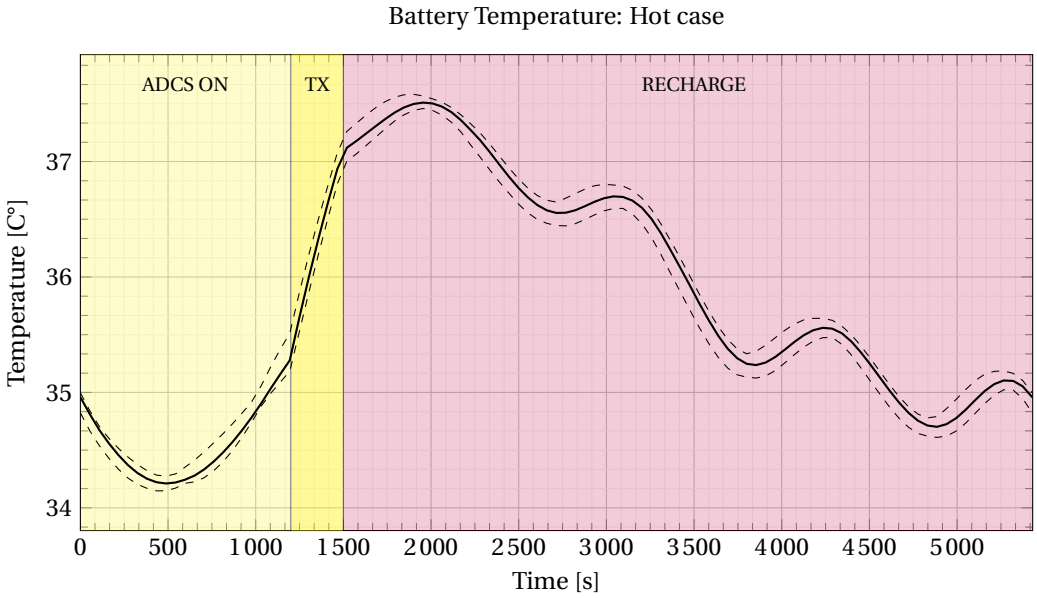

Figure C.3: Average, minimum and maximum temperatures for the batteries on orbit. Hot case.

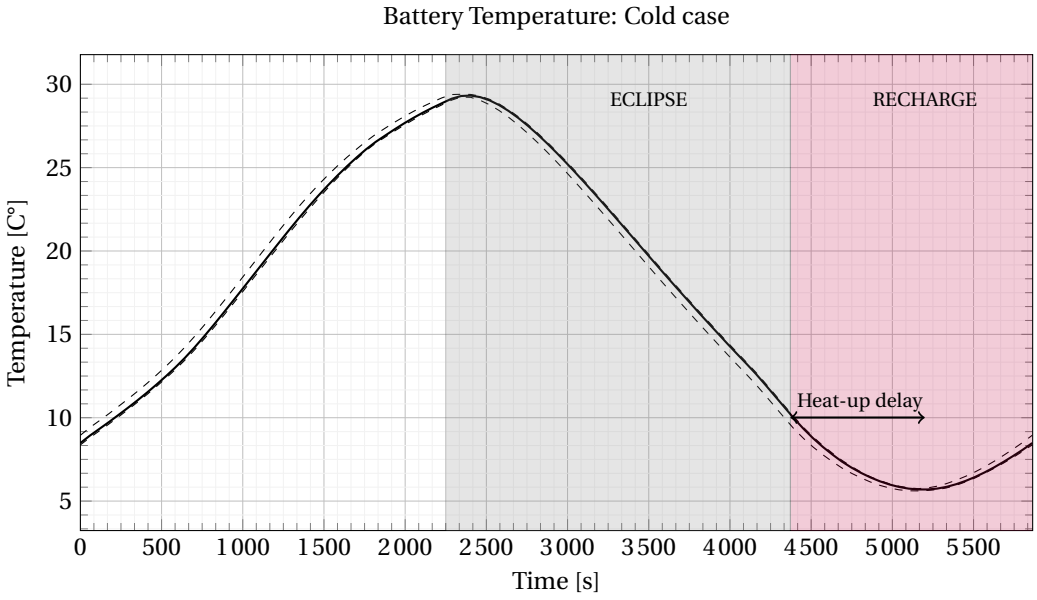

Figure C.4: Average, minimum and maximum temperatures for the batteries on orbit. Cold case.

D

Sensitivity Analysis Extended Results

In the following pages further results on temperature sensitivity are presented.

Sensitivity to variations om thermal capacity of the internal PCBs.

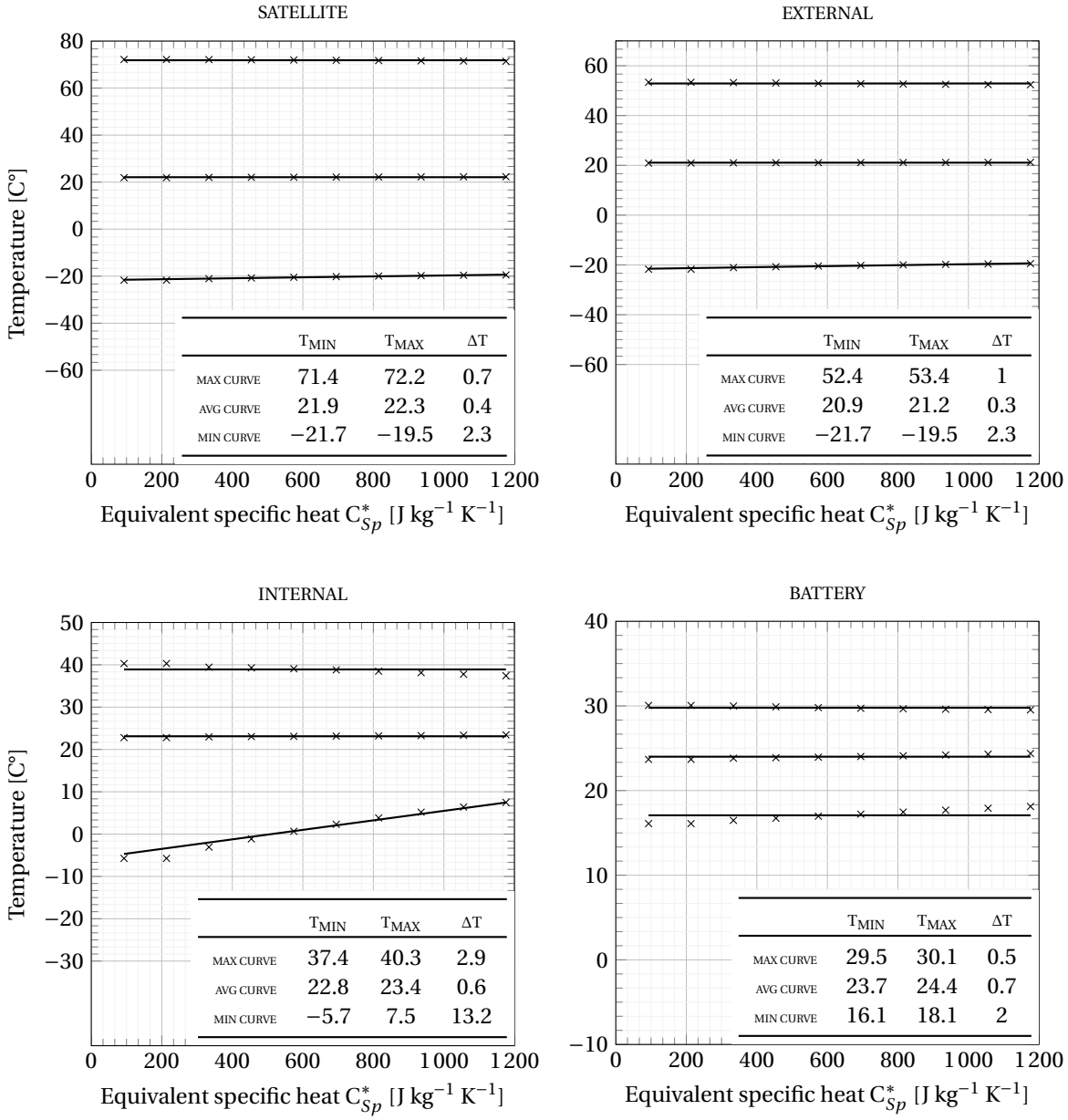

Figure D.1: Sensitivity c3

Sensitivity to variations on the thermal capacity of the batteries.

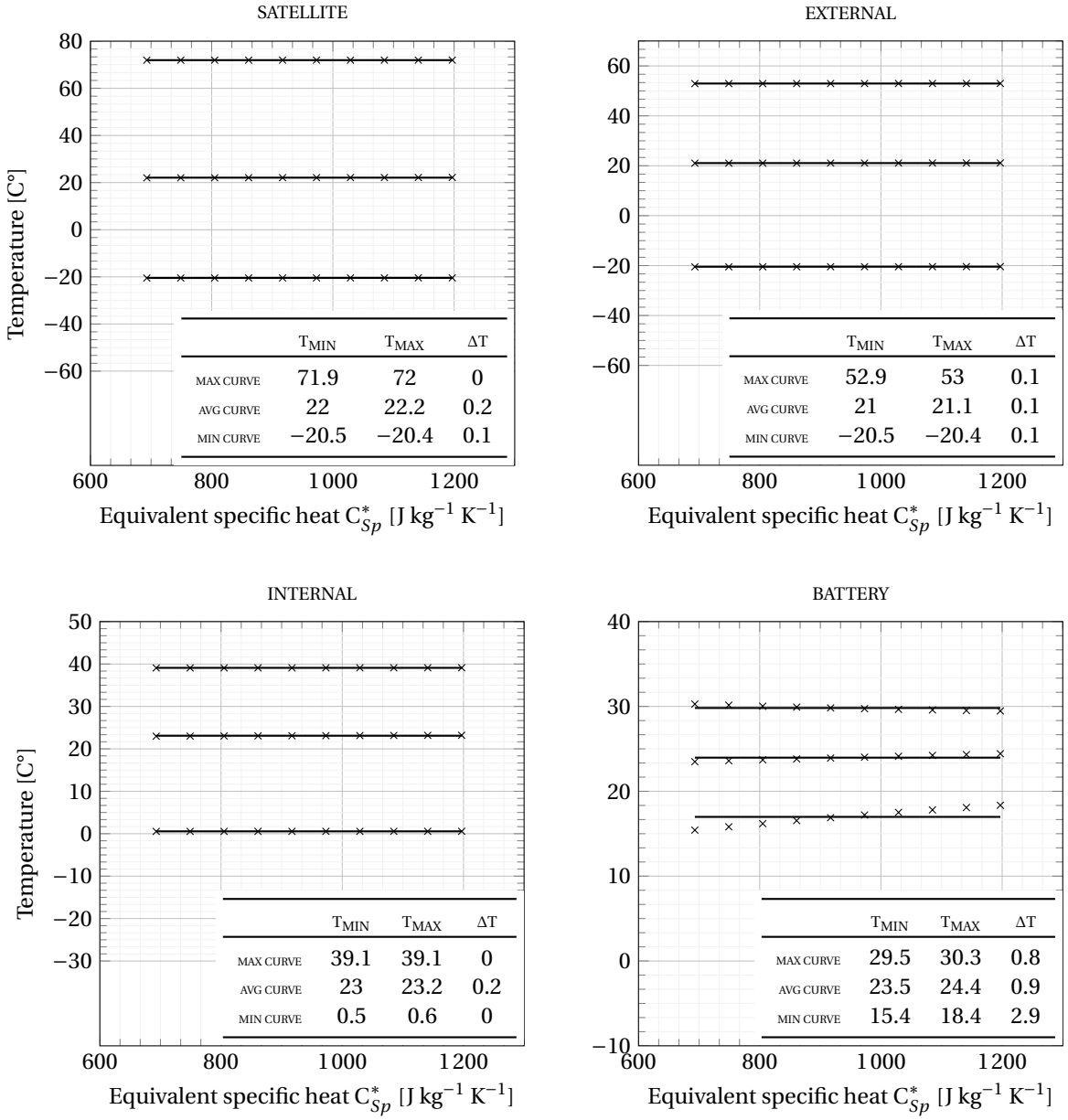

Figure D.2: Sensitivity c4

Sensitivity to variations in the thermal capacity of the electronic components, payloads, etc.

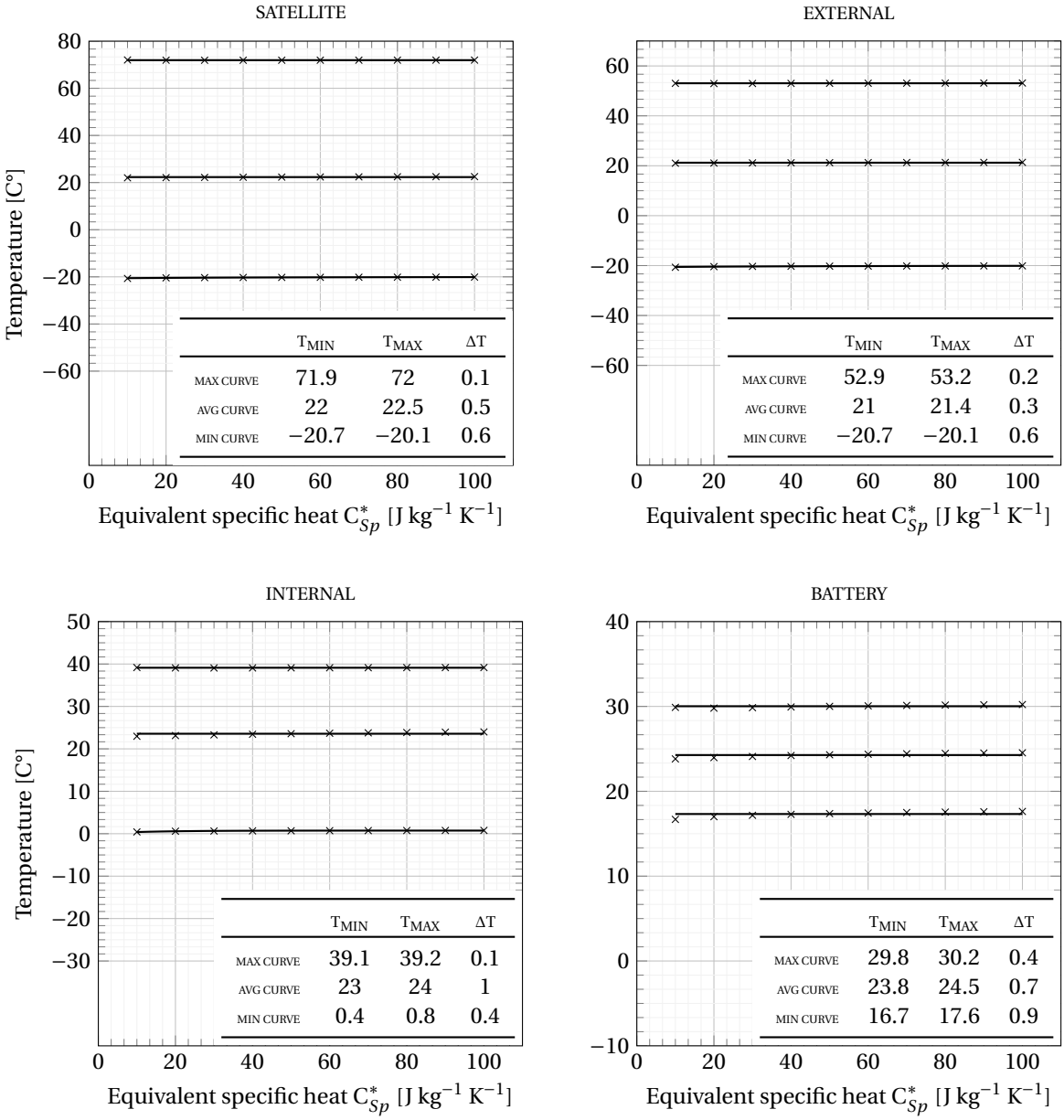

Figure D.3: Sensitivity c5

Sensitivity to variations in the thermal capacity of structural elements.

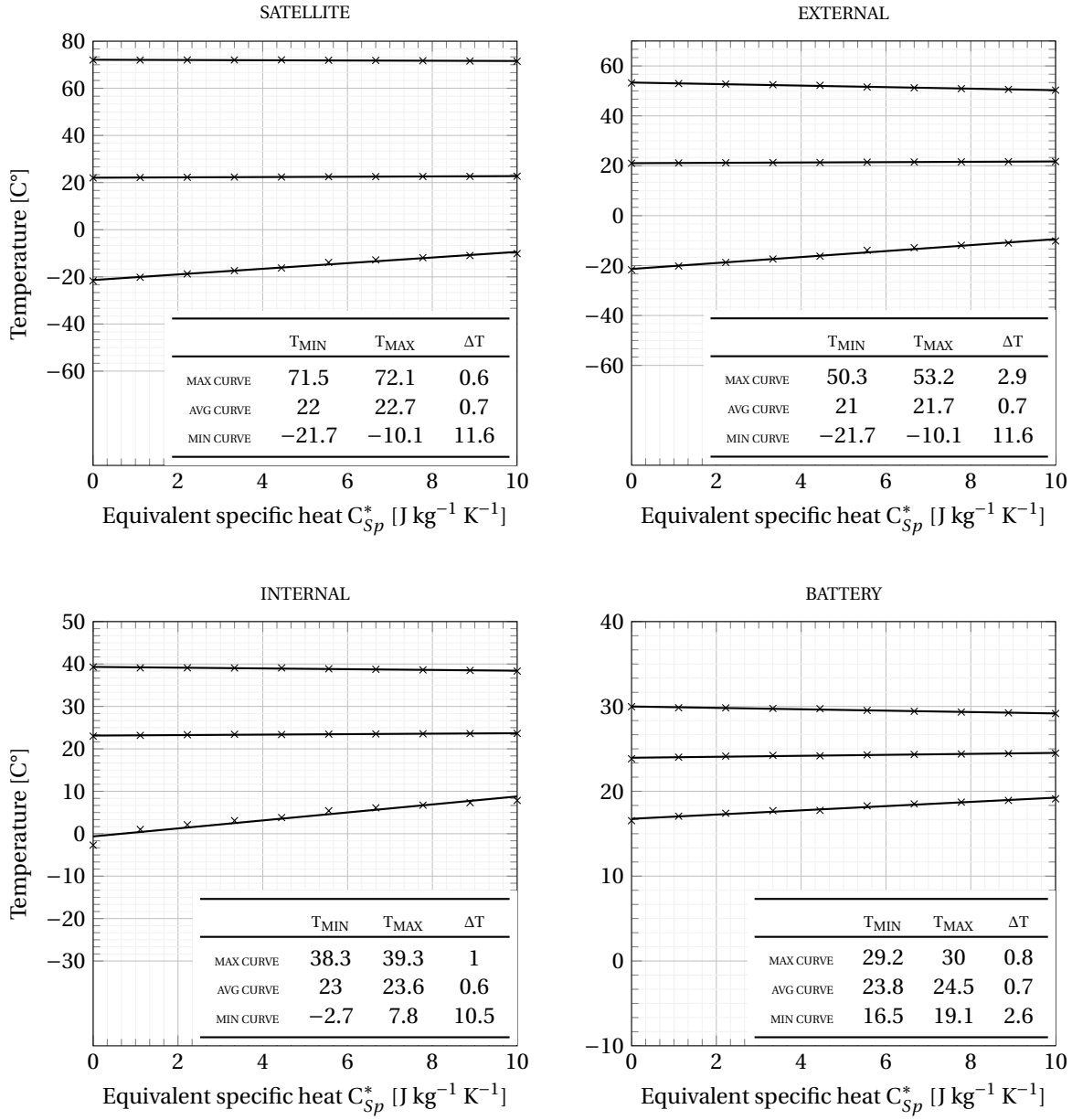

Figure D.4: Sensitivity c6

Sensitivity to conductance board to board via spacers.

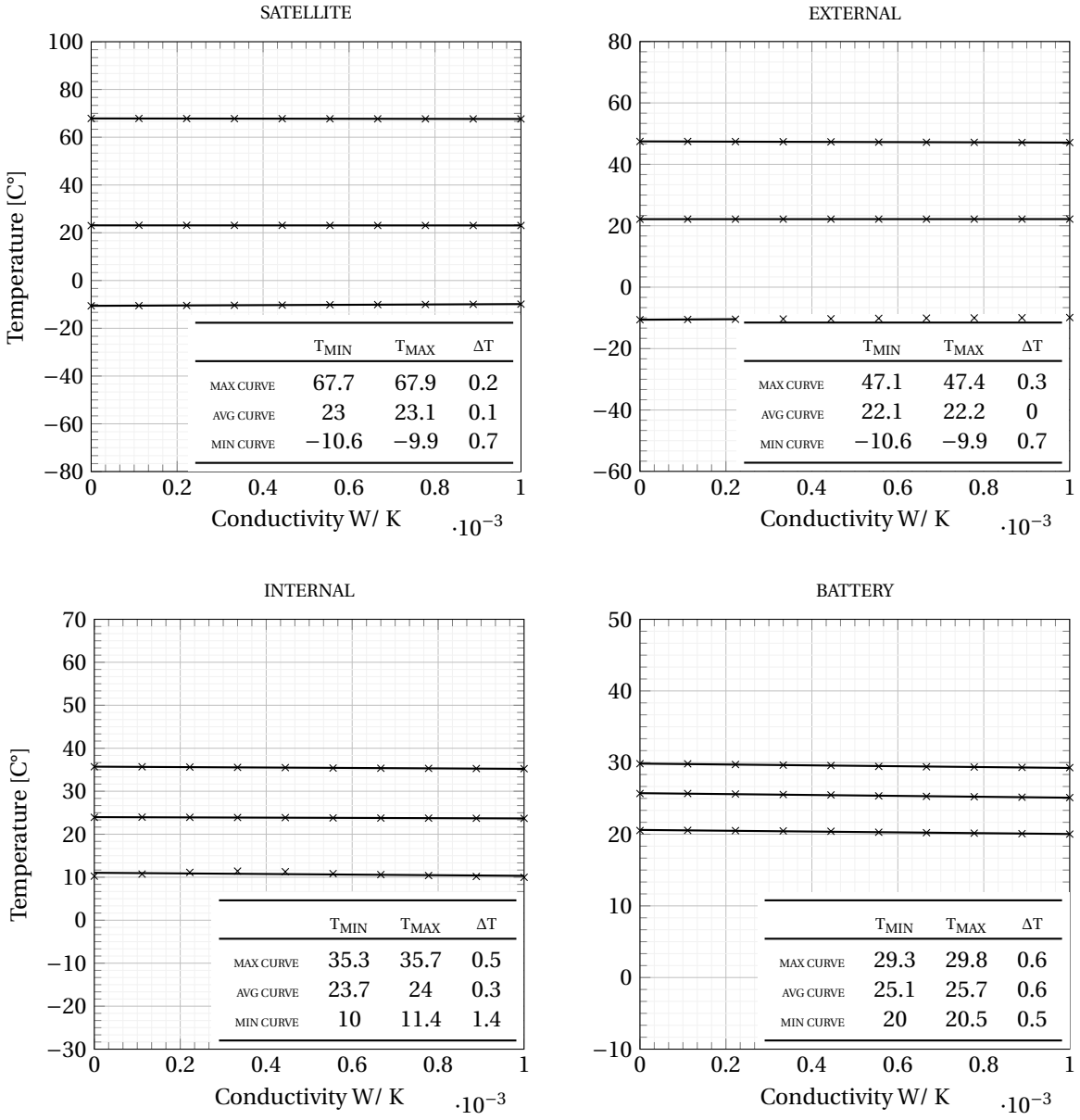

Figure D.5: Sensitivity k2

Sensitivity to conductance of internal structure to shear panels via standoffs.

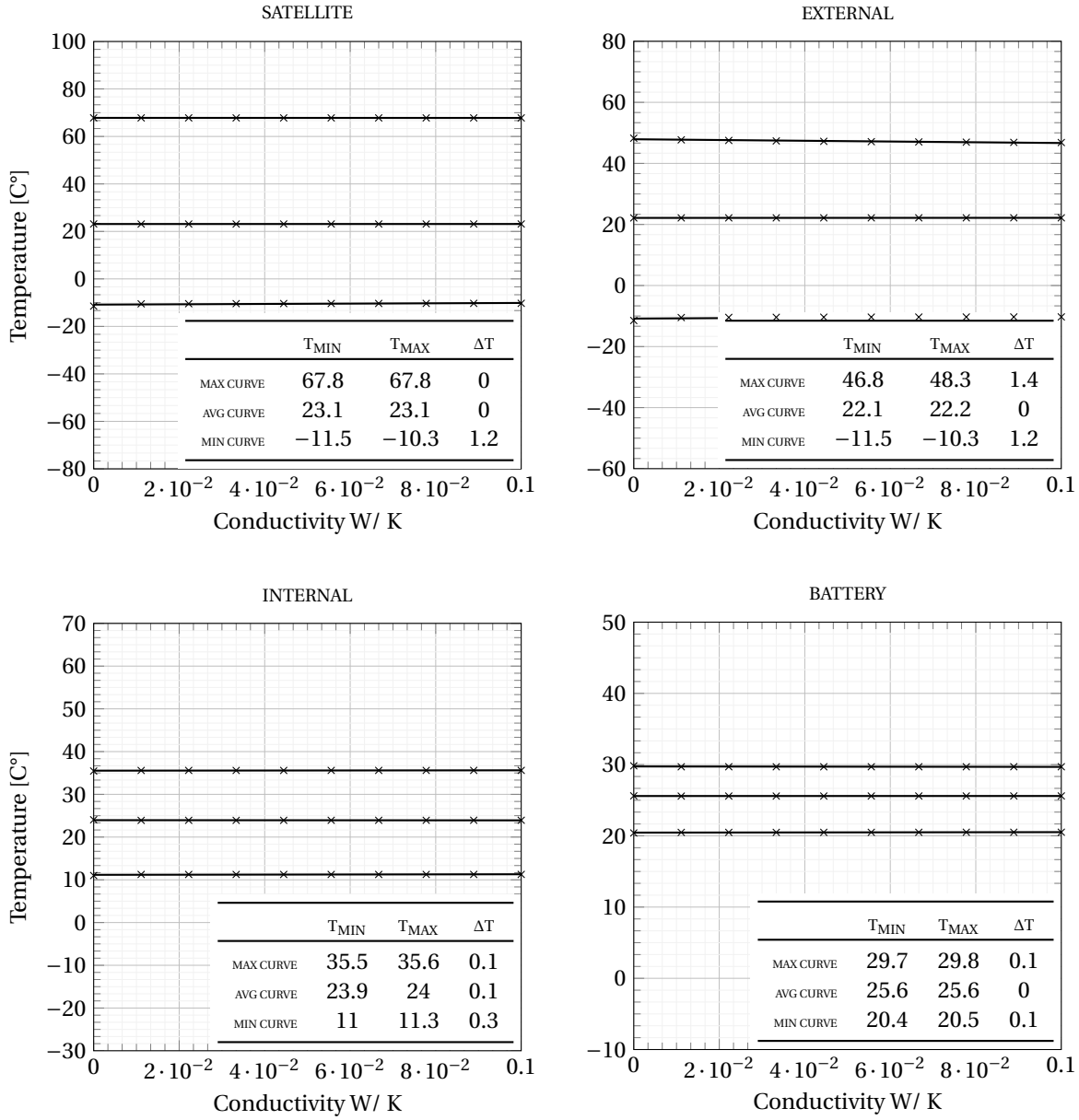

Figure D.6: Sensitivity k3

Sensitivity to conductance battery to board.

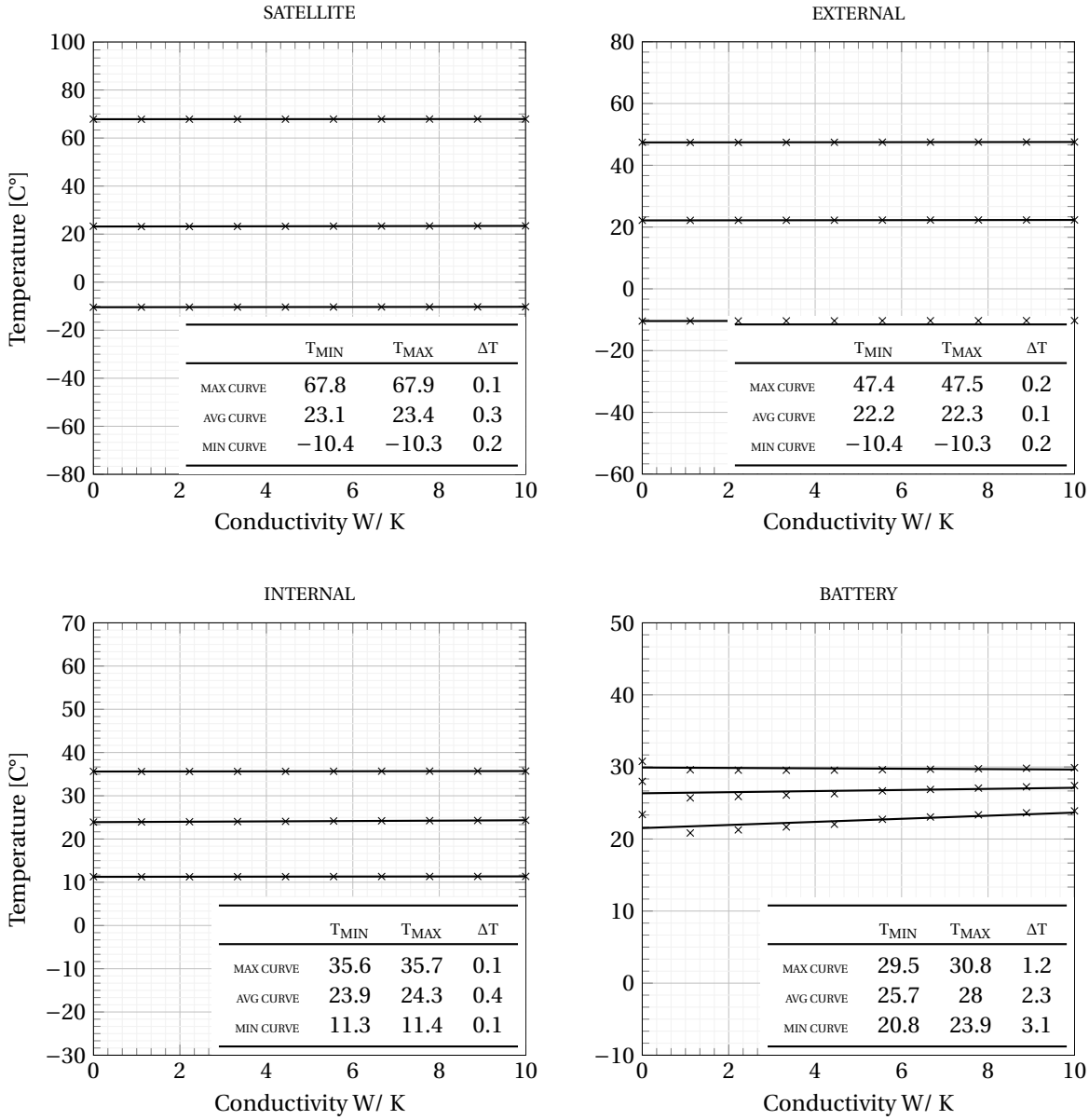

Figure D.7: Sensitivity k4

Sensitivity to conductance soldered or attached components to boards.

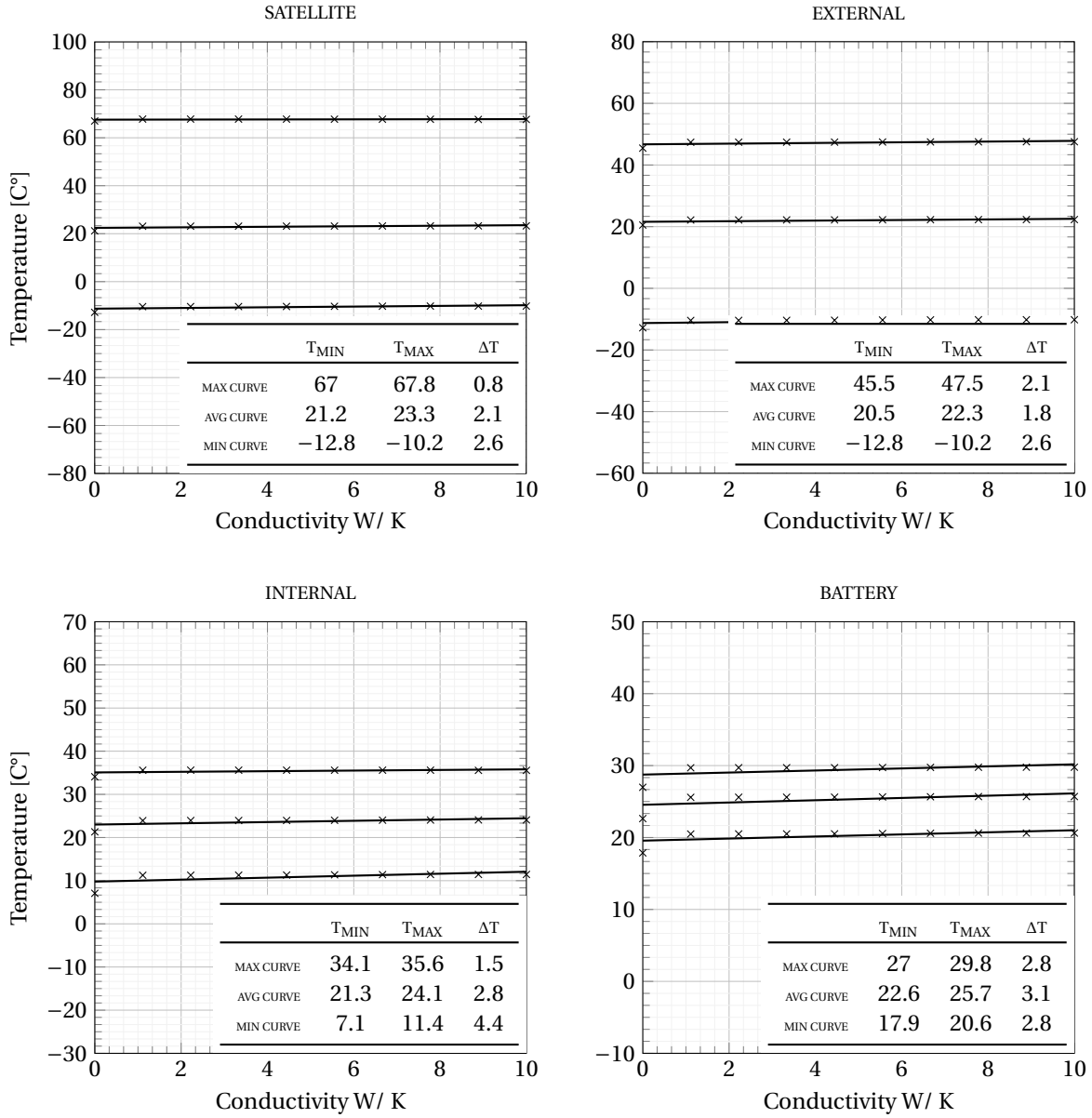

Figure D.8: Sensitivity k5

Sensitivity to conductance solar cells to shear panels.

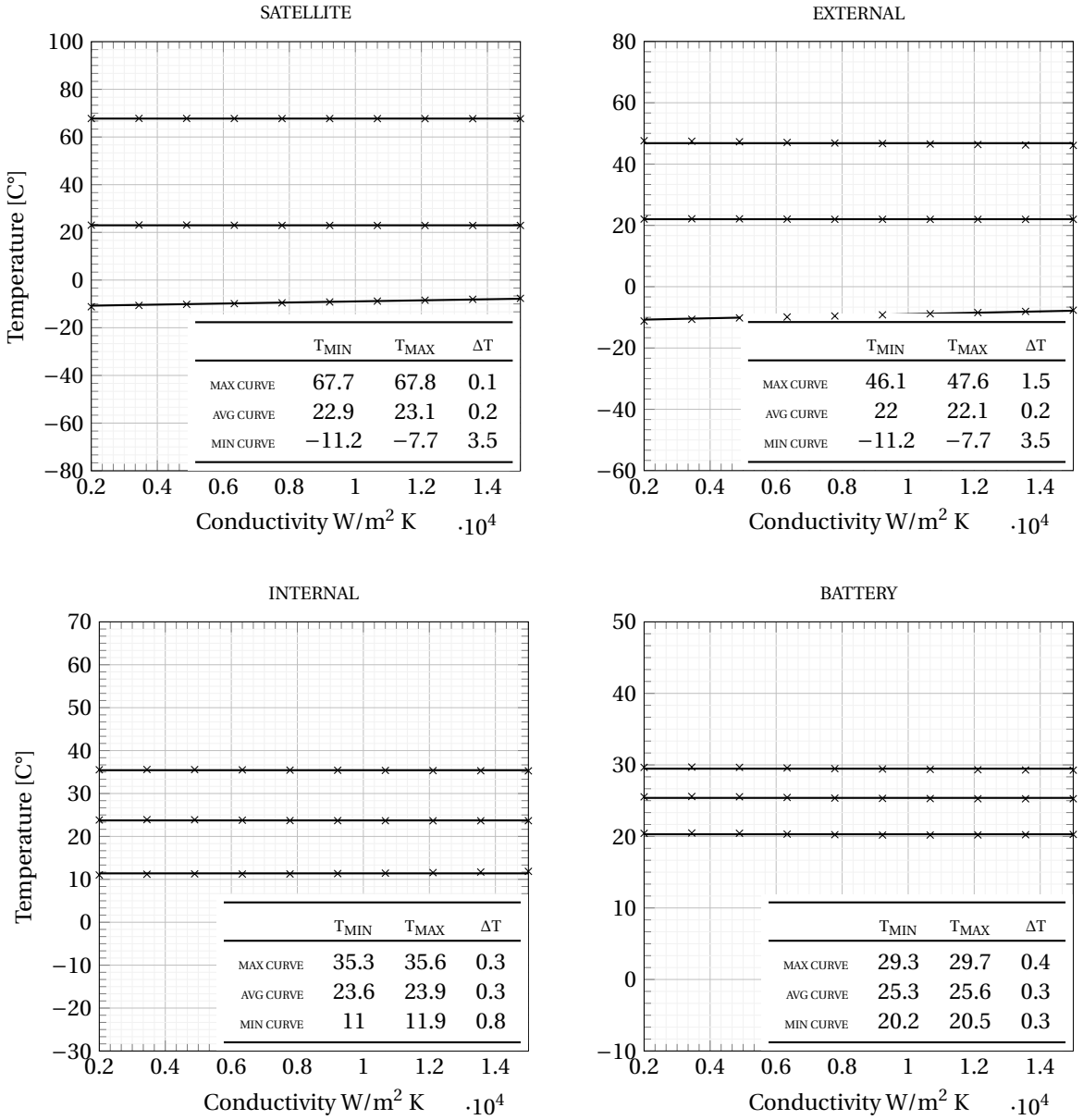

Figure D.9: Sensitivity k6

E

Matlab Code

The following Matlab code illustrates how the sensitivity analysis have been computed.

```
%clear, clc, close

cases=10;
values = [0.13,0.61,1.16,1.60,2.23,2.77,3.15,3.64,4.30,4.73,5.25];
parameter = 'o1';

% Iteration begins
for i=0:cases

% Variables
batch    = 'C:\ESATAN-TMS\2018sp1\Thermal\bin\esatan.bat';                                    % ESATAN batch file
if i<9.5
    path     = ['C:\Users\Rodrigo\Desktop\Drive\Thesis\Report\chapter3\data\',parameter,'\case_',parameter,'_0',num2str(i)
        ]; % Working folder path
    file     = ['model_v01_case_',parameter,'_0',num2str(i),'.d']; % Model file name (lowercase)
else
    path     = ['C:\Users\Rodrigo\Desktop\Drive\Thesis\Report\chapter3\data\',parameter,'\case_',parameter,'_',num2str(i)
        ]; % Working folder path
    file     = ['model_v01_case_',parameter,'_',num2str(i),'.d']; % Model file name (lowercase)
end
name     = 'MODEL_V01'; % Model name (UPPERCASE)

% Execute ESATAN
tic;
fprintf('****************** ');
fprintf('RUNNING CASE %i/%i',i,cases);
fprintf(' ****************** \r\n');

preprocess = [batch,' p "',path,'" ',name,' ',file,' % no'];
status_p = system(preprocess);
solve = [batch,' s "',path,'" ',name,' % % no'];
status_s = system(solve);

% Import data from .out
if i<9.5
    M=csvread(['C:\Users\Rodrigo\Desktop\Drive\Thesis\Report\chapter3\data\',parameter,'\case_',parameter,'_0',num2str(i)
        ,'\temp.csv'],3,0);
else
    M=csvread(['C:\Users\Rodrigo\Desktop\Drive\Thesis\Report\chapter3\data\',parameter,'\case_',parameter,'_',num2str(i),
        '\temp.csv'],3,0);
end
t=(M(1:601,1));
T=M(size(M,1)-600:size(M,1),2:3296);

% NODE DISTRIBUTION
% 1-1876 -> external panels
% 1877-2260 -> solar cells
% 2261-2428 -> battery
% 2429-2536 -> battery case
% 2537-2616 -> antenna
% 2617 -> EPS components
% 2618 -> antenna components
% 2619 -> ADCS components
% 2620-2631 -> standoff
% 2632-2647 -> spacers
% 2648-3295 -> boards

maxT = max(T);
```

```
minT = min(T);
avgT = mean(T);

% The entire satellite max
S_max = max(maxT);
% The entire satellite min
S_min = min(minT);
% The entire satellite average
S_avg = mean(avgT);

% The external panels max
E_max = max(maxT(1:2260));
% The external panels min
E_min = min(minT(1:2260));
% The external panels average
E_avg = mean(avgT(1:2260));

% The internal boards max
I_max = max(maxT(2648:3295));
% The internal boards min
I_min = min(minT(2648:3295));
% The internal average
I_avg = mean(avgT(2648:3295));

% The batteries max
B_max = max(maxT(2261:2428));
% The batteries min
B_min = min(minT(2261:2428));
% The batteries average
B_avg = mean(avgT(2261:2428));

timeleft=datevec(toc*(cases-i)/(60*60*24));
fprintf('SOLVED. Estimated Time Left: %ih %im %is \r\n',timeleft(4),timeleft(5),round(timeleft(6)));

%% Save useful reduced processed data
DATA(1,i+1) = values(i+1);
DATA(2,i+1) = S_max;
DATA(3,i+1) = S_min;
DATA(4,i+1) = S_avg;
DATA(5,i+1) = E_max;
DATA(6,i+1) = E_min;
DATA(7,i+1) = E_avg;
DATA(8,i+1) = I_max;
DATA(9,i+1) = I_min;
DATA(10,i+1) = I_avg;
DATA(11,i+1) = B_max;
DATA(12,i+1) = B_min;
DATA(13,i+1) = B_avg;
end
DATA=DATA'
csvwrite('DATA.csv',DATA)
fprintf('MATLAB FINISHED; PROCESSING DATA FOR LATEX');

dataprocessing
```

```
%% DATA PROCESSING FOR LATEX
clear,clc,close
DATA = csvread('DATA.csv');
precission = 30;

fitco(:,1)=zeros(2,1);
DATAFIT(:,1)=linspace(DATA(1,1),DATA(size(DATA,1),1),precission);

for ii =2:size(DATA,2)
    if min(DATA(:,ii))<0
        data = DATA(:,ii) - min(DATA(:,ii));
    else
        data = DATA(:,ii);
    end
    f=fit(DATA(:,1),data,'a*(1-exp(-(x)*b))','StartPoint',[DATA(1,1),data(1)]);
    fitco(:,ii)=coeffvalues(f)';
    for jj =1:precission
        if min(DATA(:,ii))<0
            DATAFIT(:,ii)=f(DATAFIT(:,1))+ min(DATA(:,ii));
        else
            DATAFIT(:,ii)=f(DATAFIT(:,1));
        end
    end
end

fid1 = fopen('data.txt','wt');
for ii = 1:size(DATA,1)
    fprintf(fid1,'%g\t',DATA(ii,:));
    fprintf(fid1,'\n');
```

```
end
fclose(fid1);

fid2 = fopen('datafit.txt','wt');
for ii = 1:size(DATAFIT,1)
    fprintf(fid2,'%g\t',DATAFIT(ii,:));
    fprintf(fid2,'\n');
end
fclose(fid2);

fid3 = fopen('coeff.txt','wt');
for ii = 1:size(fitco,1)
    fprintf(fid3,'%g\t',fitco(ii,:));
    fprintf(fid3,'\n');
end
fclose(fid3);

min = min(DATA);
max = max(DATA);

fid4 = fopen('delta.txt','wt');

fprintf(fid4,'%.1f\t',min(2));
fprintf(fid4,'%.1f\t',max(2));
fprintf(fid4,'%.1f\t',max(2)-min(2));

fprintf(fid4,'%.1f\t',min(5));
fprintf(fid4,'%.1f\t',max(5));
fprintf(fid4,'%.1f\t',max(5)-min(5));

fprintf(fid4,'%.1f\t',min(8));
fprintf(fid4,'%.1f\t',max(8));
fprintf(fid4,'%.1f\t',max(8)-min(8));

fprintf(fid4,'%.1f\t',min(11));
fprintf(fid4,'%.1f\t',max(11));
fprintf(fid4,'%.1f\t',max(11)-min(11));

fprintf(fid4,'\n');

fprintf(fid4,'%.1f\t',min(4));
fprintf(fid4,'%.1f\t',max(4));
fprintf(fid4,'%.1f\t',max(4)-min(4));

fprintf(fid4,'%.1f\t',min(7));
fprintf(fid4,'%.1f\t',max(7));
fprintf(fid4,'%.1f\t',max(7)-min(7));

fprintf(fid4,'%.1f\t',min(10));
fprintf(fid4,'%.1f\t',max(10));
fprintf(fid4,'%.1f\t',max(10)-min(10));

fprintf(fid4,'%.1f\t',min(13));
fprintf(fid4,'%.1f\t',max(13));
fprintf(fid4,'%.1f\t',max(13)-min(13));

fprintf(fid4,'\n');

fprintf(fid4,'%.1f\t',min(3));
fprintf(fid4,'%.1f\t',max(3));
fprintf(fid4,'%.1f\t',max(3)-min(3));

fprintf(fid4,'%.1f\t',min(6));
fprintf(fid4,'%.1f\t',max(6));
fprintf(fid4,'%.1f\t',max(6)-min(6));

fprintf(fid4,'%.1f\t',min(9));
fprintf(fid4,'%.1f\t',max(9));
fprintf(fid4,'%.1f\t',max(9)-min(9));

fprintf(fid4,'%.1f\t',min(12));
fprintf(fid4,'%.1f\t',max(12));
fprintf(fid4,'%.1f\t',max(12)-min(12));

%print results
header = ['*****';'S max';'S min';'S avg';'E max';'E min';'E avg';'I max';'I min';'I avg';'B max';'B min';'B avg'];
for j=1:12
figure(j)
hold on
scatter(DATA(:,1),DATA(:,j+1),'xk')
plot(DATAFIT(:,1),DATAFIT(:,j+1),'r')
title(['TEMP:  ', header(j+1,:)])
end
```